AN EXPERIMENTAL INVESTIGATION OF A FULLY CAVITATING TWO-DIMENSIONAL FLAT PLATE HYDROFOIL NEAR A FREE SURFACE

Thesis by

Thomas Emmett Dawson

Major, U. S. Marine Corps

In Partial Fulfillment of the Requirements

For the Degree of

Aeronautical Engineer

California Institute of Technology

Pasadena, California

1959

ACKNOWLEDGEMENT

It gives the author great pleasure to express his deep appreciation to Dr. A. J. Acosta who originally suggested the idea for this experiment and whose advice and assistance have been of enormous value during the course of this work. He also wishes to acknowledge the assistance of Mr. Ted Bate on the experimental program. The author would be remiss if he did not acknowledge the United States Marine Corps and the Department of the Navy which made the entire course of graduate study possible.

ABSTRACT

A fully cavitating two-dimensional flat plate hydrofoil at and below a free surface was investigated. The effects of proximity to the free surface, angle of attack, cavitation number and Froude number or gravity on the normal force, the moment about the leading edge, the center of pressure location, the cavity length and the air flow rate into the cavity are discussed. Comparisons to other experiments and theories also are made.

TABLE OF SYMBOLS

Symbol	Definition	Unit
b	Span	Feet
c	Chord length	Feet
$C_f = \frac{F_n}{\rho U^2 c/2}$	Normal force coefficient	Dimensionless
$C_{m_{LE}} = \frac{M}{\rho U^2 bc/2}$	Moment coefficient about leading edge (positive nose up)	Dimensionless
$C_Q = \frac{Q}{Ubc \sin\alpha}$	Air volume flow rate coefficient	Dimensionless
$C_P = \frac{p-p_c}{\rho U^2/2}$	Pressure coefficient	Dimensionless
F_n	Normal force	Pounds
$K = \frac{p_\infty - p_c}{\rho U^2/2}$	Cavitation number	Dimensionless
l	Cavity length from the leading edge	Feet
M	Moment about leading edge	Foot pounds
p_c	Cavity pressure	Pounds per square foot
p_∞	Stream pressure far upstream at depth of leading edge	Pounds per square foot
S	Submergence	Feet
U	Free stream velocity	Feet per second
α	Angle of attack	Degrees
δ	Spray sheet thickness	Feet
ρ	Density	Slugs per cubic foot
$F = \frac{U}{\sqrt{gc}}$	Froude number	Dimensionless

TABLE OF CONTENTS

I. INTRODUCTION

The continued interest in cavitation and in the practical aspects of this phenomenon in various fields of application has sustained an active program of theoretical and experimental research in hydrodynamics for some years. Cavitation is frequently considered to be an undesirable or destructive agent in most fluid flow situations. Examples of mechanical damage due to cavitation erosion on propellers or pump and turbine impellers are usually cited as the undesirable part. Again it is well known that the occurrence of extensive cavitation in most turbomachines, i.e., propellers, pumps and hydrofoil sections, causes serious deterioration in performance. However, in some types of devices, notably hydrofoils, it was noticed that extensive cavitation, of the type called by Tulin "supercavitating", on hydrofoils does not necessarily lead to poor performance at all. ("Supercavitation" is said to occur when the length of the cavity is significantly greater than the chord.) The realization of this fact and the outstanding interest in the applications of hydrofoils to propellers, ship stabilization, hydrofoil craft and various other aspects of naval architecture have stimulated all phases of hydrofoil research.

The focus of most activity in this area is the theory and performance of two-dimensional cavitating hydrofoils. In brief most of these works are concerned with the exploration of hydrofoil behavior and verification of two-dimensional theories in an infinite fluid. In this category we can cite the closed tunnel experiments of Parkin (1), and those by Silberman (2) in a free jet tunnel.

The appropriate theories were initiated by Wu (3), Tulin (4) and again Wu (5). It was realized early that the close proximity of the tunnel walls could significantly influence the results. However, it was found by Plesset, Simmons and Birkhoff (6) that drag results on lamina in closed tunnels were essentially unchanged from infinite stream values although the proportions of the cavity shape might change drastically. Further calculations of the wall effect for other shapes were worked out by Cohen and Tu (7) from which it was deduced that the same result should be true also for lift. (This result was experimentally confirmed by Parkin in (1)). The effect of gravity was worked out (approximately) by Parkin (8) to account for this variable in water tunnel tests. Here again, the fluid was taken as infinite.

However, not all or even most hydrofoils are used in an infinite fluid. In fact, most are operated near a free surface. Certainly this is the case for a hydrofoil supported boat. The free surface, one would think, would be a feature of considerable importance. For deep submergences, infinite fluid theory should prevail. On approaching the surface, on the other hand, the super-cavitating foil becomes in the limit a planing surface. For this situation we will have, in addition to the effects of angle of attack and cavitation number, the relative submergence of the foil and the influence of gravity in perturbing the shape of the free surface. Of course in an actual tunnel test there must be another bounding surface as well which in the case of the present experiments is a rigid wall. In view of the added complications and increasing number of separately variable parameters incurred by the presence

of the free surface it is not surprising that there exist few experiments exploring this effect. In fact for cavitating flows of the sort described herein we know only of the work of Johnson (9) on curved hydrofoils of low aspect ratio. With the high speed of his tests and with the low aspect ratios used it is not possible to determine separately the effects of free surface proximity and cavitation number; nor was it possible to make direct experimental comparison with the theory of two-dimensional hydrofoils so well developed in (3), (4), (5) or reported in the other experiments previously mentioned.

Similarly, the theory of a cavitating hydrofoil near a free surface is not to be found - especially if the effects of gravity are to be included. Special cases, however, do exist. The work of Green (10) and (11) considers the planing of a flat plate on a surface of infinite and finite depth with arbitrary submergence. Gravity is not considered and the cavitation number is always zero (resulting in an infinite cavity length). Finally Cumberbatch (12) and Wu (in an unpublished work) considered the effect of gravity on the planing of a flat plate at small angles of attack and infinitesimal submergences in a fluid of infinite depth.

From the foregoing remarks it is obvious that much work, experimental as well as theoretical, remains to be done before all situations of possible interest to users of hydrofoils become reasonably clear. It is also evident that no one theory or combination of theories now available will cover adequately the range of variables that could reasonably be expected to occur. The present program is an experimental one and it is intended to give some

preliminary information on the effect of the proximity of a free surface on the cavitating flow past a flat plate two-dimensional hydrofoil.

The primary data sought were the normal force coefficient, moment coefficient about leading edge, center of pressure location, bubble length and air flow rate as functions of the angle of attack, cavitation number and relative submergence of the hydrofoil beneath the surface. In addition, the possible effect of gravity or Froude number on these results is a feature of great interest and will be checked within the limitations of the equipment.

As a further item of interest the linearized free streamline theory of flow past a fully cavitated flat plate hydrofoil beneath a free surface is worked out and compared to the results of Green (10), so that the accuracy of this method can be determined for this type of flow as well.

II. EXPERIMENTAL PROGRAM

Experimental Facility

The experiment was carried out in the Free Surface Water Tunnel of the Hydrodynamics Laboratory at the California Institute of Technology. Knapp et al (13) give a complete description of this tunnel and Fig. 1a shows a picture of the working section. This tunnel is a vertical-return, closed-loop capable of a velocity up to 26 fps. The test section is 7.5 ft. long, 1.6 ft. wide, and has a nominal depth to the free surface of 1.6 ft. The rather low velocity of the working section does not permit vapor cavitation at the deepest submergences. To obtain a supercavitating flow under the circumstances of the present test, air was forced into the wake of the hydrofoil to form a constant pressure cavity. Such "ventilated" or "forced" cavitation simulates in all important respects vapor cavitation and permits thereby cavitation research in low speed facilities that do not have pressurization control. O'Neill and Swanson (14) report experiments on such artificial cavities behind disks.

The installation of a full span hydrofoil in the test section of the main tunnel was not considered feasible due to mounting and instrumentation difficulties. Therefore, it was decided to construct a smaller two-dimensional test section.

Data Desired

The primary purpose of this experiment was to determine the effects of a free surface, cavitation number, angle of attack, and Froude number upon the force and moment acting on a two-dimensional, fully cavitating flat plate hydrofoil and also upon the

cavity length. Realizing that in order to maintain stable cavity flow at the deeper submergences it was going to be necessary to force air into the cavity, it was decided to measure this air flow rate as an additional feature of the experiment.

In order that the above results could be achieved, it was necessary to obtain the following data: tunnel free stream velocity, force and moment acting on the hydrofoil, angle of attack, submergence, cavity pressure, cavity length, and air volume flow rate. These data were obtained by measuring the pressure distribution on the flat plate since the installation of devices to measure the total force and moment directly was considered impractical. In addition it was felt that sample plots of these pressure distributions would be of interest since none are available. (Plots of pressure distributions are referred to later in the report.)

Design and Fabrication of Equipment

The two-dimensional test section, Fig. 1b, was fabricated from plexiglas and aluminum to fit at the upstream end of the larger test section on the centerline. The two-dimensional section is 4.25 ft. long, 2 ft. high, and has an inside width at the leading edges of 0.25 ft.. The leading edges are wedge-shaped pieces of aluminum with sharp upstream edges and parallel inner surfaces. This two-dimensional section has a means for holding a mounting plate, Fig. 2a, which in turn holds the hydrofoil, Figs. 2b and 3. The mounting plate can be positioned vertically by inserting or removing aluminum shims under it. In addition, the mounting plate has a circular plate, to which the hydrofoil is

attached, that can be rotated to vary the angle of attack. The hydrofoil is also attached to the wall of the two-dimensional test section opposite the mounting plate to prevent any tendency of the wall to bow out during operation.

The wedge hydrofoil itself, Figs. 2b and 3, was constructed of 416 stainless steel. Grooves were milled at the desired location of the pressure taps and then brass tubes of 1/16-in. diam. were laid in these grooves and covered with transparent epoxy resin and the surfaces were ground smooth. Piezometer orifices of 0.020 in. diam. were then drilled perpendicular to the wetted surface of the hydrofoil into the brass tubes. The pressure measured at each of these taps was led off through the brass tubes behind the mounting plate and thence into flexible tubing and to the manometer board.

Leading down behind the mounting plate and through the face of the circular plate just downstream of the hydrofoil were the lines for feeding air to the cavity and for measuring the cavity pressure. To insure that there was no water in the line that measured the cavity pressure, a three-way valve was put in this line with one side connected to laboratory air pressure. This enabled the experimenter to blow this line clear prior to each reading (see Fig. 4 for schematic drawing).

The Free Surface Water Tunnel, as originally designed and constructed, had a boundary layer remover, or skimmer, on the upper surface just prior to the test section. This served to remove the boundary layer which had built up through the

tunnel in order that the velocity be uniform up to the free surface in the test section. It was found, however, that a more level free surface in the two-dimensional test section was obtained when the skimmer was blocked off. The great majority of the test runs were conducted in this configuration. In this condition there was a velocity defect at the free surface. Fig. 5 shows the results of a velocity survey near the free surface on the centerline of the two-dimensional test section. It can be seen that the velocity at the free surface is about 75 per cent of the free-stream value. The velocity at one inch below the free surface has returned to 98 per cent of the free-stream value. In order that the effect of this velocity defect could be investigated, additional runs at the end of the major part of the experimental program were made with the skimmer unplugged. This effect was small and will be discussed in more detail later.

In order to test and calibrate the two-dimensional section, preliminary runs without the hydrofoil were made. The velocity in the two-dimensional test section was correlated to the existing calibration curve of the tunnel. Boundary layer surveys were made with an impact probe at the position of the leading edge of the hydrofoil. The results of these boundary layer surveys are shown in Fig. 6. The boundary layers were slightly larger than predicted by turbulent boundary layer theory. The displacement thickness was found to be 0.045 in. as compared to 0.032 in. from turbulent boundary layer theory. This displacement thickness was not considered large enough to warrant a redesign of the

two-dimensional test section. Mendelsohn (15) shows that a boundary layer of thickness equal to four per cent of the span does not affect the forces acting at the centerline of a two-dimensional fully wetted airfoil by more than one per cent. The effects on a fully wetted model and the present fully cavitating model with a boundary layer thickness equal to about ten per cent of the span should be approximately the same. In addition to the measurement of the boundary layer thickness, a check for ventilation at the leading edges of the two-dimensional test section also was made. Infrequent and shortlived ventilation cavities were noted at velocities above 15 fps. This was apparently the result of sporadic turbulence pockets coming through the tunnel. It is possible that the effect of this free-stream turbulence is responsible for the thickened boundary layer observed on the side walls. Moreover, the leading edges are beveled on one side only - to suppress surface waves. This may cause local separation at the leading edges some distance below the free surface and result in the slightly larger boundary layer than the theory predicts.

Instrumentation

The instrumentation of the experiment was very simple. The pressures from the 10 orifices on the foil were measured on a water-filled manometer board, as was the tunnel total head. The cavity pressure was measured on a separate water-filled manometer. The air volume flow rate was measured by means of a Fisher Porter flowmeter of 4.0 cu. ft. per min. capacity, see Figs. 1a and 4 for photographs of the entire setup and a

schematic drawing. In order to measure the cavity lengths, a yardstick was fixed to the tunnel wall so that zero corresponded to the leading edge of the hydrofoil. Then by sighting perpendicular to the flow at the estimated point of closure of the cavity, it was possible to measure the cavity lengths.

All pressure measurements are considered accurate to within 0.01 ft. of water. The air flow rate is considered accurate to within the calibration of the instrument, 5.0 per cent. However, the cavity lengths were at best visual averages, accurate only to one-half inch for any length, due to fluctuations in the rear of the cavity from one to two inches.

Prior to the commencement of the actual experimental program, an angle of attack calibration was made. This was accomplished by drilling two additional piezometer orifices in the hydrofoil. One was located on the upper surface and one on the lower surface of the hydrofoil at equal distances from the leading edge. By reducing the pressure difference between these two orifices to zero, it was possible to align the chordline of the hydrofoil with respect to the flow. This angle was repeatable to within one-fourth of a degree. The angle of attack as used in this experiment is with respect to the wetted or lower surface and since the included wedge angle is six degrees the zero was shifted by three degrees.

III. EXPERIMENTAL PROCEDURE

The experimental program was started at the deepest submergence, 0.811 ft. below the free surface or S/c = 2.16, and continued up to and through the free surface at submergence ratios of 1.5, 0.83, 0.16, 0.05 and -0.06. Submergence, S, as used in this report, is the distance from the undisturbed free surface to the pivot point on the hydrofoil - positive if below the surface and negative if above. At each of the above submergences, runs were made at six angles of attack: 6°, 8°, 10°, 12°, 14° and 16°. With the skimmer blocked, five runs were made at each submergence and at each angle of attack. The cavity pressure was varied from run to run as was the velocity. This program permitted a range of cavitation numbers, $-0.05 < K < 0.20$, and a small range of Froude numbers, $2.7 \leq F \leq 4.8$, which are two of the basic parameters of the present experiment. After the above program was completed, another program similar to the one above was undertaken at S/c = 0.09, $\alpha = 6^{\circ}$, 8°, and 10°, and velocities higher than before, up to 20 fps. These tests were done with the skimmer unplugged in order to find the effect of the free surface velocity defect noted earlier, as well as to obtain a Froude number as high as the present experiment would permit, F = 5.75. An additional part of the experiment was carried out at S/c = 1.60. Numerous runs at two velocities and one angle of attack, $\alpha = 8^{\circ}$, were made. The only measurements taken were the cavity length and cavity pressure so that a better overall average cavity length measurement could be obtained. These data are shown in a separate figure in the report, Fig. 44, and will be discussed later.

Procedure for a Typical Run

In order that the reader may more thoroughly understand the experimental procedure, a typical run will be described briefly below:

The hydrofoil was installed at the desired depth. Since the lines from the pressure orifices on the hydrofoil to the top of the mounting plate were small, it was imperative for accuracy that all air and bubbles be out of all lines. This was found to be best accomplished by application of a reduced pressure to the tops of the manometer tubes. After the air was removed, the manometer board was allowed to stabilize as an additional check for air in the lines. The tunnel then was brought up to the desired speed. The angle of attack was adjusted to the desired value and the air flow was regulated, if necessary, to obtain a stable cavity of the desired length. It was found that about 10 minutes was required for all pressure readings to stabilize after the speed, angle of attack, and cavity length were fixed. After this time period all readings were taken as nearly simultaneously as possible.

It should be pointed out here that the closure of the cavity that was observed in this experiment was primarily the reentrant type which was controlled by the air flow rate. There was a minimum air flow rate for this type of cavity; below this rate the cavity became unstable and collapsed, and above this rate the excess air blew out the end of the cavity with no appreciable effect on cavity pressure. However, when this latter condition occurred it was impossible to define the cavity closure point. Photographs of typical cavities are shown in Figs. 7 through 11.

Data Reduction and Definitions

The data were reduced to the form of normal force coefficient, moment coefficient, center-of-pressure location, cavity-length to chord-length ratio, and air-volume flow-rate coefficient. These results were found as functions of the cavitation number, angle of attack, submergence to chord-length ratio, and Froude number*.

The normal force and moment coefficients were obtained by means of numerical integration. It was assumed for this purpose that the stagnation point was at the leading edge of the flat plate. This assumption is substantiated by Wu's exact theory (3) for the angles of attack under consideration and was also verified by direct visual observation of the flow near the leading edge by means of a tuft on a probe. The pressure distributions were plotted and the numerical integration procedure was checked by a planimeter. The difference was less than 2 per cent which is not significant. Some representative plots of pressure distributions are shown in Figs. 12 through 17.

Note: The pressure coefficient as used is known to go to zero at both the leading and trailing edges.

---

*All terms used in this paragraph are defined in the table of symbols.

IV. RESULTS AND DISCUSSION

Presentation of Results

The results of the present experiment are presented in Figs. 18 through 46. The quantities desired and obtained as results were: the normal force coefficient, C_f; the moment coefficient about the leading edge, $C_{m_{LE}}$; the center-of-pressure location aft of leading edge; the cavity length ratio, ℓ/c; and the air volume flow rate coefficient, C_Q. The results will be discussed in the above order with respect to the following parameters: the angle of attack, α; the cavitation number, K; the submergence ratio, S/c; and the Froude number, F. The normal force coefficient also will be discussed in relation to the ratio, c/δ, where δ is spray sheet thickness. For $S/c > 0.16$, δ was defined as the depth of water between the free surface and the leading edge, and for $S/c \leq 0.16$ the spray sheet thickness was estimated visually. The results also will be compared to other experiments and to the theories available.

Normal Force Coefficient

The basic normal force coefficient data are plotted on Figs. 18 through 23 for the six submergence ratios. It is seen that C_f increases parabolically with K as the infinite fluid theory of Wu (3) indicates. Extrapolation of the data at $S/c = 2.16$ shows that C_f increases from 0.16 to 0.29 for $\alpha = 6^\circ$, and from 0.373 to 0.48 at $\alpha = 16^\circ$ as K increases from zero to 0.20. It can be seen that similar increases are true for other submergences at which a sufficient range of K was attainable for extrapolation. In order to separate the effect of angle of attack changes from cavitation number changes, the experimental data on these figures were

extrapolated to K = 0 and replotted on Fig. 24a. This figure shows that C_f increases linearly with angle of attack for all submergence ratios. The slope, $dC_f/d\alpha$, is equal to 0.021 per degree. This linear relationship and the rate of change both agree with the infinite fluid theory of Wu (3). The experimental values extrapolated to K = 0 also were plotted on Fig. 25 to show the effect of the free surface. The effect of the free surface is first noted at about S/c = 0.7 for all angles of attack. At S/c = 0 the increase in C_f over the C_f at S/c > 0.7 is 13 per cent at $\alpha = 16^\circ$ and 25 per cent at $\alpha = 6^\circ$ with skimmer plugged. With the skimmer operating, the increase in C_f over the value obtained with the skimmer plugged is 8.5 per cent at $\alpha = 10^\circ$, and 7.0 per cent at $\alpha = 6^\circ$.

We now compare our normal force coefficients with the two experiments that are available. Parkin (1) performed an experiment with a flat plate in full cavity flow in a closed tunnel. For proper comparison then, we should use our results at S/c = 2.16. However, Parkin's data are for $K \geq 0.20$ while ours extends only up to about K = 0.19. If we extrapolate both data to K = 0.20, we find the present experimental values higher than that of Parkin by 4.0 per cent at $\alpha = 8^\circ$ and higher by 7.0 per cent at $\alpha = 12^\circ$. Silberman (2) also did some recent work with a flat plate in a free jet tunnel. Since his model of two inch chord was approximately 5 in. from the edge of the jet, his results should be compared to the present experiment at S/c = 2.16 also. Silberman's experiments were carried out in same cavitation number range as the present experiments. Extrapolating both data at $\alpha = 8^\circ$ to K = 0.20, again we find that the present data are higher than that of Silberman by

about 4.0 per cent. At K = 0.10 we are higher still; this time by about 16 per cent. Before we discuss these discrepancies, let us first look at the theories applicable to the normal force coefficient.

As was mentioned in the introductory section of this report, there is no theoretical treatment of the total problem as proposed in this work. The available theories are: the infinite fluid theory with no gravity (both exact and linearized) of Wu (3), (5), the infinite fluid theory with gravity of Parkin (8), the planing theory of Green (10) with no gravity, the linearized planing surface theory of Cumberbatch (12), and an unpublished theory of Wu that accounts for the effect of gravity. In addition, we have the linearized wall effect theories due largely to Cohen (7) that can be extended to account for the effect of the free surface and a rigid bottom (with no gravity). This latter theory requires laborious calculation for the present geometry, and due to the press of time it was not carried out. Furthermore, Green (11) has also worked out the case of planing on a finite channel for zero cavitation number. Again no numerical results are available. In order to make some attempt to fill the obvious gap in theory, two simplified linearized theories are proposed, -- one for the free surface effect, (App. I), and one for the bottom effect, (App. II), which will be discussed with the others in due course.

We will first look at the infinite fluid theories, Wu (3) and Parkin (8), and compare them to our results at S/c = 2.16. Looking again at Fig. 18 we see that the data of the present experiment are consistently higher than Wu at all angles of attack. The data are higher by 4.0 per cent at $\alpha = 6^{\circ}$, K = 0.20, by 5.0 per cent at

$\alpha = 6^\circ$ K = 0, by 4.0 per cent at $\alpha = 16^\circ$ K = 0.20, and by 5.5 per cent at $\alpha = 16^\circ$ K = 0. We look to Parkin for the effect of gravity and find that his theory for $F^2 = 16$ predicts a slight decrease (two per cent estimated from his charts) in C_f from the zero gravity case. Thus, at least at the deepest submergence, the effect of gravity on our tests is negligible. However, the discrepancy with Wu's theory and the experiments of Parkin and Silberman remains to be resolved.

We now consider the possible effect of the free surface. There are two theories available; the exact theory of Green (10) and the linearized theory of App. I. Both of these theories are basically the same in origin and apply for K = 0. Looking at Fig. 26, the two theories may be seen plotted as C_f divided by the value of C_f for the infinite fluid versus the chord to spray sheet thickness ratio. It is seen that the effect of the free surface is to increase C_f in both theories. The linearized theory, however, overestimates the effect of the free surface. At $c/\delta = 0.4$, which corresponds to $S/c = 2.16$, the linearized curve is 14 per cent higher than the exact when the latter is evaluated at an angle of attack of 8°. It is seen from Fig. 26, as well as Figs. 27 through 30, that the theoretical effect of the free surface is much larger than shown by experiment. Green's theory is 16 per cent higher than the experimental points at $\alpha = 8^\circ$, 10°, 12°, 14°. Thus the trend of the experiment is in the right direction but much too small in magnitude.

Although the linearized theory of the bottom effect, App. II, is strictly correct only at or near the free surface, we might look

at this effect at S/c = 2.16 for comparative purposes. It is seen that this effect is to increase C_f by 1.5 per cent, which is in the same direction as the experiment although the effect is far too small to be of importance.

Now we turn our attention from the case of deepest submergence to the one in which the hydrofoil is at or near the free surface. There are no other experiments with which to make a comparison, but here again the results of Green and the linear theory should be applicable. We find as before in Figs. 27 through 30 that both theories overestimate the effect of the free surface. The experimental results are lower than those of Green at all angles of attack by 14.0 per cent at c/δ = 6.0 and by 23 per cent at c/δ = 18.0. The linear theory is still higher than Green's theory by about 13 per cent in this range of c/δ.

The possibility of gravity causing the lift decrease at the free surface was next examined. Here we have only the planing theories of Cumberbatch and Wu as previously mentioned. Strictly speaking, these theories apply only for zero spray sheet thickness. For comparative purposes, however, the Froude number asymptotes at $c/\delta = \infty$ of these theories have been shown on Fig. 26 along with the theory of Green and that of App. I, and the experimental points. It appears that the experimental data approach an asymptote for a Froude number of 3.5 to 4.0, which is the average Froude number of the present experiment. This would lead to the conclusion that C_f for shallow submergences is strongly Froude-number sensitive. It was, in fact, to check this point that additional data were taken at S/c = 0.09 with as wide a range

in F as the equipment would allow. The resulting curves of C_f versus F are shown in Fig. 31, in which it is seen that there is no particular dependency on F over the range $2.7 \leq F \leq 5.8$. However, planing surface theory predicts a decrease in C_f with decreasing F. This result is not observed in the present tests and presumably the accuracy of the experiment is sufficient to detect this variation.

The effect of the bottom, App. II, when the hydrofoil is at the free surface, is still to increase the lift but by only 0.4 per cent, which is negligible.

With respect to the normal force coefficient, we find ourselves in somewhat of a dilemma at both the deeper submergences and near the free surface. At the deeper submergences the present data are higher by about five per cent than comparable experiments and the infinite-fluid-no-gravity theory. Parkin's theory with gravity will not account for this discrepancy and both theories for the free surface effect overcorrect badly. At and near the free surface, on the other hand, we find that the present data are about 20 per cent lower than the exact no-gravity planing theory, and considerably further below the linearized theory without gravity. It appears that gravity will account for the observed lift near the free surface with the average Froude number of these tests, but the experimental data do not show the Froude number sensitivity predicted by the linearized planing theory.

The conditions required by these theories are not perfectly fulfilled in the experiments and this may have a bearing on the result. For example, there is a sidewall boundary layer and a free surface velocity defect. The force reduction due to the sidewall

boundary layer according to the previously mentioned work of Mendelsohn should not influence the centerline force coefficient appreciably (one per cent). An additional complicating factor is that for the smaller submergences the spray sheet fell in front of the hydrofoil and the resulting turbulent wake passed under the hydrofoil. This effect is to thicken the surface velocity defect and change the local flow inclination and hence to result in a departure from the assumed flow conditions of the theory. It may be that the combined effects of the sidewalls, boundary layer and spray sheet interference mask the Froude number sensitivity required by Cumberbatch's theory of planing.

On the other hand, at the deepest submergences we can see no outstanding defect of the experiment that will account for the observed discrepancy between the extrapolated experimental data and Green's theory. Gravity, as we have mentioned, does not account for this result, at least in an infinite fluid. Neither do the wall effect theories of Appendices I, II or those of Cohen and Tu. However, it is definitely possible that the combined effect of gravity and the neighboring free surface may well result in the observed behavior. For example, we know that the presence of gravity reduces the excursion of the free surface. Or to put it in other terms, the surface is partly "rigidified" by the effect of gravity. In the limit as the Froude number goes to zero, the free surface becomes plane. Cohen and Tu have calculated this latter case for zero cavitation number for a limited range of c/δ and found that the lift coefficient is lower than the infinite fluid value. Thus, there is every reason to believe that gravity

acting in the presence of a free surface can significantly alter the force coefficients. To repeat, in the present case at an average Froude number of 3.5, the normal force coefficient is 16 per cent lower than Green's theory (the experimental data are extrapolated to $K = 0$) and five per cent higher than the infinite fluid theories and closed water tunnel experiments. Certainly, further experiments over a range of Froude numbers wider than those of the present tests are desirable to clear up this matter.

Moment Coefficient about Leading Edge

The basic moment coefficient data are plotted on Figs. 32 through 37 for the six submergence ratios. As with the normal force coefficient, it can be seen that the moment coefficient decreases parabolically with cavitation number as the infinite fluid theory of Wu (3) predicts. At $S/c = 2.16$ the data show that as K increased from zero to 0.20 the moment coefficient decreased as follows: $\alpha = 10^{\circ}$ from $C_{m_{LE}} = -0.085$ to -0.127; $\alpha = 16^{\circ}$ from $C_{m_{LE}} = -0.137$ to -0.177. A similar decrease with cavitation number exists at other submergences. Fig. 24b shows $C_{m_{LE}}$ extrapolated to $K = 0$ plotted versus angle of attack. This figure shows a linear decrease in $C_{m_{LE}}$ with α at all submergences. The slope $dC_{m_{LE}}/d\alpha$ is equal to -0.008. This linear decrease and slope again agree well with Wu. The values of $C_{m_{LE}}$ extrapolated to $K = 0$ were also plotted versus S/c on Fig. 38 to show the effect of the free surface. Again the primed points are those obtained with the skimmer unplugged and operating. The effect of the free surface to increase the magnitude of the moment coefficient is first noted at about $S/c = 0.7$ for all angles of attack. At

$S/c = 0$, with the skimmer plugged, the increase in the value of $C_{m_{LE}}$ over the value of $C_{m_{LE}}$ below $S/c = 0.7$ is 13 per cent at $\alpha = 8^{\circ}$ and 13.5 per cent at $\alpha = 16^{\circ}$. When the skimmer was unplugged an additional increase in the value of $C_{m_{LE}}$ of 13.0 per cent at $\alpha = 8^{\circ}$ and of 6.0 per cent at $\alpha = 10^{\circ}$ was noted.

For experimental comparison in this case we have only Parkin (1) whose experiment was performed in a closed tunnel in the cavitation number range generally greater than 0.20. Extrapolation of both data to $K = 0.20$ at $\alpha = 12^{\circ}$ and for our deepest submergence, we find that the agreement is very good.

The basic theory available for comparison to the experimental moment coefficient is the infinite fluid no-gravity theory of Wu. Looking at Fig. 32 at $S/c = 2.16$ we see that the experimental data are larger negatively by 7.5 per cent at $K = 0$ $\alpha = 10^{\circ}$, by 6.0 per cent at $K = 0.20$ $\alpha = 10^{\circ}$, by 11.0 per cent at $K = 0$ $\alpha = 16^{\circ}$, and by 7.5 per cent at $K = 0.20$ $\alpha = 16^{\circ}$. No numerical comparison with the infinite fluid gravity theory of Parkin (8) is possible at the angles of attack of the present tests. However, upon inspecting his data at smaller angles of attack, $\alpha = 3^{\circ}$ and 5°, it is seen that gravity tends to decrease the magnitude of $C_{m_{LE}}$ from the infinite fluid theory by about two per cent, which is negligible.

The theories of Green (10), App. I or App. II, have not been extended to cover the moment coefficient. Therefore, we cannot compare the data to theory at or near the free surface.

Thus we find ourselves in a position similar to the one of the force coefficient. We have found that the moment coefficients

are smaller than the infinite fluid theory by 6.0 to 11.0 per cent and that the gravity effect is negligible for the case of an infinite fluid. The present data compare well with the only experiment available. No comparison to theory was made for the effect of the free surface or for the case of the hydrofoil at or near the free surface. Hence, the only discrepancy noted was between the infinite fluid theory and the experimental data. Some possible reasons for this difference have been proposed in normal force coefficient section and will not be further mentioned here.

Center of Pressure

The location and movement of the center of pressure will be discussed next. Fig. 39 shows the effect of angle of attack. It can be seen from this figure that for all submergences the center of pressure moves aft on the hydrofoil on the order of 5.0 per cent as the angle of attack is increased from 6° to 16°. To be specific, at S/c = 2.16, the center of pressure moves from the 31.5 per cent chord position at $\alpha = 6^{\circ}$ to the 36.0 per cent chord position at $\alpha = 16^{\circ}$. At S/c = -0.06, the center of pressure moves from the 32.5 per cent chord position at $\alpha = 8^{\circ}$ to the 37.0 per cent chord position at $\alpha = 16^{\circ}$. Cavitation number was not taken out of the experimental data. It should be remembered that the data at the lower three submergences are between K = 0 and K = 0.20 and at the upper three are essentially zero. We see from the figures that the experimental points lie between the K = 0 and K = 0.20 "boundaries" from the infinite fluid theory of Wu (3). (When center-of-pressure location was plotted versus cavitation number there

was little, if any, dependence.) Hence the comparison to the theory is good. However, upon comparison to the experiment of Parkin (1) it is found that there is some difference. In his experiment at $K = 0.20$ $\alpha = 12^{\circ}$ the center of pressure was located at the 41 per cent chord position, while in the present experiment, Fig. 39, at $K = 0.20$, $\alpha = 12^{\circ}$, the center of pressure was located at the 35 per cent chord position.

We now look at the effect of the free surface on the center-of-pressure location, Fig. 40. We see that the location is essentially a constant for each angle of attack up to the free surface. Upon passing through the free surface, however, the center of pressure starts a sudden movement aft on the flat plate for all angles of attack. For a change up through the free surface of one-tenth of a chord length for $\alpha = 10^{\circ}$ through 16°, the center of pressure moves aft about one per cent of the chord. At $\alpha = 8^{\circ}$ this change in submergence shifts the center of pressure 6.0 per cent aft. This latter case approaches the gravity planing theory of Wu (unpublished) in which the center of pressure is located at about the 65 per cent chord position for $F = 3.5$. Thus the experimental trend is in the right direction. However, no quantitative statement of the gravity effect on the center-of-pressure location can be made since the true planing case is never reached experimentally nor is there a zero gravity planing theory for center-of-pressure location with which to compare.

Cavity Length

The original data of cavity-length to chord-length ratio, ℓ/c, are plotted in Figs. 41 through 43 at the submergence ratios of 2.16,

1.50, and 0.83. It can be seen that the effect at all angles of attack and submergences of increasing cavitation number is to decrease ℓ/c. The decrease is slower for $\alpha = 8^\circ$ than for the case of $\alpha = 16^\circ$. For instance, at $S/c = 2.16$ and $\alpha = 8^\circ$, the decrease is from $\ell/c = 4.5$ to $\ell/c = 2.5$ as K varies from 0.08 up to 0.14, while at the same submergence, and $\alpha = 16^\circ$, ℓ/c decreases from 7.0 to 5.5 for an increase in K from 0.137 to 0.14 only. Similar decreases in ℓ/c with K of a more gradual nature can be seen at the other two submergences. The effect of angle of attack can also be seen from Figs. 41 through 43. At $S/c = 0.83$, $K = 0.12$, ℓ/c decreases from 3.9 to 2.1 as α decreases from 16° to 8°. From the same figures, the effect of reducing the submergence at constant K is to decrease the length-ratio at all angles of attack. For instance at $K = 0.10$ $\alpha = 12^\circ$ the length-ratio decreases from 6.2 to 4.2 as S/c decreases from 2.16 to 0.83.

Few experimental data are available for comparison of length ratios. However, we can cite Silberman (2) again. The comparison of the additional length data mentioned earlier and that of Silberman at $\alpha = 8^\circ$ can be seen on Fig. 44. No fairing of curves through the experimental data of Ref. 2 was attempted, hence no accurate quantitative comparison is possible. However, it can be seen that in the present work at a given cavitation number, say $K = 0.10$, that the length ratio is less than Silberman by a factor of about two for the submergence ratio, 1.60. This difference could be due to the gravity effect since the Minnesota experiment was performed in a vertical, free-jet tunnel in which the gravity effect was absent. Parkin (8) in his infinite-fluid-gravity theory suggests

this. Fig. 44 shows the experimental results at $\alpha = 8^{\circ}$ as well as the theory of Parkin both for $F = 2.83$ and 3.68. As can be seen from this figure, which bears out the previous experimental data on length ratios, the Froude number dependence is practically negligible. It can also be seen that the experimental length ratios for a given cavitation number and Froude number are smaller than the theoretical lengths by a factor of about 2. For a comparison of experimental cavity lengths to the exact and linear theories of Wu (3), (5) we again look at Fig. 44 on which are plotted these theories also. We can see that at $K = 0.10$, $S/c = 1.60$ $\alpha = 8^{\circ}$ the exact theory is higher than the experimental points by a factor of 1.2. The linear theory predicts even longer cavity lengths than the exact theory and hence is farther from the experiment.

Thus we find that the experimental cavity lengths decrease with decreasing submergence, with decreasing angle of attack, and with increasing cavitation number as would be expected. The experimental data do not agree well with the only other experiment available nor do they agree well with the linearized theory of Wu (5) or the infinite-fluid-gravity theory of Parkin (8). The agreement is good with the exact infinite-fluid theory of Wu (3). The effects of gravity on cavity lengths at $S/c = 1.60$ and in velocity range of this experiment were found to be negligible.

The discrepancy between the experiments cannot be accounted for. The discrepancy between the present experiment and the theories can be attributed to the possible influence of the sidewalls, bottom and the free surface. However the "dissipation" model used by Wu in his exact theory gives values closest to the

experimental results.

Air-Volume Flow-Rate

The air-volume flow-rate coefficient data are plotted on Figs. 45 and 46 at S/c = 2.16 and S/c = 0.83. The difficulty of measurement of the air-flow plus the little-understood phenomenon of air entrainment make the data somewhat scattered and not too reproducible. However, Fig. 45 and Fig. 46 do show the order of magnitude of the air flow at two submergences. For S/c = 2.16, C_Q lies in the range, generally, from 0.70 to 1.20 for K between 0.11 and 0.15. At S/c = 0.83 C_Q lies in the range from 0.55 to 0.80 for K between 0.06 to 0.15. No experiments of air-flow rate measurements behind two-dimensional bodies are known. However, one three-dimensional experiment and theory of Cox and Clayden (16) and another three-dimensional experiment of Swanson and O'Neill (14) are available. The data of these two experiments which correlate the theory are plotted on Figs. 45 and 46. It is seen that these curves form "boundaries" for various values of Froude number. The results of this experiment lie in the Froude number range that is higher than that of the present tests. It can be seen from the figures that as the submergence is decreased at constant angle of attack and cavitation number that the air flow also is decreased. The curves of Cox and Clayden and Swanson and O'Neill show a radical decrease in air-flow for a small increase in K. The results of this experiment do not show this behavior. However, the results of the air-flow measurements on the disk were obtained when the downstream end of the cavity

consisted of twin vortices and the sharp reduction in air-flow noted in their experiments occurred when the vortices disappeared and a reentrant cavity formed, whereas in the present experiment the majority of the data were taken with a reentrant type of cavity closure (see Figs. 7 through 11). Entirely different mechanisms govern the entrainment rate of the twin vortex and reentrant jet. This explains the difference between the disk experiments and the present experiment with regard to the radical change of air-flow with cavitation number.

Pressure Distributions

Some representative plots of typical pressure distributions on a fully cavitating flat plate have been referred to before and are presented in Figs. 12 through 17. They are shown in this report solely for the possible interest they might hold for the reader. Their primary use was in the determination of the normal force coefficient. It would be of great interest to compare these distributions to the distributions calculated from Wu's theory. However, time did not permit such a comparison. Cumberbatch in his planing theory does show some pressure distributions for various Froude numbers. One of these for a Froude number of about 3.2 is shown in Fig. 17b for comparison.

V. SUMMARY

In the preceding sections the effects on a two-dimensional cavitating flat plate due to varying the submergence below a free surface and due to varying the angle of attack, cavitation number and Froude number have been shown. The effects on the force and moment coefficient, center of pressure location and cavity length due to changes in angle of attack and cavitation number at submergences greater than seven-tenths of a chord length are generally what are predicted by the gravity free infinite fluid theory of Wu (3). The airflow rates are of the same order of magnitude as previous three-dimensional experiments have found. No particular dependence of any of the results on Froude number at these submergences was found.

The effect of the free surface was first noted at a submergence of about seven-tenths of a chord length. The effect was to increase the force and moment coefficient, to decrease the cavity lengths and airflow rates. No effect on the center of pressure location due to the free surface was observed until planing was approached at which time the center of pressure started a movement aft. The increase in the magnitude of the force and moment coefficient at the free surface over the magnitude at submergences greater than seven-tenths of a chord was about 30 per cent. The gravity free infinite fluid theories, both linear of App. I and the exact of Green (10), predict an increase in the force due to the free surface. Green predicts 28 per cent and App. I 14 per cent more than is shown by the experiment. The force data appear to approach the Froude number asymptote predicted by the gravity planing theory of Cumberbatch (12) and Wu. However,

the Froude number dependence predicted by this theory at the free surface was not confirmed. The linearized theory for the bottom effects, App. II, at and near the free surface indicates these effects are negligible.

It has been seen that the effect of the free surface and the effect of gravity, individually, do not account accurately for the experimental results. But it is felt that a combination of the two probably gives a more realistic picture of what is actually occurring. However, it remains for further experimental and theoretical work to be done in order that the points in question can be resolved.

Addendum

After completion of this report it was learned from the author of Ref. 8 that an error had been made in that linearized theoretical development. The correction of this error showed no significant change in the cavity length; however it did show that the effect of gravity on the force coefficient in an infinite fluid was to decrease its value by about ten per cent. This brings the theory closer to the experiment at the deeper submergences and strengthens the conclusions of this report with respect to the influence of gravity.

REFERENCES

1. Parkin, Blaine R., "Experiments on Circular Arc and Flat Plate Hydrofoils in Noncavitating and Full Cavity Flows", California Institute of Technology, Hydrodynamics Laboratory Report No. 47-6, February 1956, 45 pages.

2. Silberman, Edward, "Experimental Studies of Supercavitating Flow about Simple Two-Dimensional Bodies in a Jet", St. Anthony Falls Hydraulic Laboratory, University of Minnesota, Project Report No. 59, April 1958, 45 pages.

3. Wu, T. Y., "A Free Streamline Theory for Two-Dimensional, Fully Cavitated Hydrofoils", California Institute of Technology, Hydrodynamics Laboratory Report No. 21-17, July 1955, 36 pages.

4. Tulin, M. P., "Supercavitating Flow Past Foils and Struts", Symposium on Cavitation in Hydrodynamics, National Physical Laboratory, Teddington, England, Paper No. 16, September 1955.

5. Wu, T. Y., "A Note on the Linear and Nonlinear Theories for Fully Cavitated Hydrofoils", California Institute of Technology, Hydrodynamics Laboratory Report No. 22-22, August 1956, 24 pages.

6. Birkhoff, C., Plesset, M., and Simmons, N., "Wall Effects in Cavity Flow", Parts I and II, Quarterly of Applied Mathematics, Vol. VIII, No. 2, July 1950.

7. Cohen, Hirsch, and Tu, Yih-o, "Wall Effects on Supercavitating Flow Past Foils", Rensselaer Polytechnic Institute, RPI Math Rep. No. 6, October 1956, 13 pages.

REFERENCES (Cont'd)

8. Parkin, Blaine R., "A Note on the Cavity Flow Past a Hydrofoil in a Liquid with Gravity", California Institute of Technology, Engineering Division Report No. 47-9, December 1957, 36 pages.

9. Johnson, Virgil E., Jr., "The Influence of Depth of Submersion, Aspect Ratio and Thickness on Supercavitating Hydrofoils Operating at Zero Cavitation Number", Second Symposium on Naval Hydrodynamics, Washington, D.C., August 1958, 50 pages.

10. Green, A. E., "Note on the Gliding of a Plate on the Surface of a Stream", Proceedings of Cambridge Philosophical Society, Vol. 32, 1936, pages 248-252.

11. Green, A. E., "The Gliding of a Plate on a Stream of Finite Depth", Proceedings of Cambridge Philosophical Society, Part I, Vol. 31, 1935, pp. 584-603, Part II, Vol. 32, 1936, pp. 67-85.

12. Cumberbatch, E., "Two Dimensional Planing at High Froude Number", Journal of Fluid Mechanics, Vol. 4, Part 5, September 1958, pp. 466-478.

13. Knapp, R. T., Levy, J., O'Neill, J. P., and Brown, F. P., "The Hydrodynamics Laboratory at the California Institute of Technology", Transactions, A.S.M.E., Vol. 70, No. 5, July 1948, pp. 437-457.

REFERENCES (Cont'd)

14. Swanson, W. M. and O'Neill, J. P., "The Stability of an Air-maintained Cavity Behind a Stationary Object in Flowing Water", California Institute of Technology, Hydrodynamics Laboratory Memorandum Report No. M-24.3, September 1951, 10 pages.

15. Mendelsohn, R. A. and Polhamus, J. F., "Effect of the Tunnel-Wall Boundary Layer on Test Results of a Wing Protruding from a Tunnel Wall", NACA TN No. 1244, April 1947, 9 pages.

16. Cox, R. N. and Clayden, W. A., "Air Entrainment at the Rear of a Steady Cavity", Symposium on Cavitation in Hydrodynamics, National Physical Laboratory, Teddington, England, Paper No. 12, September 1955, 19 pages.

APPENDIX I

LINEARIZED FLOW PAST A FULLY CAVITATING FLAT PLATE NEAR A FREE SURFACE

Notation

c	Chord length (normalized to unity)
S	Depth below free surface
t	Auxiliary mapping plane
u	Perturbation velocity in x-direction
U	Free stream velocity (normalized to unity)
v	Perturbation velocity in y-direction
$V = u - iv$	Complex velocity function
w	Auxiliary mapping plane
$z = x + iy$	Physical plane

The linearized free streamline theory allows the problem to be treated easily by conformal mapping. The boundary conditions are shown in the physical or z-plane, Fig. I-1, where u and v, the perturbation velocities, are much smaller than the free stream velocity, U. The pressure on the cavity is assumed to be the same as on the free surface and the pressure condition is that u = 0.

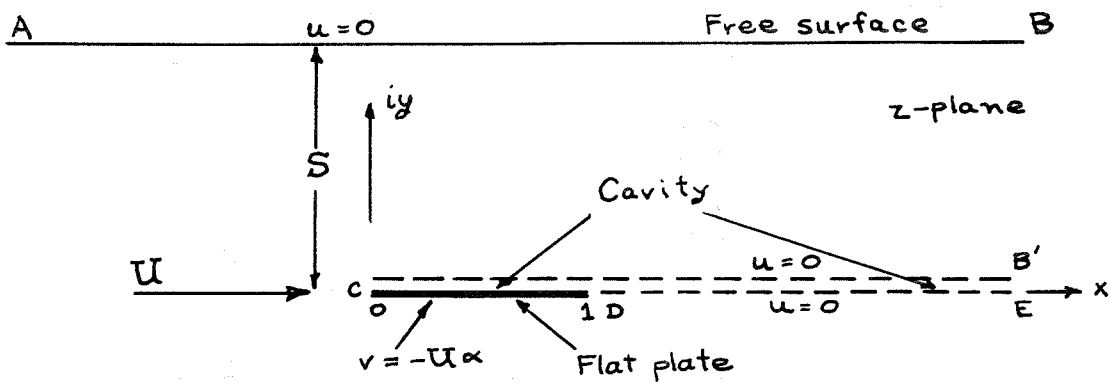

Fig. I-1

In order to map the physical plane into the upper half t-plane through the w-plane, the following mapping functions were obtained by the use of the Schwatz-Christoffel Theorem:

$$z = A\left[(\lambda-1)\ \ln\ (w-\lambda) + w\right] + B \tag{1}$$

$$w = \tfrac{1}{2}\left(t + \tfrac{1}{t}\right). \tag{2}$$

Evaluation of the constants gives

$$A = -\frac{S}{\pi}(\lambda-1) \tag{3}$$

$$B = \frac{S}{\pi(\lambda-1)}\left[(\lambda-1)\ \ln|\lambda-1| + 1\right] + iS \tag{4}$$

$$\frac{\pi}{S} = \frac{2}{\lambda-1} - \ln\left|\frac{\lambda+1}{\lambda-1}\right|. \tag{5}$$

The t-plane and boundary conditions then are shown in Fig. I-2.

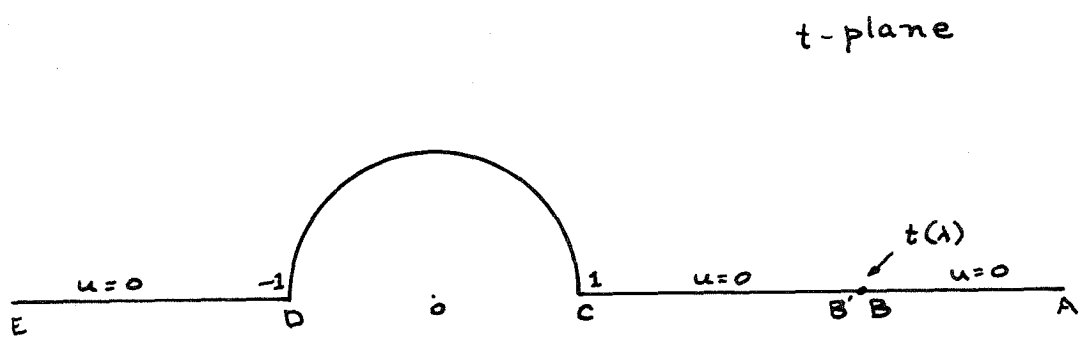

Fig. I-2

It can be seen that as $t \to \infty$, $z \to \infty$ and that $V = u - iv \to 0$ (i.e., no perturbations at ∞). The only permissible function satisfying these conditions (V is the same at corresponding points in the z, w and t-planes) is

$$V(t) = u - iv = -\frac{2i\alpha}{t-1} \tag{6}$$

since a leading edge but not a trailing edge singularity is permissible.

Now we look at the lift on the plate, which is

$$L = \int_0^1 (P - P_a)\, dx$$

and the lift coefficient is

$$C_L = \frac{L}{\rho U^2 c/2} = \int_0^1 C_p\, dx = \int_0^1 C_p\, dz$$

since dy = 0 on the plate. From linearized theory it can be shown that $C_p = -2u$ so that the lift coefficient becomes

$$C_L = -2\, \mathrm{Re} \int_0^1 \bar{V}(z)\, dz$$

or

$$C_L = -2\, \mathrm{Re} \int_C^D V(z)\, dz \tag{7}$$

where Re denotes the real part of the complex function.

It is obvious that the velocity function in the z-plane, V(z), is now needed, but it is given only by the complicated relationships of equation 1, 2 and 6. However, V(z) is regular in the entire z-plane except as $z \to 0$ where t - 1 behaves like $z^{1/4}$. Thus $V(z) \propto \frac{1}{t^{1/4}}$ and hence is integrable there.

Now consider the line integral

$$J = \int_{-R, B, B', C, D, R''} V(z)\, dz + \int_{\Gamma} V(z)\, dz$$

where Γ is the semicircular contour of large radius, R, in the lower half plane as shown in Fig. I-3

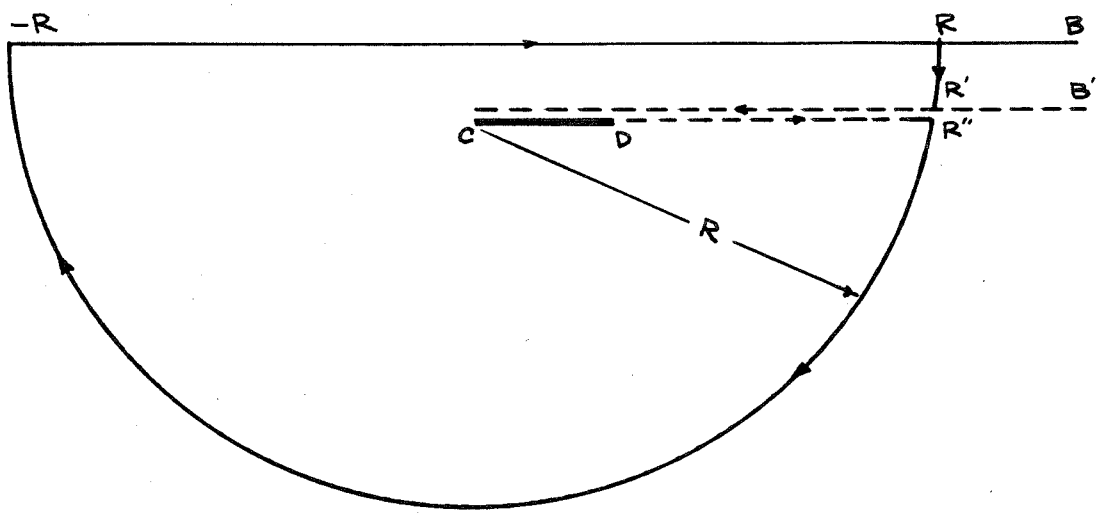

Fig. I-3

Since V(z) has no poles inside the contour, -R, R, R', C, D, R'', -R; J = 0.

But

$$Rl\, J = Rl_{-R}\int_{R} + Rl_{R}\int_{R'} + Rl_{R'}\int_{C} + Rl_{C}\int_{D} + Rl_{D}\int_{R''} + Rl_{\Gamma}\int = 0. \qquad (8)$$

By inspection of the above integrals and the boundary conditions, it can be seen that

$$Rl_{-R}\int_{R} = Rl_{R'}\int_{C} = Rl_{D}\int_{R''} = 0 .$$

Thus

$$-Rl_{C}\int_{D} = Rl_{R}\int_{R'} + Rl_{\Gamma}\int .$$

Also from equation 7

$$\tfrac{1}{2} C_L = -R\ell \int_{C_D} \bar{V}(z)\, dz$$

therefore

$$\tfrac{1}{2} C_L = R\ell \int_{R'R} \bar{V}(z)\, dz + R\ell \int_{\Gamma} \bar{V}(z)\, dz .$$

Since the contour can be distorted so that $R \to \infty$, it can be shown that as $z \to \infty$, $t \to \infty$ and

$$V(t) \longrightarrow -\frac{2i\alpha}{t} , \tag{9}$$

and from equations 1 and 2 it is seen that

$$z \longrightarrow \frac{At}{2} \tag{10}$$

So, by combining equations 9 and 10 it is seen that

$$\bar{V}(z) \longrightarrow \frac{iA\alpha}{z} .$$

Let $z = Re^{i\theta}$ so that

$$R\ell \int_{\Gamma} = -i\alpha A \int_{0}^{-\pi} \frac{iRe^{i\theta}}{Re^{i\theta}}\, d\theta = -\alpha A \pi . \tag{11}$$

Along the segment RR', as $R \to \infty$, $w = \lambda$ and from equation 2 it is seen that $2\lambda = t + 1/t$ or $t = \lambda + \sqrt{\lambda^2 - 1}$ and from equation 6

$$u - iv = \frac{-2i\alpha}{\lambda - 1 + \sqrt{\lambda^2 - 1}} . \tag{12}$$

It is obvious that $u = 0$ so that

$$R\ell \int_{BB'} \bar{V}(z)\, dz = -iv_B \int_{S}^{0} i\, dy = -v_B S .$$

Using equation 12 it is seen that

$$R\ell_{B}\int_{B'} = \frac{2\alpha S}{\lambda - 1 + \sqrt{\lambda^2 - 1}} \tag{13}$$

Therefore, gathering up terms for the lift coefficient from equation 11 and equation 13, it is seen that

$$C_L = -2A\alpha\pi - \frac{4\alpha S}{\lambda - 1 + \sqrt{\lambda^2 - 1}}$$

or that

$$C_L = \frac{2\alpha S}{\lambda - 1}\left[1 - \frac{2}{1 + \sqrt{\frac{\lambda + 1}{\lambda - 1}}}\right] . \tag{14}$$

The parameter, λ, is a function of the depth below the surface and can be found from equation 5. From equation 5 as $S \to \infty$ it is seen that

$$\lambda^2 \longrightarrow \frac{2S}{\pi} .$$

Substituting this in equation 14 the lift coefficient becomes

$$C_L \doteq \frac{\pi\alpha}{2}\left(1 + \sqrt{\frac{\pi}{2S}}\right) . \tag{15}$$

Of more interest is the ratio C_L/C_{L_∞} which can be obtained from equations 14 and 15 and is

$$\frac{C_L}{C_{L_\infty}} = \frac{4S}{\pi(\lambda - 1)}\left[1 - \frac{2}{1 + \sqrt{\frac{\lambda + 1}{\lambda - 1}}}\right] . \tag{16}$$

Values of S and λ found from equation 5 can be substituted into equation 16 to obtain the curve shown in Fig. 26 of the report.

APPENDIX II

A SIMPLE ESTIMATE OF THE BOTTOM EFFECT ON A PLANING SURFACE AT INFINITESIMAL ANGLES OF ATTACK

The effect that is developed here is the influence on the lift coefficient due to the proximity of a solid lower boundary to a hydrofoil near a free surface. This effect is calculated by the simplified solution shown below.

For a planing surface when the angles of attack approaches zero ($\alpha \rightarrow 0$) the lift coefficient approaches $\pi\alpha$. This can be interpreted $L = \rho U \Gamma/2$ where ρ is the density of the fluid and U is the free stream velocity. To calculate the circulation, Γ, the Weissinger two-point method will be used. A vortex of strength Γ is placed at the one-quarter chord point, the center of pressure of a flat plate airfoil, and the value of Γ is adjusted so that the boundary condition is satisfied at the three-quarter chord point. If v is the perturbation velocity perpendicular to the plate then at the three-quarter chord point the boundary condition is $v/U = dy/dx = -\alpha$ or $v = -\alpha U$. The flow is sketched in Fig. II-1.

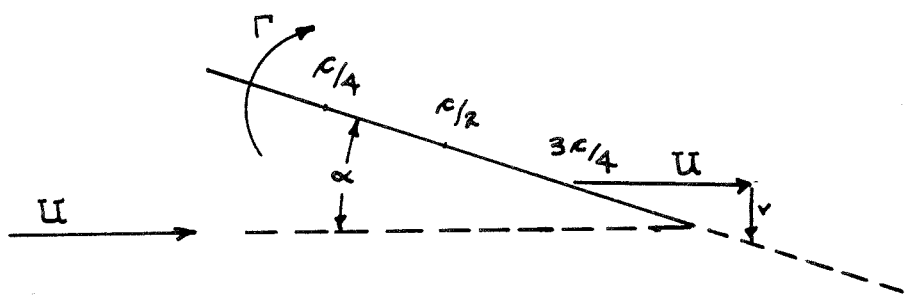

Fig. II-1

The velocity at a distance $c/2$ from a vortex of strength Γ is $v = -\Gamma/2\pi c/2$ so that $\Gamma = -v\pi c = dU\pi c$. The lift is then

$$L = \tfrac{1}{2}\rho U \pi \alpha U c$$

and the lift coefficient is

$$C_L = \frac{L}{\rho U^2 c/2} = \pi\alpha$$

Now a planing surface as the limit of a cavitating flat plate hydrofoil near a free surface is considered, Fig. II-2.

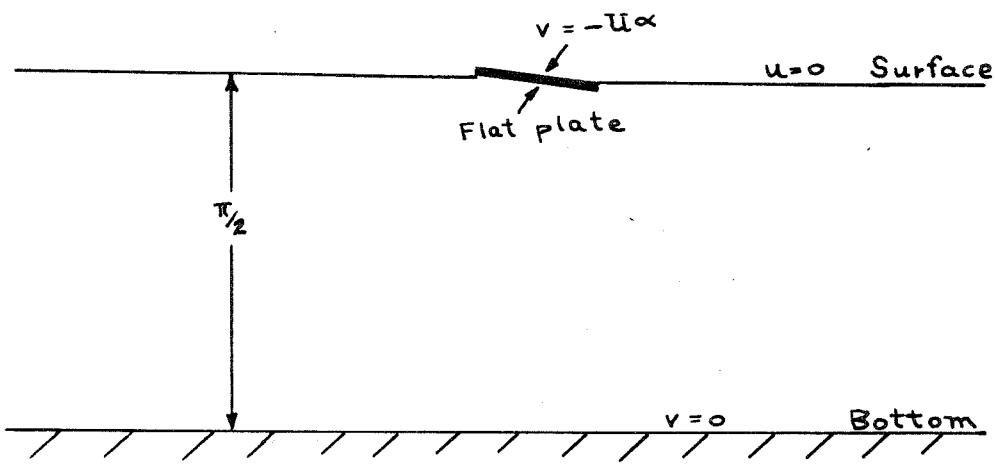

Fig. II-2

The flat plate can be replaced by a vortex at the one-quarter chord point but in order to satisfy the boundary conditions shown in Fig. II-2, the sequence of alternating vortices of equal strength, as shown in Fig. II-3, will be necessary.

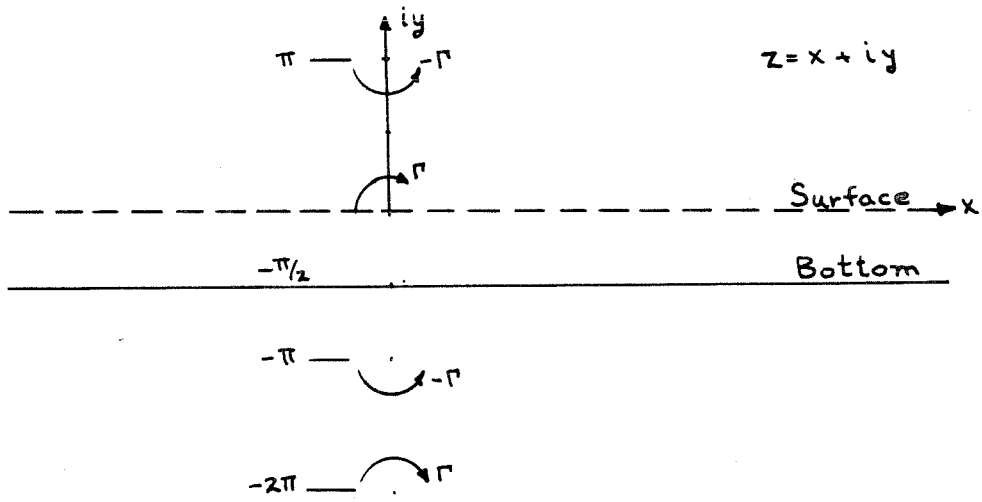

Fig. II-3

On the lines of symmetry $z = 0 \pm n\pi i$ there are no horizontal velocities, u, due to the vortices. Similarly on the lines of symmetry, $z = -\frac{\pi}{2} \pm n\pi i$ there are no vertical velocities, v, due to the vortices.

The potential due to a single vortex is

$$G(z) = \phi + i\psi = \frac{i\Gamma}{2\pi} \ln z$$

and for the sequence in Fig. II-3 the total potential due to all vortices is

$$F(z) = \frac{i\Gamma}{2\pi} \sum_{-\infty}^{+\infty} (-1)^n \ln (z - n\pi) .$$

This series has a sum*

$$F(z) = \frac{i\Gamma}{2\pi} \ln \tanh \frac{z}{2}$$

so that

$$u - iv = \frac{dF}{dz} = \frac{i\Gamma}{2\pi} \operatorname{cosech} z .$$

---

*Copson, E.T., Theory of Functions of a Complex Variable

At $z = c/2$,

$$v = -\frac{\Gamma}{2\pi} \operatorname{cosech} \frac{c}{2} = -U\alpha,$$

hence,

$$\Gamma = 2\pi U \alpha \sinh \frac{c}{2}$$

and

$$L = \pi \rho U^2 \alpha \sinh \frac{c}{2}$$

Finally the lift ceofficient is obtained,

$$C_L = \frac{L}{\rho U^2 c/2} = \frac{2\pi\alpha}{c} \sinh \frac{c}{2}.$$

However, the dimension of interest is the distance to the solid boundary, h. Let the ratio of the chord to this distance, h, be $\sigma = c/h = c/\pi/2$ or $c = 2\sigma/\pi$. Therefore,

$$C_L = \frac{4\alpha}{\sigma} \sinh \frac{\pi\sigma}{4}$$

is the lift coefficient of a planing flat plate hydrofoil at zero submergence with a solid lower boundary and no gravity.

When $\sigma \rightarrow 0$ (i.e., lower boundary infinitely far away) the hyperbolic sine can be expanded

$$\sinh x \longrightarrow x + \frac{1}{6}x^3 + ----$$

so that

$$C_L \doteq \frac{4\alpha}{\sigma}\left[\frac{\pi\sigma}{4} + \frac{1}{6}\left(\frac{\pi\sigma}{4}\right)^3 + ----\right]$$

or

$$C_L \doteq \pi\alpha\left[1 + 0.103\,\sigma^2 + ----\right]$$

Therefore, it can be seen that the presence of a lower boundary always increases the lift. The effect is fairly small even for $\sigma = 1$

in which case there is a ten per cent increase in lift. In the case of this experiment near the surface, $\sigma \doteq 0.2$ so that

$$\frac{C_L}{C_{L_\infty}} \doteq 1.004$$

which is not significant.

At the deepest submergences of this experiment (which is no longer planing and this theory does not hold in the true sense) $\sigma \doteq 0.4$ and therefore

$$\frac{C_L}{C_{L_\infty}} \doteq 1.016$$

or a one and one-half per cent increase, which is not significant.

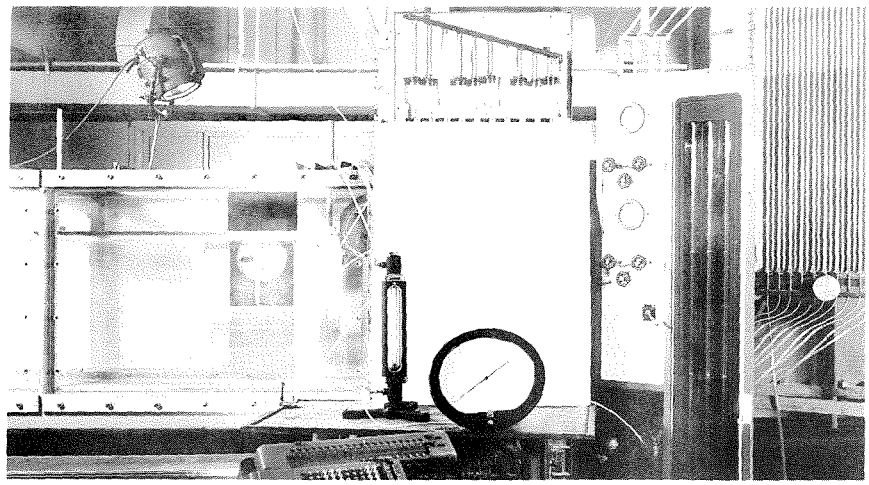

Fig. 1a The general arrangement of the experimental apparatus showing the two-dimensional test section installed in the working section of the free surface water tunnel. The hydrofoil also can be seen in a position corresponding to S/c = - 0.06.

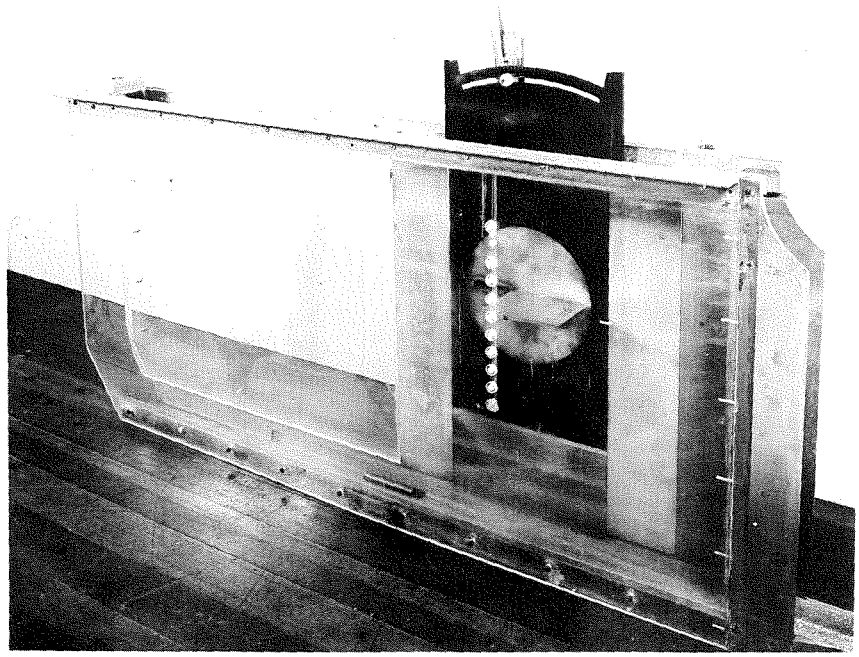

Fig. 1b A view of the two-dimensional test section showing the leading edges and general construction. The mounting plate and hydrofoil can also be seen installed.

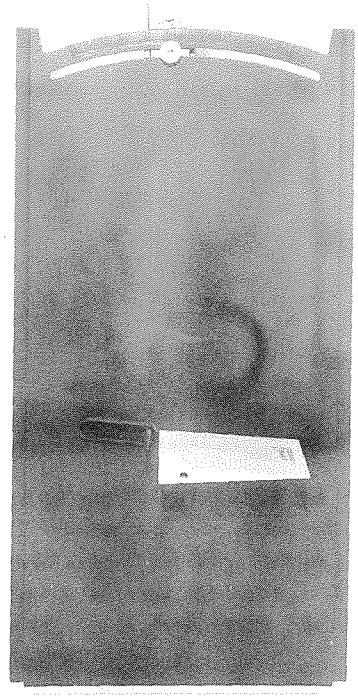

Fig. 2a The mounting plate and the hydrofoil showing the cavity pressure probe and the opening for forcing air into the cavity. The circular plate and arc for varying the angle of attack also can be seen.

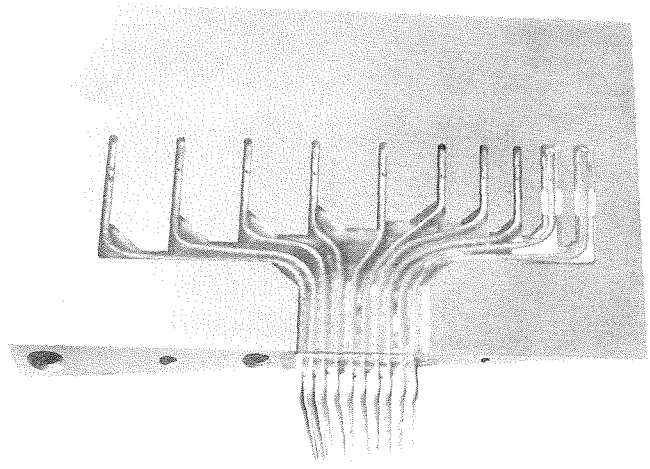

Fig. 2b A view of the wedge hydrofoil showing the wetted surface, piezometer orifices, and general construction.

A	B	C	D	E	F
.500"	.500"	.497"	.506"	.433"	.314"
G	H	I	J		
.253"	.245"	.239"	.413"		

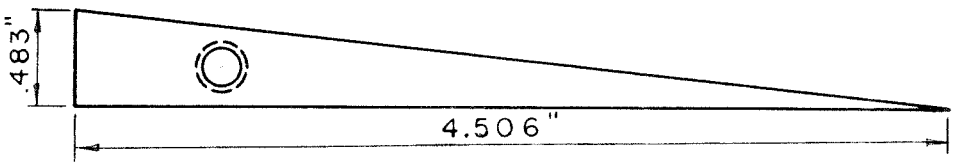

NOTE: PRESSURE TAP POSITIONS
NOT TO SCALE

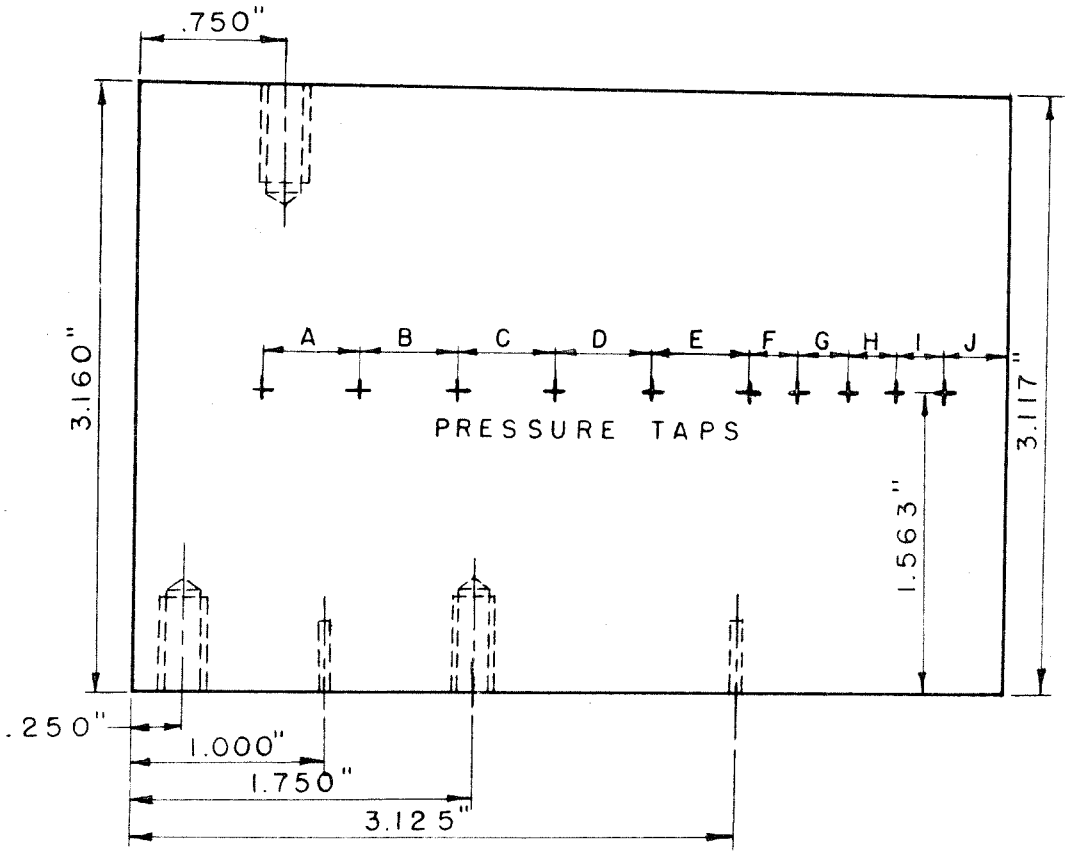

Fig. 3. A side and bottom view of the wedge hydrofoil tested showing additional details of the construction and the location of the piezometer orifices.

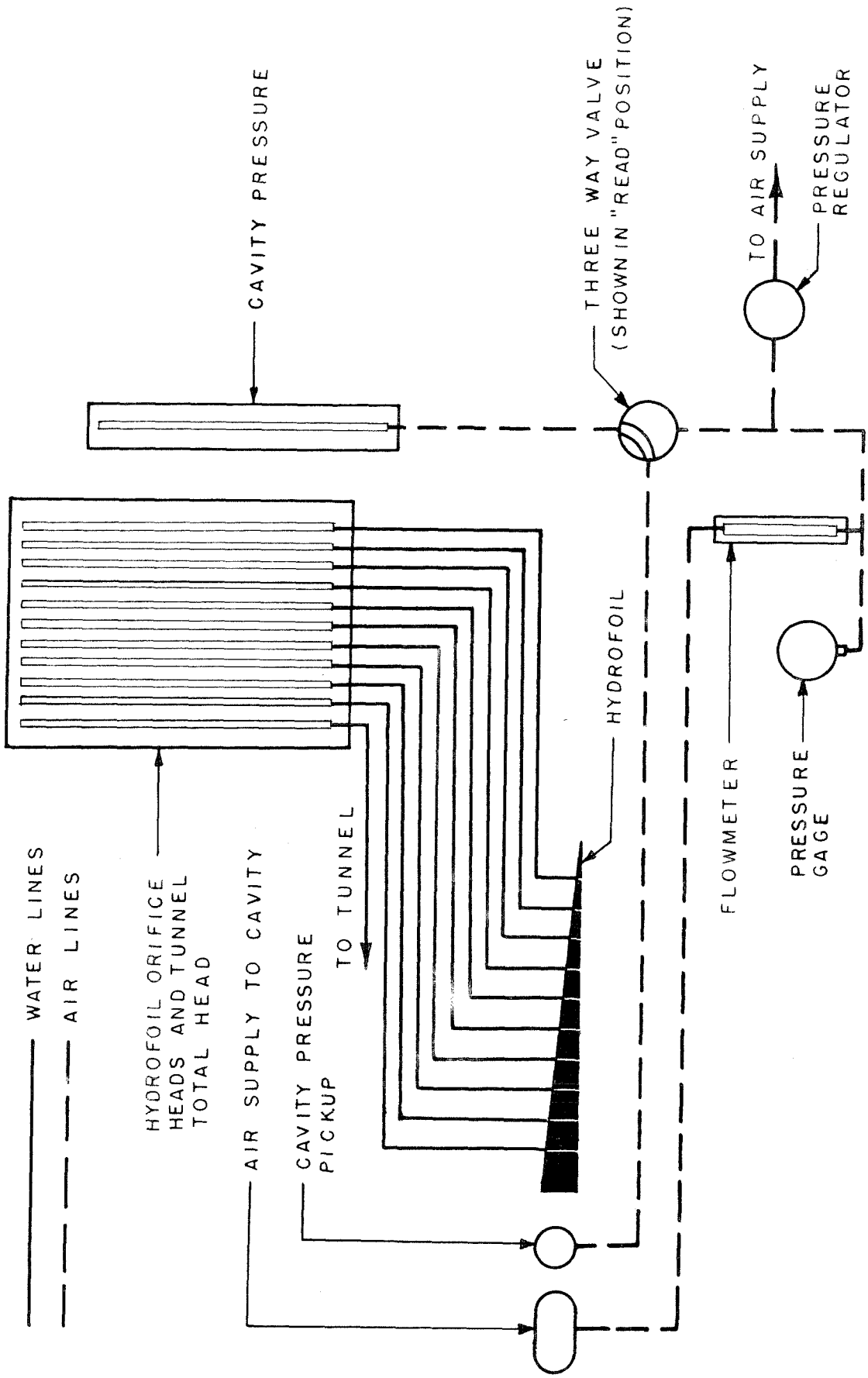

Fig. 4. A schematic diagram of the set-up of the experimental apparatus.

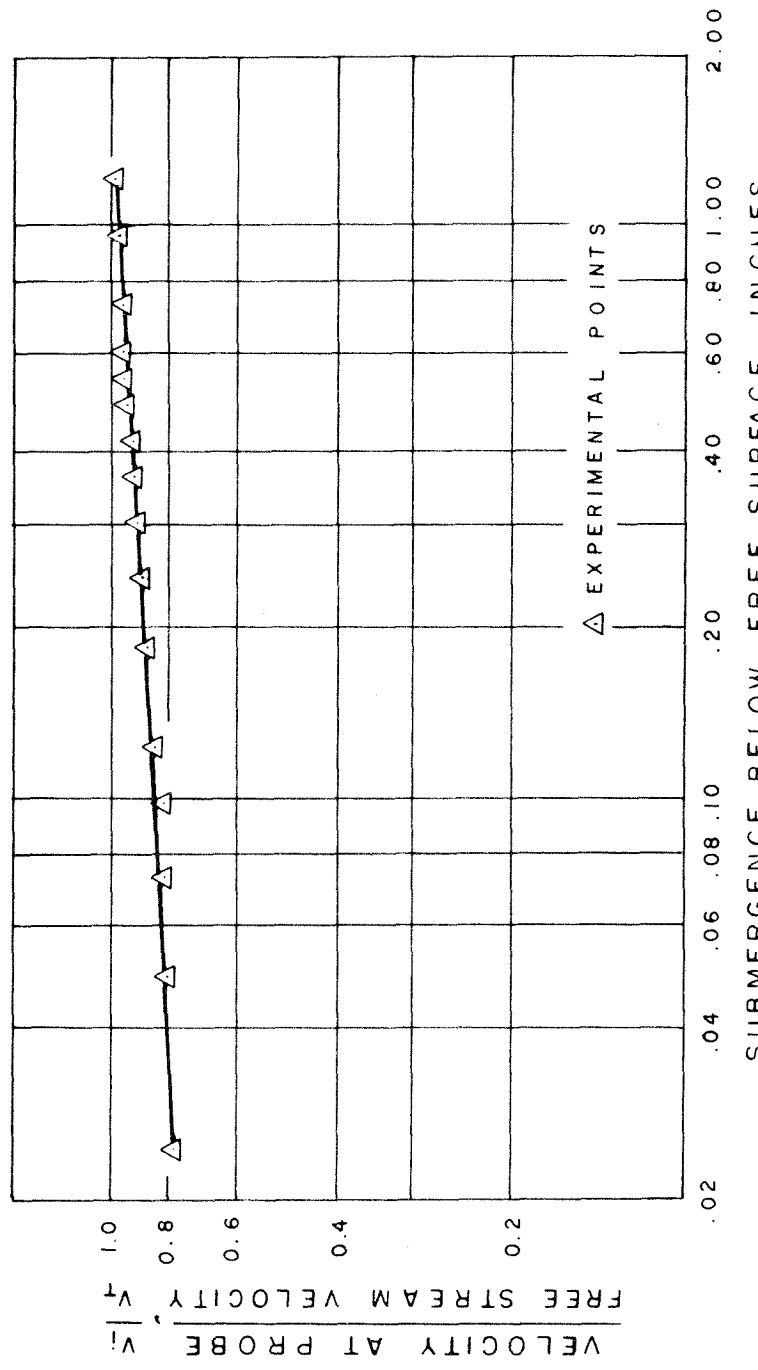

Fig. 5. A plot of the velocity profile near the free surface and on the center line of the two-dimensional test section. (Skimmer not operating.)

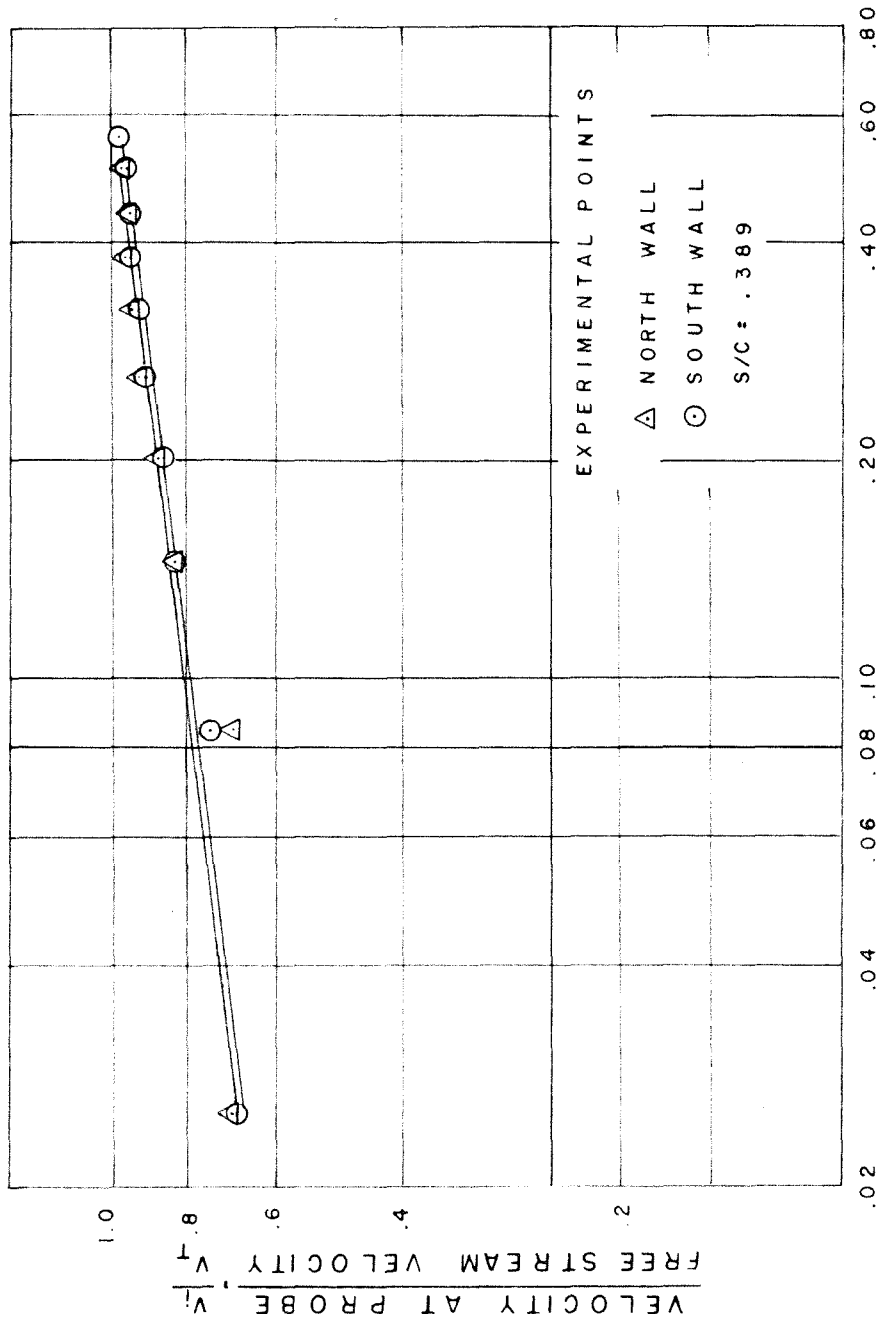

Fig. 6. A plot of the velocity profiles on the walls of the two-dimensional test section at the position of the leading edge of the hydrofoil.

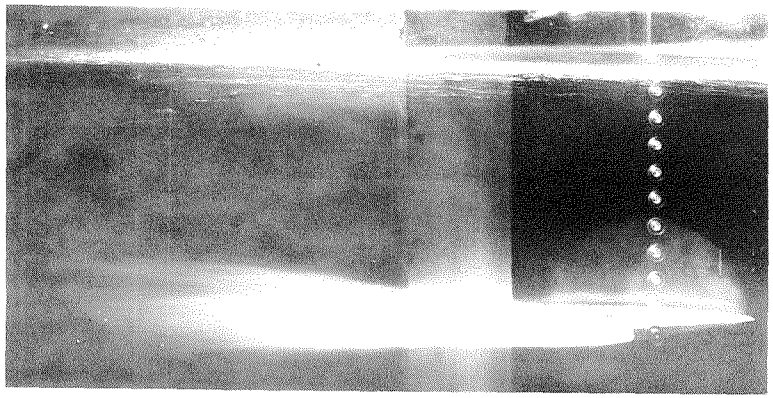

(a) S/c = 2.16, $\alpha = 10^{o}$, K = 0.182, ℓ/c = 2.53

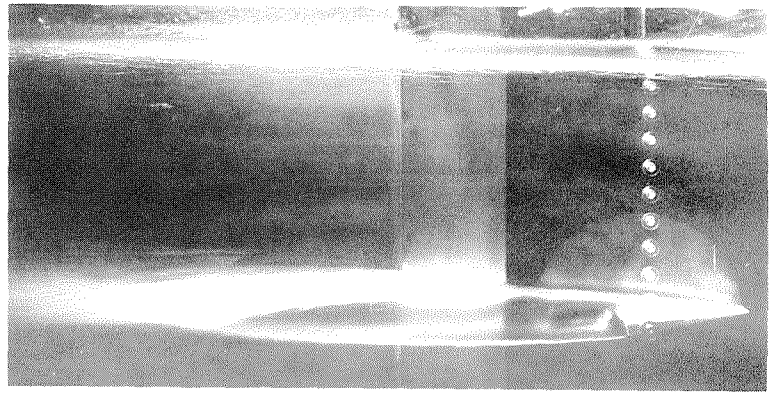

(b) S/c = 2.16, $\alpha = 12^{o}$, K = 0.132, ℓ/c = 4.18

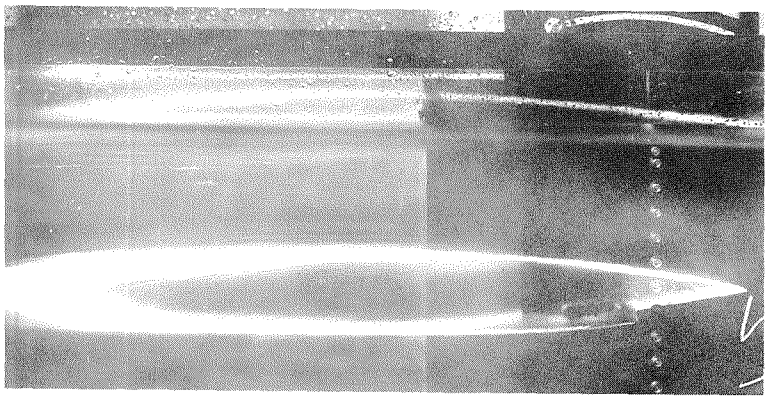

(c) S/c = 1.50, $\alpha = 16^{o}$, K = 0.109, ℓ/c = 6.92

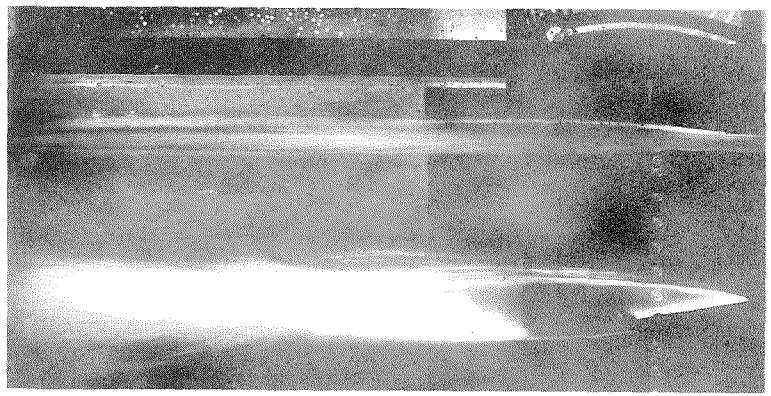

(d) S/c = 1.50, $\alpha = 16^{o}$, K = 0.144, ℓ/c = 3.60

Fig. 7 Photos of typical cavities under varying conditions which show the bowing of the free surface.

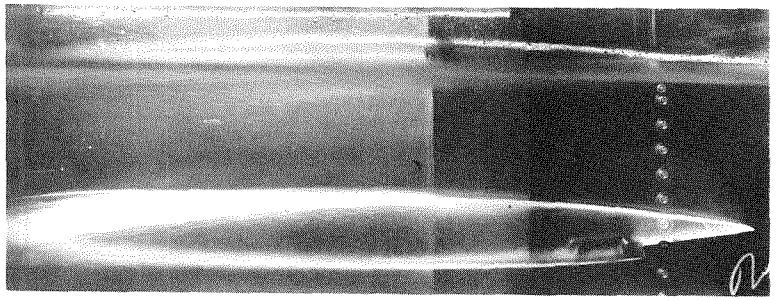

(a) S/c = 1.50, $\alpha = 14^{o}$, K = 0.099, $\ell/c = 6.58$

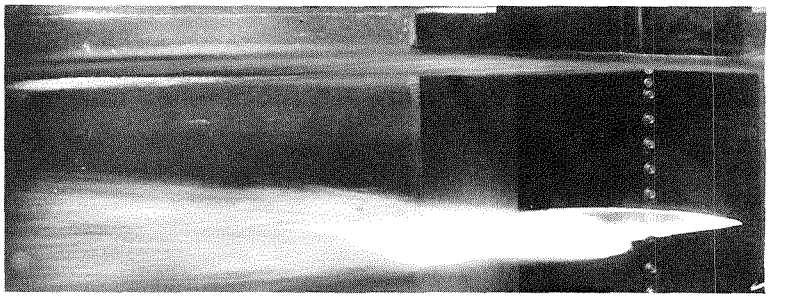

(b) S/c = 1.50, $\alpha = 14^{o}$, K = 0.190, $\ell/c = 2.80$

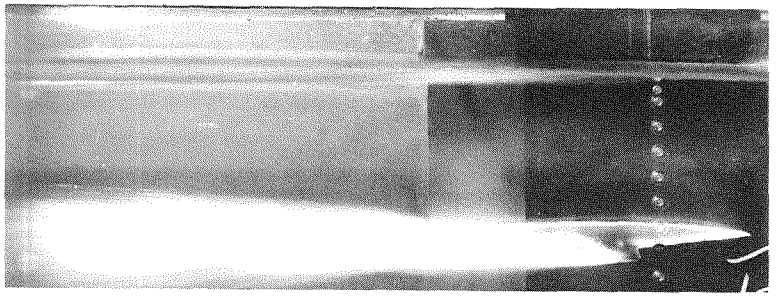

(c) S/c = 1.50, $\alpha = 12^{o}$, K = 0.169, $\ell/c = 2.80$

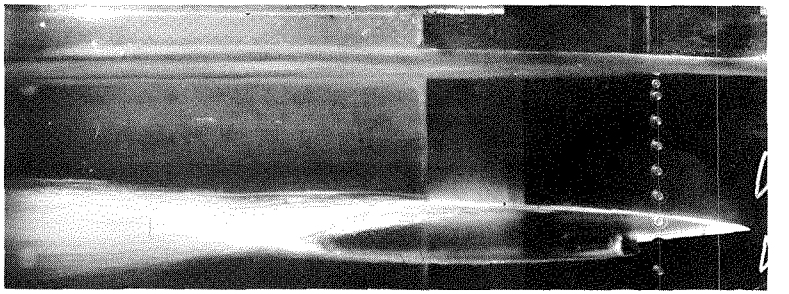

(d) S/c = 1.50, $\alpha = 12^{o}$, K = 0.109, $\ell/c = 4.26$

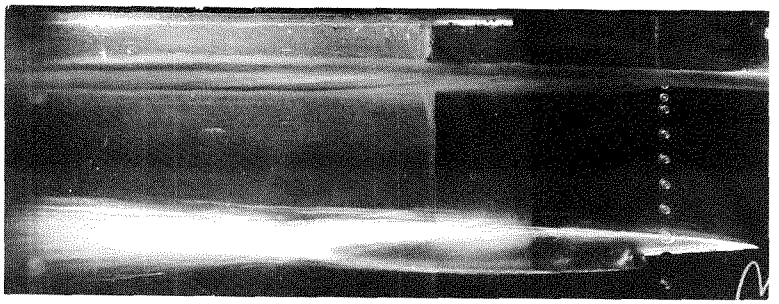

(e) S/c = 1.50, $\alpha = 10^{o}$, K = 0.101, $\ell/c = 3.86$

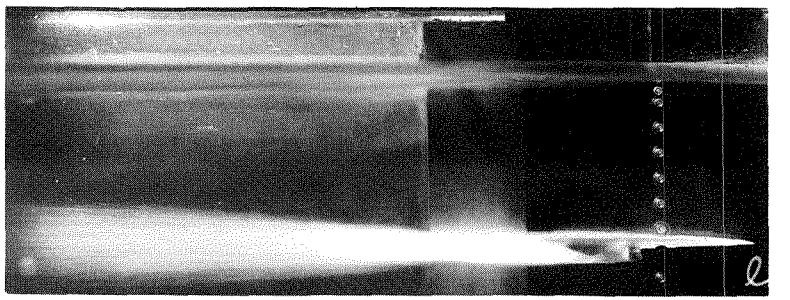

(f) S/c = 1.50, $\alpha = 8^{o}$, K = 0.115, $\ell/c = 2.53$

Fig. 8 Photos of typical cavities under varying conditions which show the bowing of the free surface.

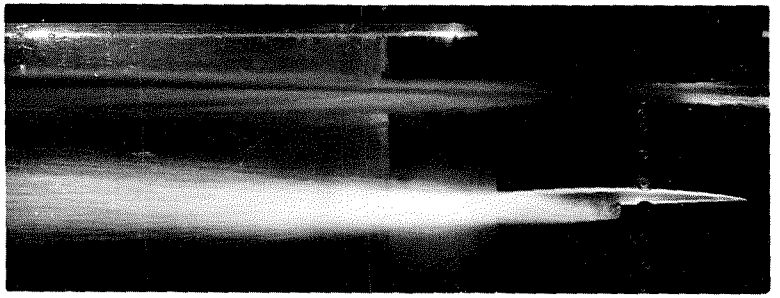

(a) S/c = 0.83, $\alpha = 8^{o}$, K = 0.128, $\ell/c = 1.86$

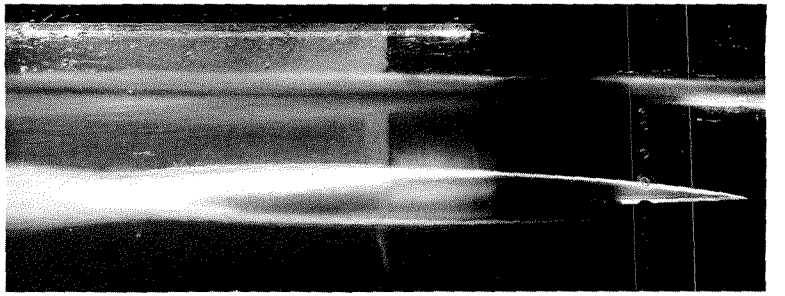

(b) S/c = 0.83, $\alpha = 8^{o}$, K = 0.058, $\ell/c = 4.93$

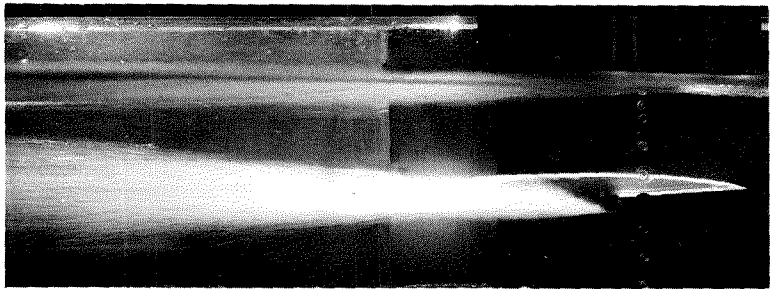

(c) S/c = 0.83, $\alpha = 10^{o}$, K = 0.146, $\ell/c = 2.13$

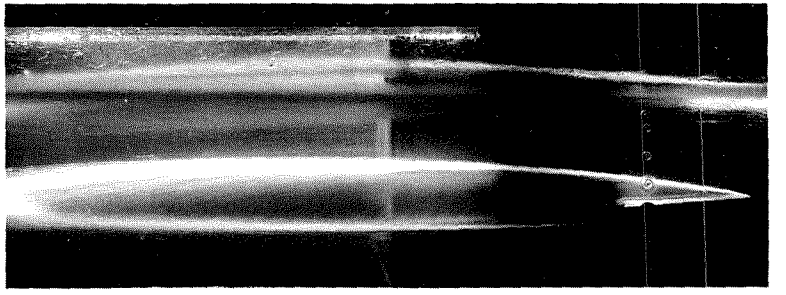

(d) S/c = 0.83, $\alpha = 10^{o}$, K = 0.061, $\ell/c = 6.26$

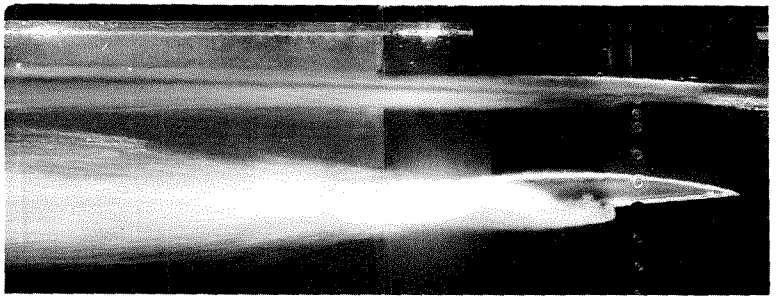

(e) S/c = 0.83, $\alpha = 12^{o}$, K = 0.145, $\ell/c = 2.53$

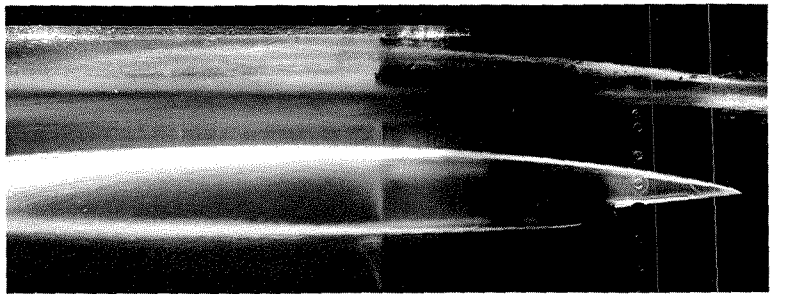

(f) S/c = 0.83, $\alpha = 12^{o}$, K = 0.063, $\ell/c = 6.92$

Fig. 9 Photos of typical cavities under varying conditions which show the bowing of the free surface.

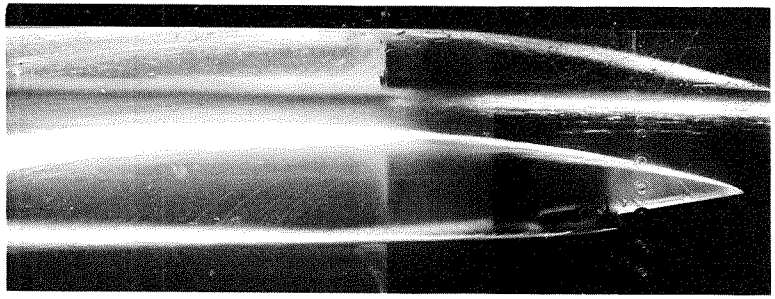

(a) S/c = 0.83, $\alpha = 16^{\circ}$, K = 0.073, $\ell/c = 7.99$

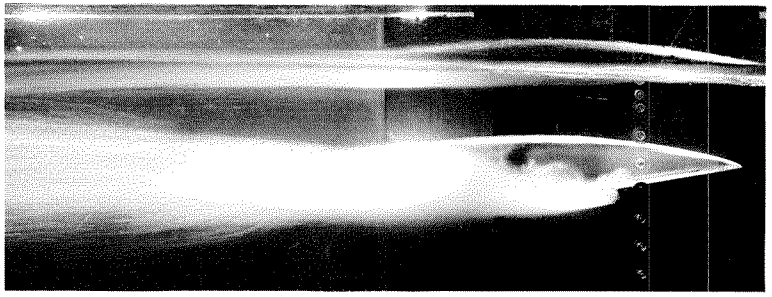

(b) S/c = 0.83, $\alpha = 16^{\circ}$, K = 0.141, $\ell/c = 2.80$

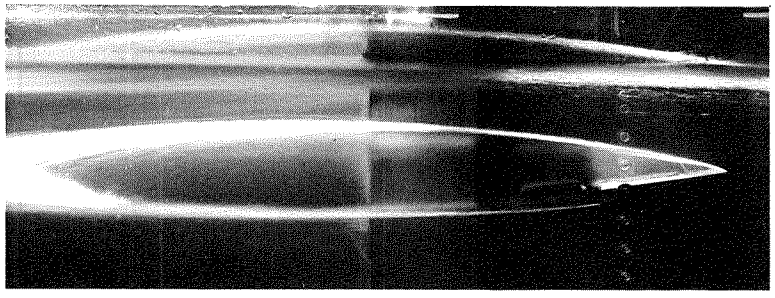

(c) S/c = 0.83, $\alpha = 14^{\circ}$, K = 0.071, $\ell/c = 6.13$

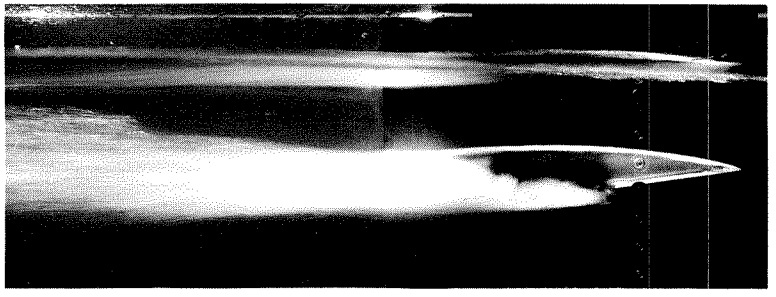

(d) S/c = 0.83, $\alpha = 14^{\circ}$, K = 0.143, $\ell/c = 2.93$

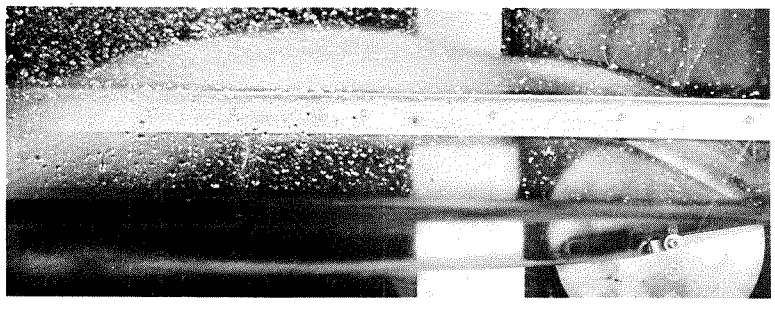

(e) S/c = 0.16, $\alpha = 16^{\circ}$, K = - 0.005

(f) S/c = 0.16, $\alpha = 16^{\circ}$, K = - 0.003

Fig. 10 Photos of typical cavities under varying conditions which show the bowing of the free surface.

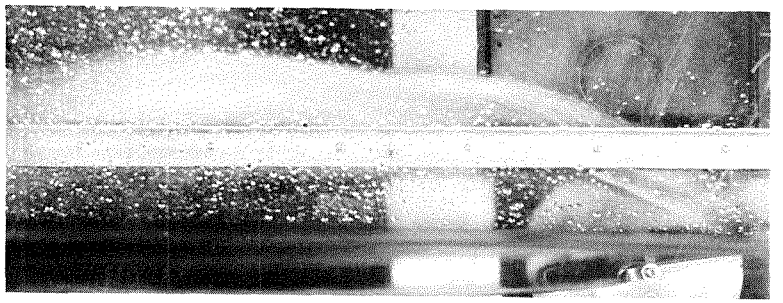

(a) S/c = 0.16, $\alpha = 14^{o}$, K = 0

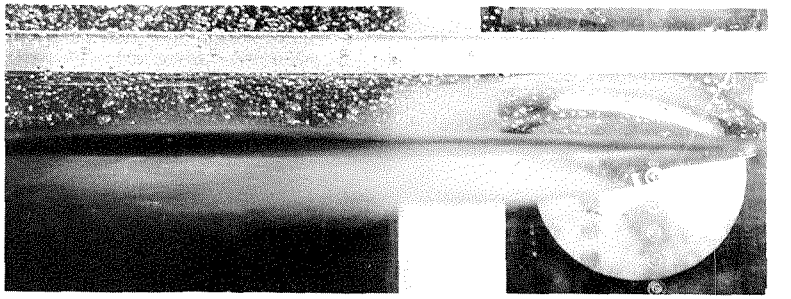

(b) S/c = 0.16, $\alpha = 14^{o}$, K = 0

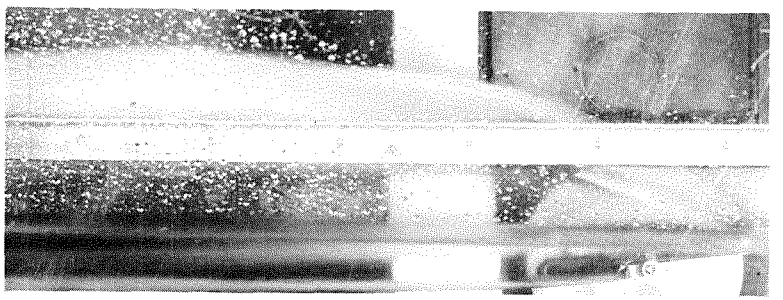

(c) S/c = 0.16, $\alpha = 12^{o}$, K = 0.005

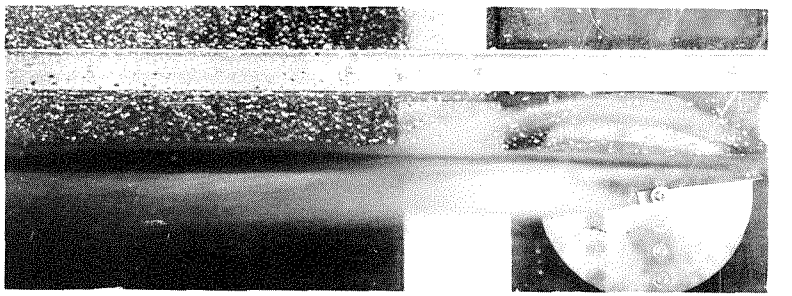

(d) S/c = 0.16, $\alpha = 12^{o}$, K = 0.055, $\ell/c = 2.26$

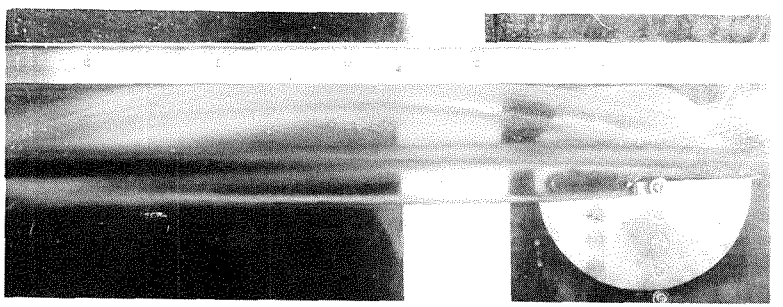

(e) S/c = 0.16, $\alpha = 8^{o}$, K = 0.016

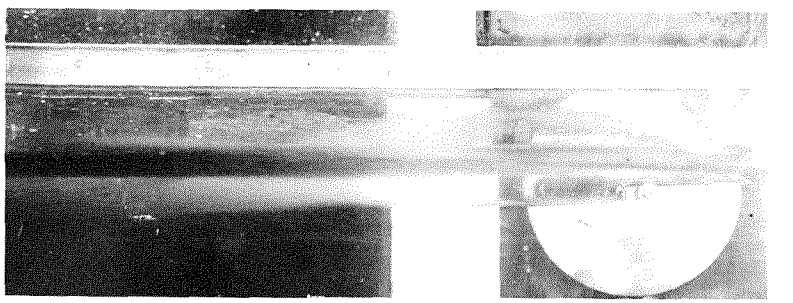

(f) S/c = 0.16, $\alpha = 8^{o}$, K = 0.039, $\ell/c = 2.80$

Fig. 11 Photos of typical cavities under varying conditions which show the bowing of the free surface.

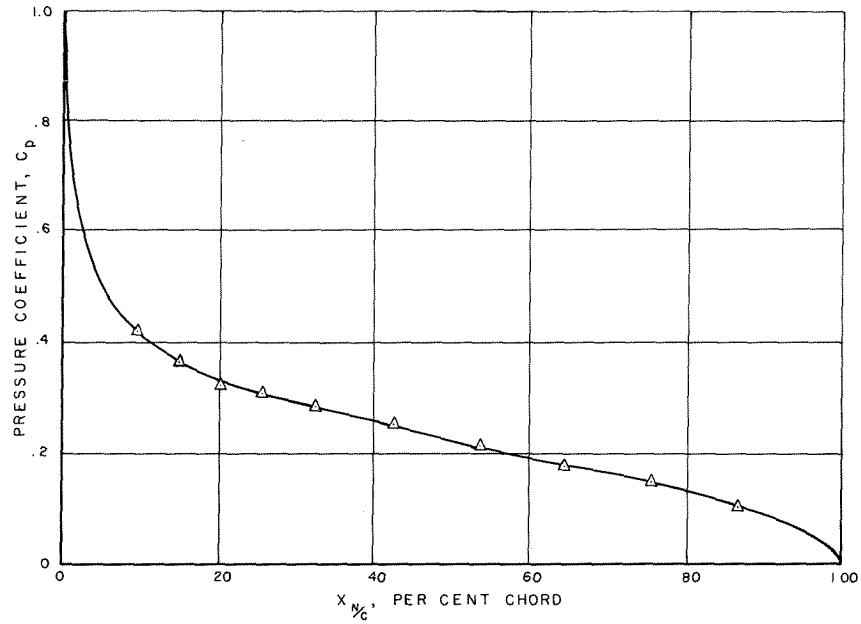

(a) S/c = 2.16, $\alpha = 8^{\circ}$, K = 0.115, C_f = 0.252

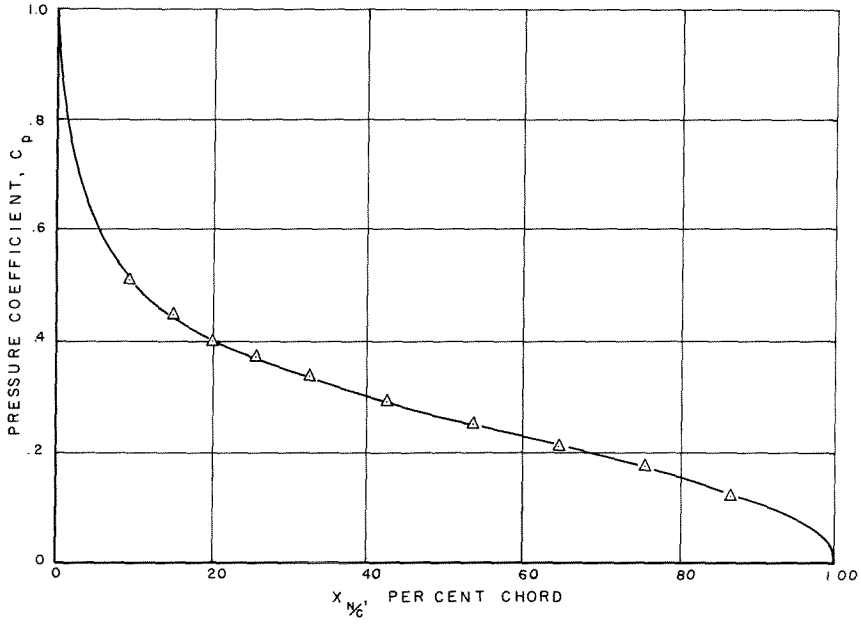

(b) S/c = 2.16, $\alpha = 10^{\circ}$, K = 0.111, C_f = 0.294

Fig. 12 Plots of pressure distributions on a fully cavitating flat plate hydrofoil at various submergences, cavitation numbers, and angles of attack.

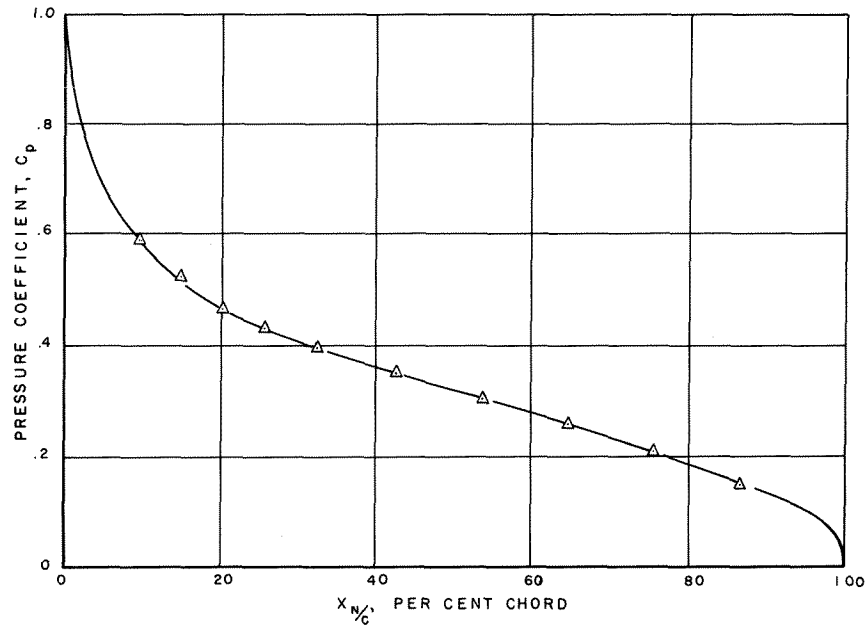

(a) S/c = 2.16, $\alpha = 12^{\circ}$, K = 0.127, $C_f = 0.343$

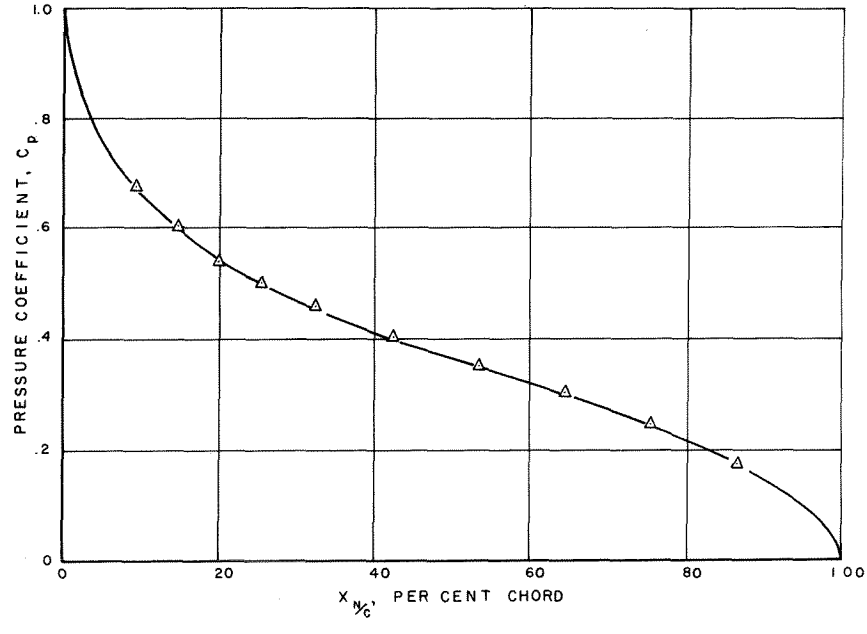

(b) S/c = 2.16, $\alpha = 14^{\circ}$, K = 0.120, $C_f = 0.391$

Fig. 13 Plots of pressure distributions on a fully cavitating flat plate hydrofoil at various submergences, cavitation numbers, and angles of attack.

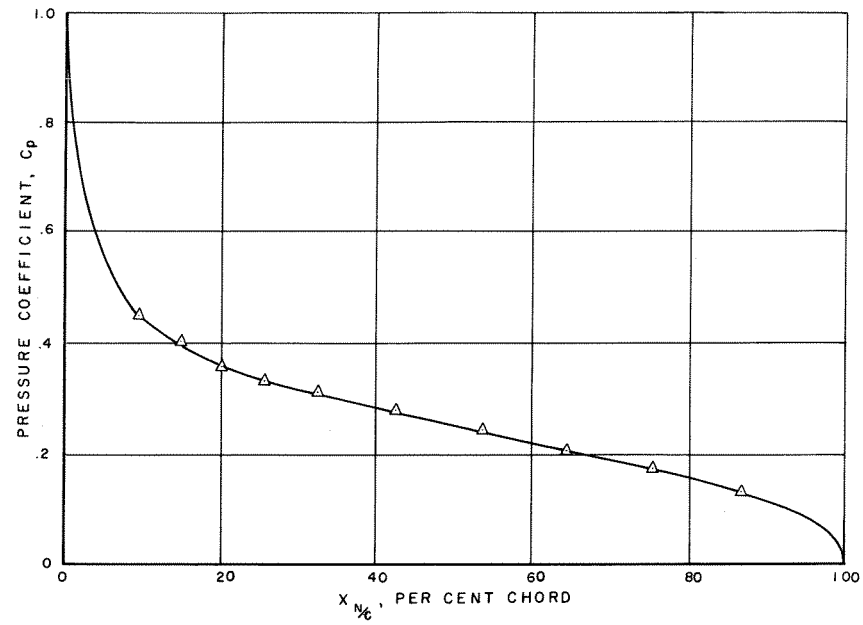

(a) S/c = 0.83, $\alpha = 8^{o}$, K = 0.128, $C_f = 0.278$

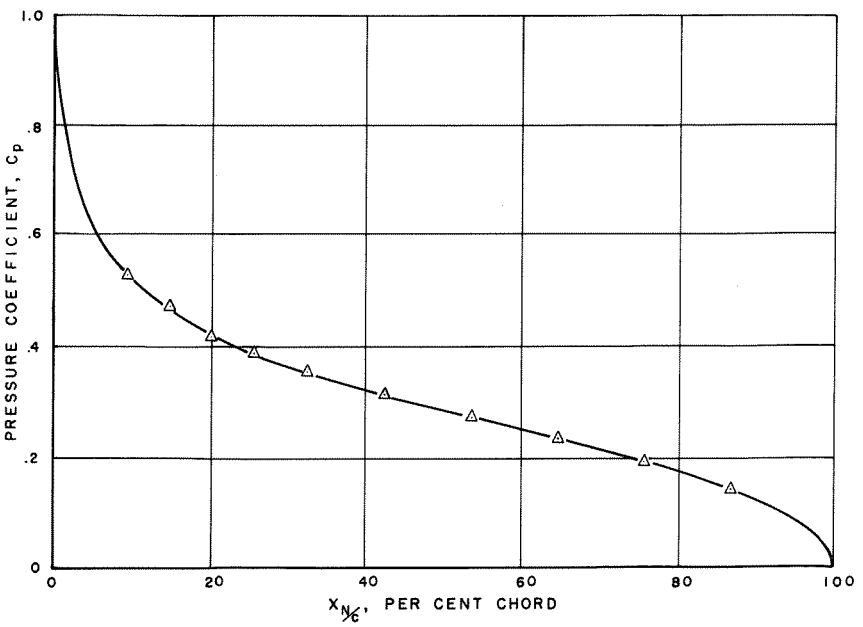

(b) S/c = 0.83, $\alpha = 10^{o}$, K = 0.123, $C_f = 0.313$

Fig. 14 Plots of pressure distributions on a fully cavitating flat plate hydrofoil at various submergences, cavitation numbers, and angles of attack.

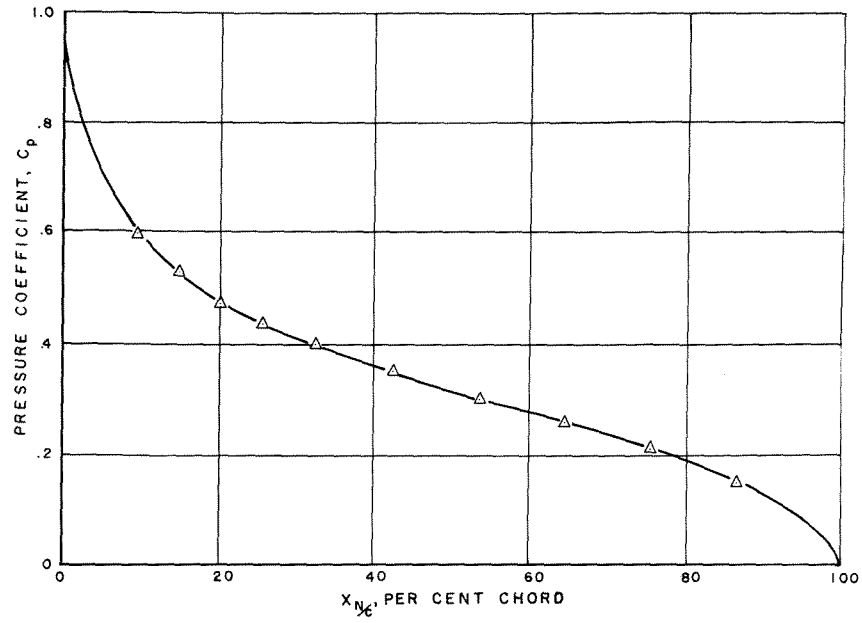

(a) S/c = 0.83, $\alpha = 12^{\circ}$, K = 0.118, $C_f = 0.346$

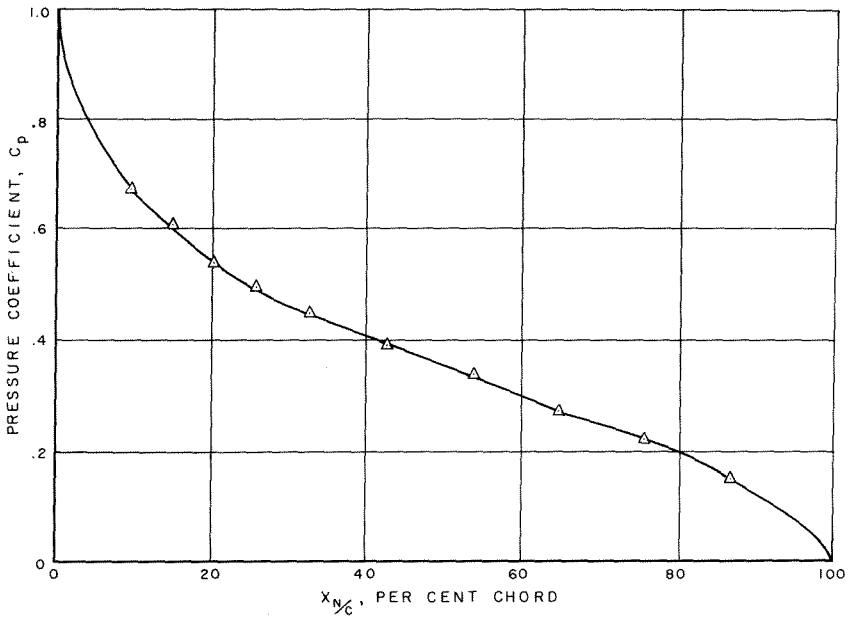

(b) S/c = 0.83, $\alpha = 16^{\circ}$, K = 0.079, $C_f = 0.380$

Fig. 15 Plots of pressure distributions on a fully cavitating flat plate hydrofoil at various submergences, cavitation numbers, and angles of attack.

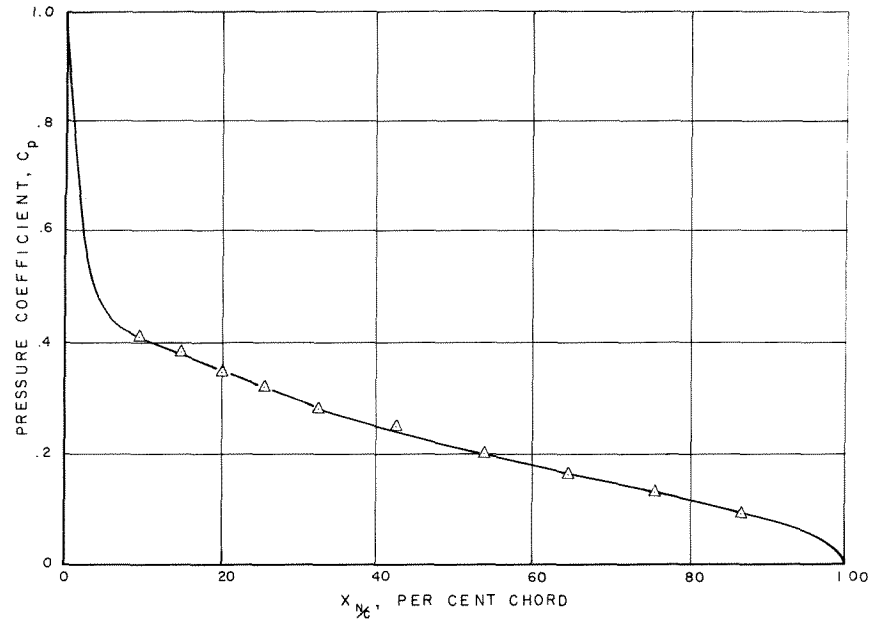

(a) S/c = -0.06, $\alpha = 8^{\circ}$, K = -0.018, $C_f = 0.217$

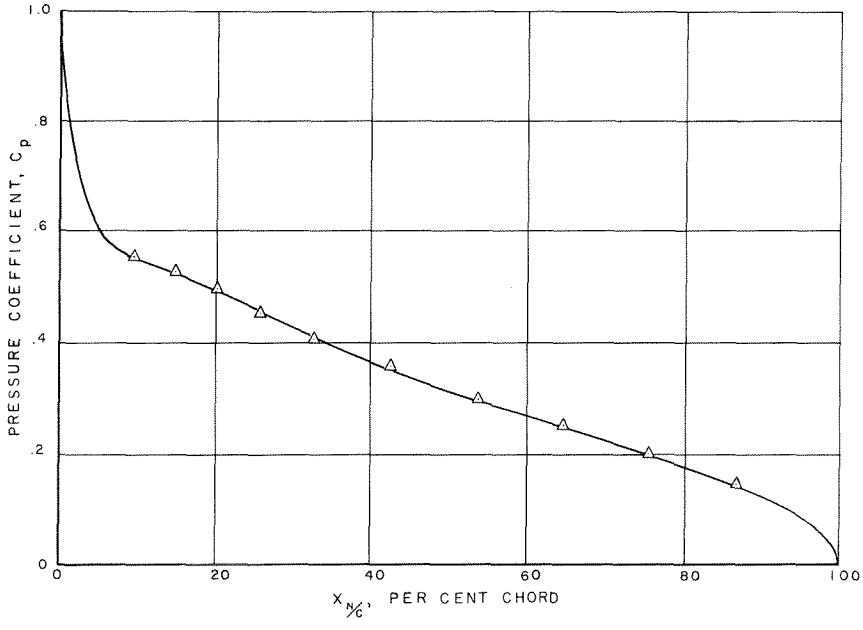

(b) S/c = - 0.06, $\alpha = 12^{\circ}$, K = - 0.021, $C_f = 0.339$

Fig. 16 Plots of pressure distributions on a fully cavitating flat plate hydrofoil at various submergences, cavitation numbers, and angles of attack.

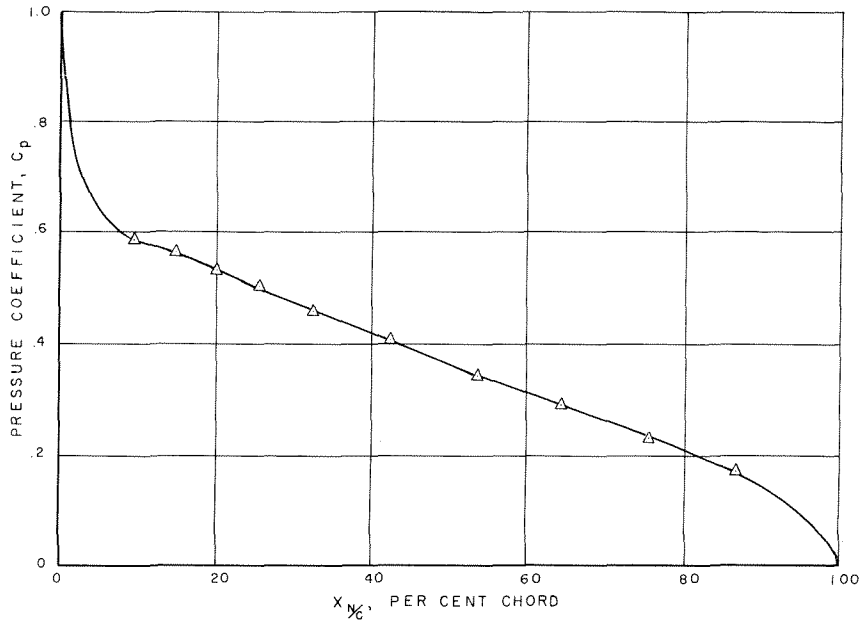

(a) $S/c = -0.06$, $\alpha = 14^{o}$, $K = -0.024$, $C_f = 0.377$

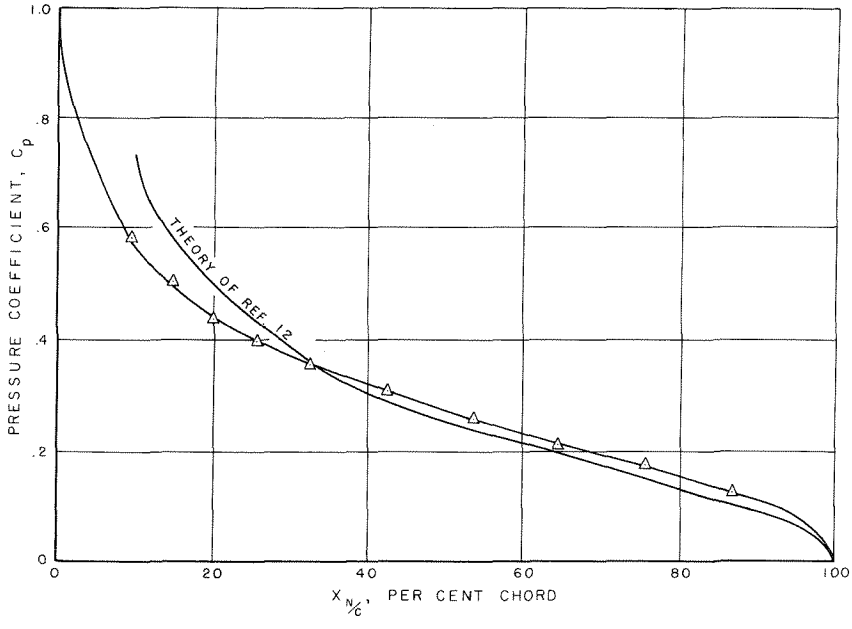

(b) $S/c = 0.09$, $\alpha = 10^{o}$, $K = -0.001$, $C_f = 0.312$

Fig. 17 Plots of pressure distributions on a fully cavitating flat plate hydrofoil at various submergences, cavitation numbers, and angles of attack.

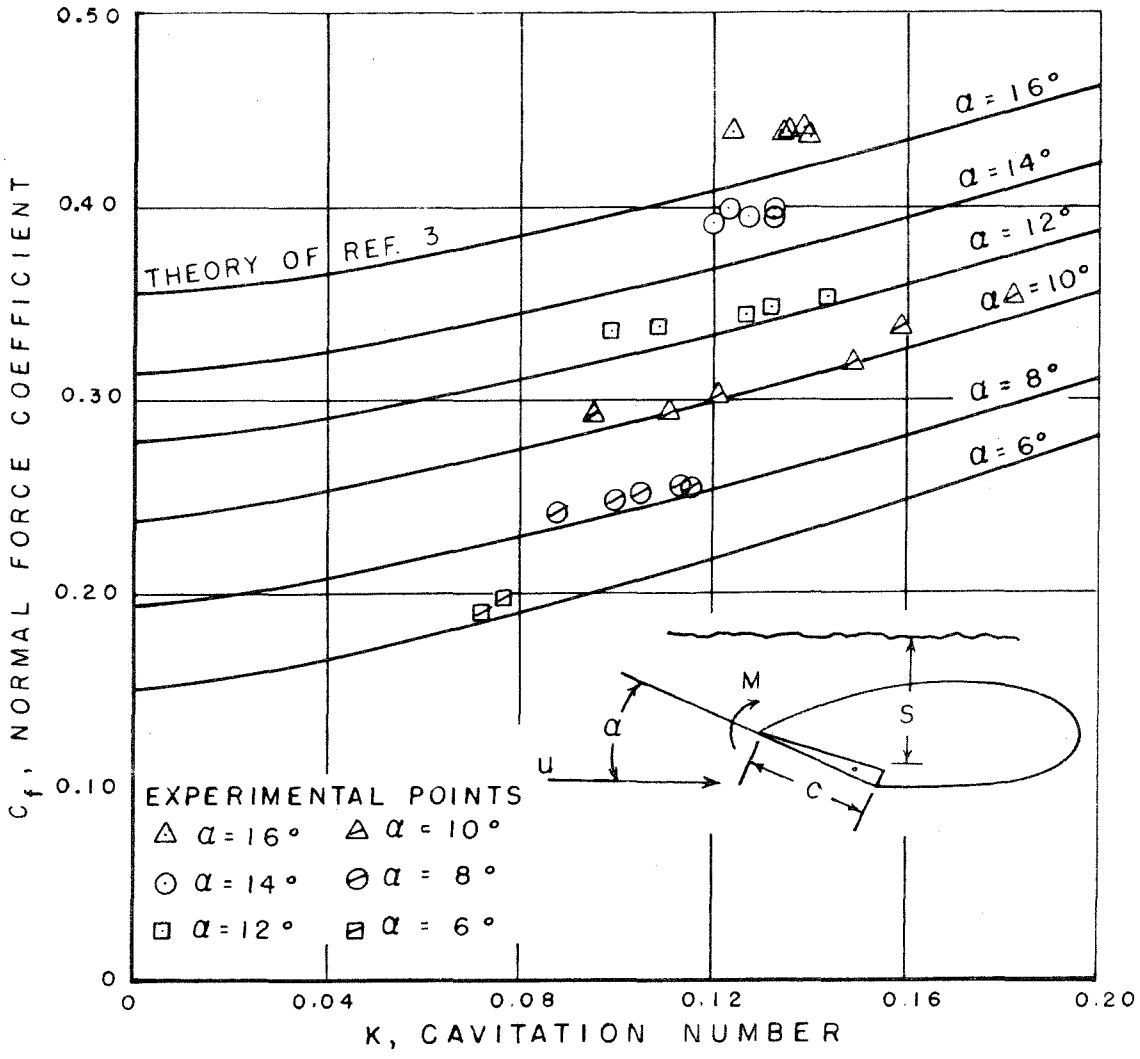

Fig. 18. The experimental normal force coefficient versus cavitation number, at six angles of attack and S/c = 2.16, as compared to Wu's exact infinite fluid theory.

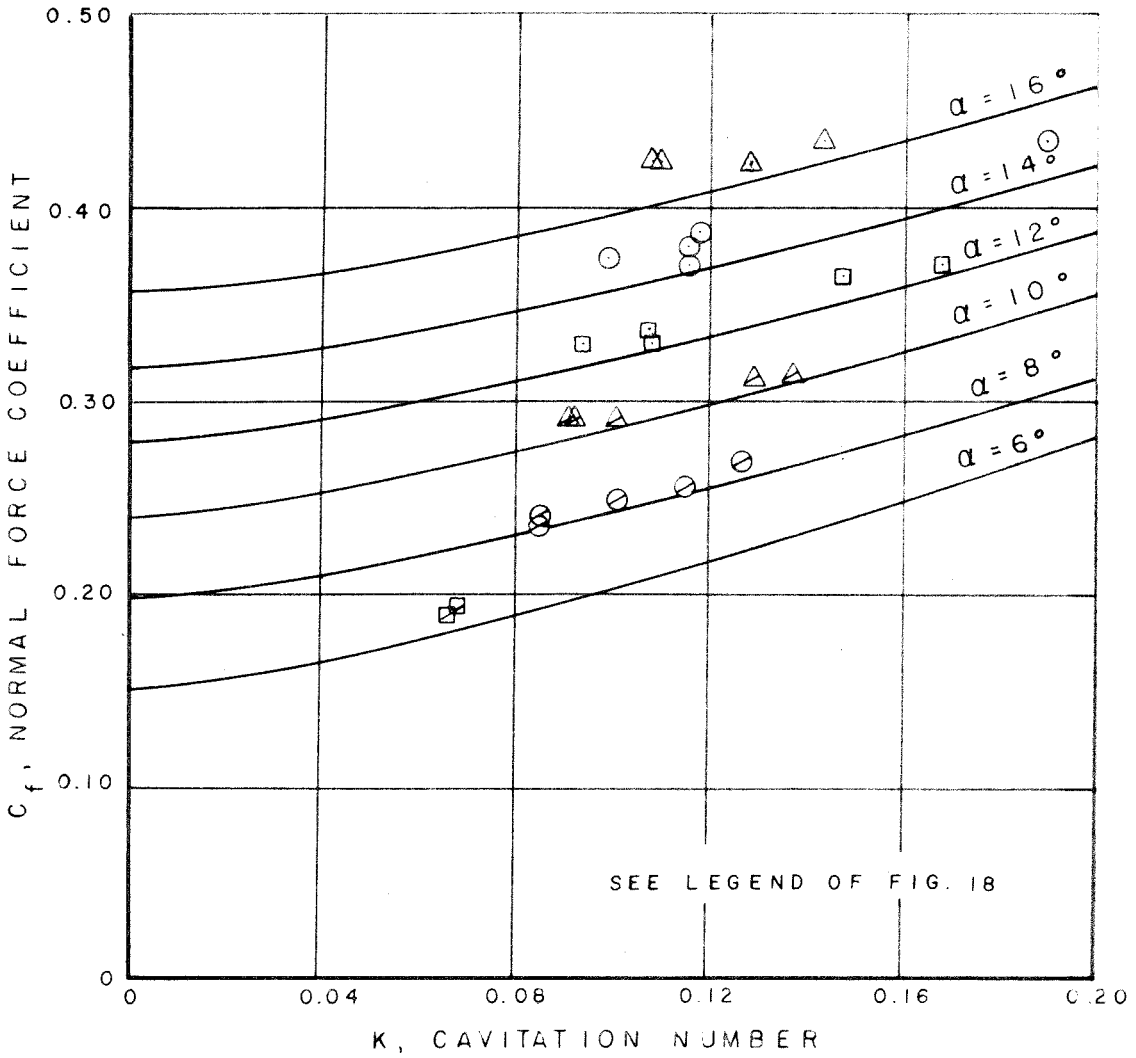

Fig. 19. The experimental normal force coefficient versus cavitation number, at six angles of attack and S/c = 1.50, as compared to Wu's exact infinite fluid theory.

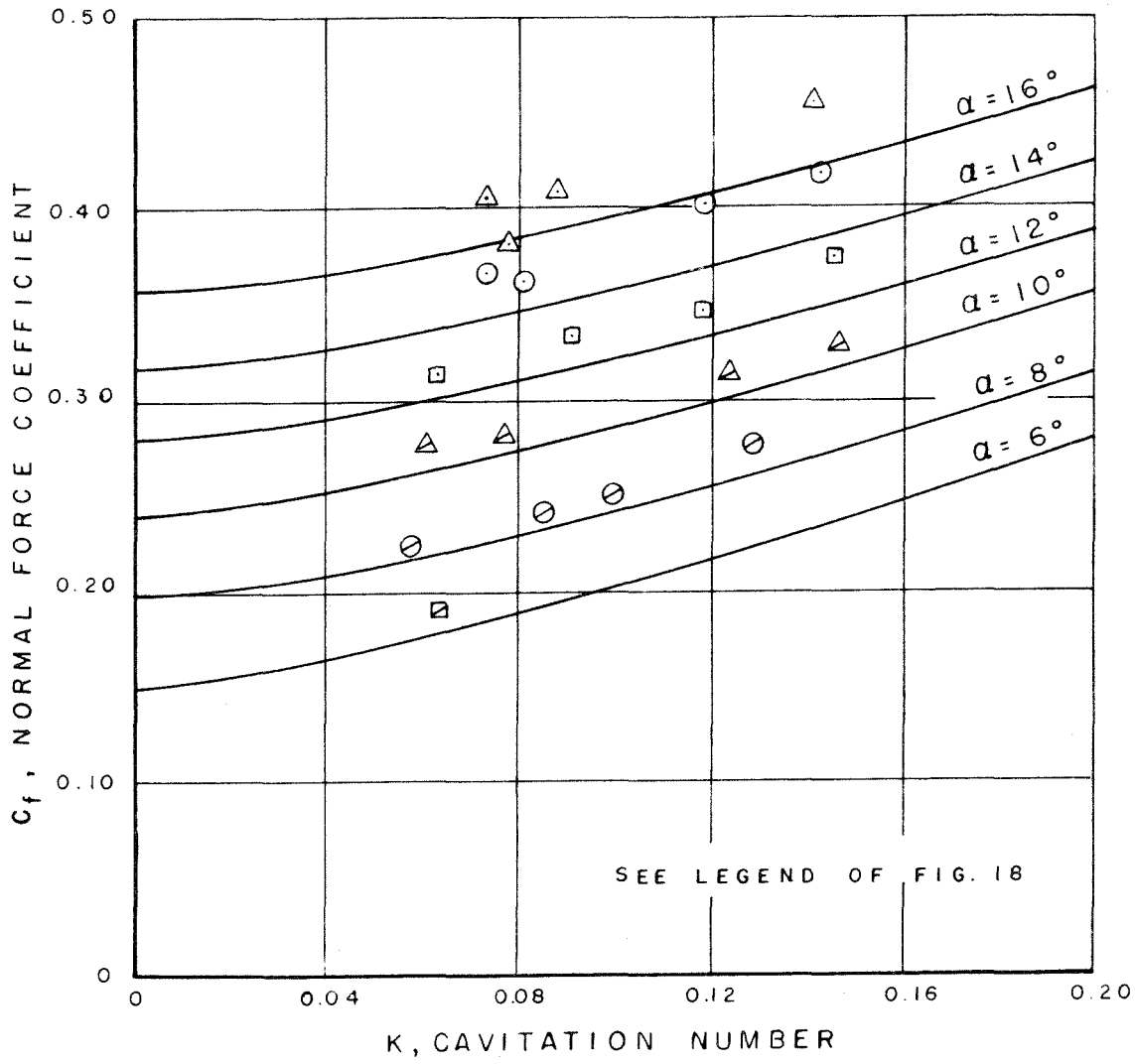

Fig. 20. The experimental normal force coefficient versus cavitation number, at six angles of attack and S/c = 0.83, as compared to Wu's exact infinite fluid theory.

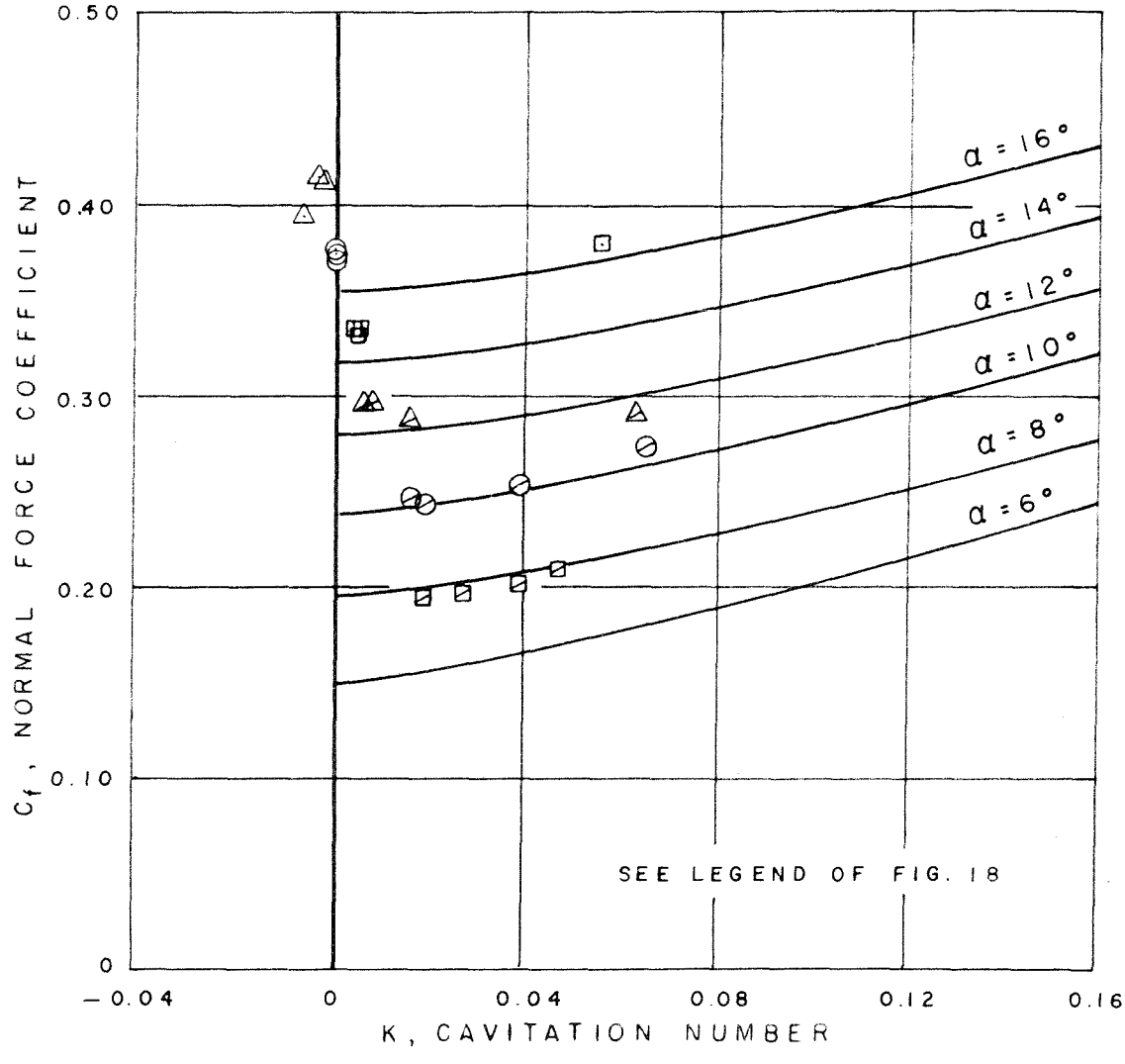

Fig. 21. The experimental normal force coefficient versus cavitation number, at six angles of attack and S/c = 0.16, as compared to Wu's exact infinite fluid theory.

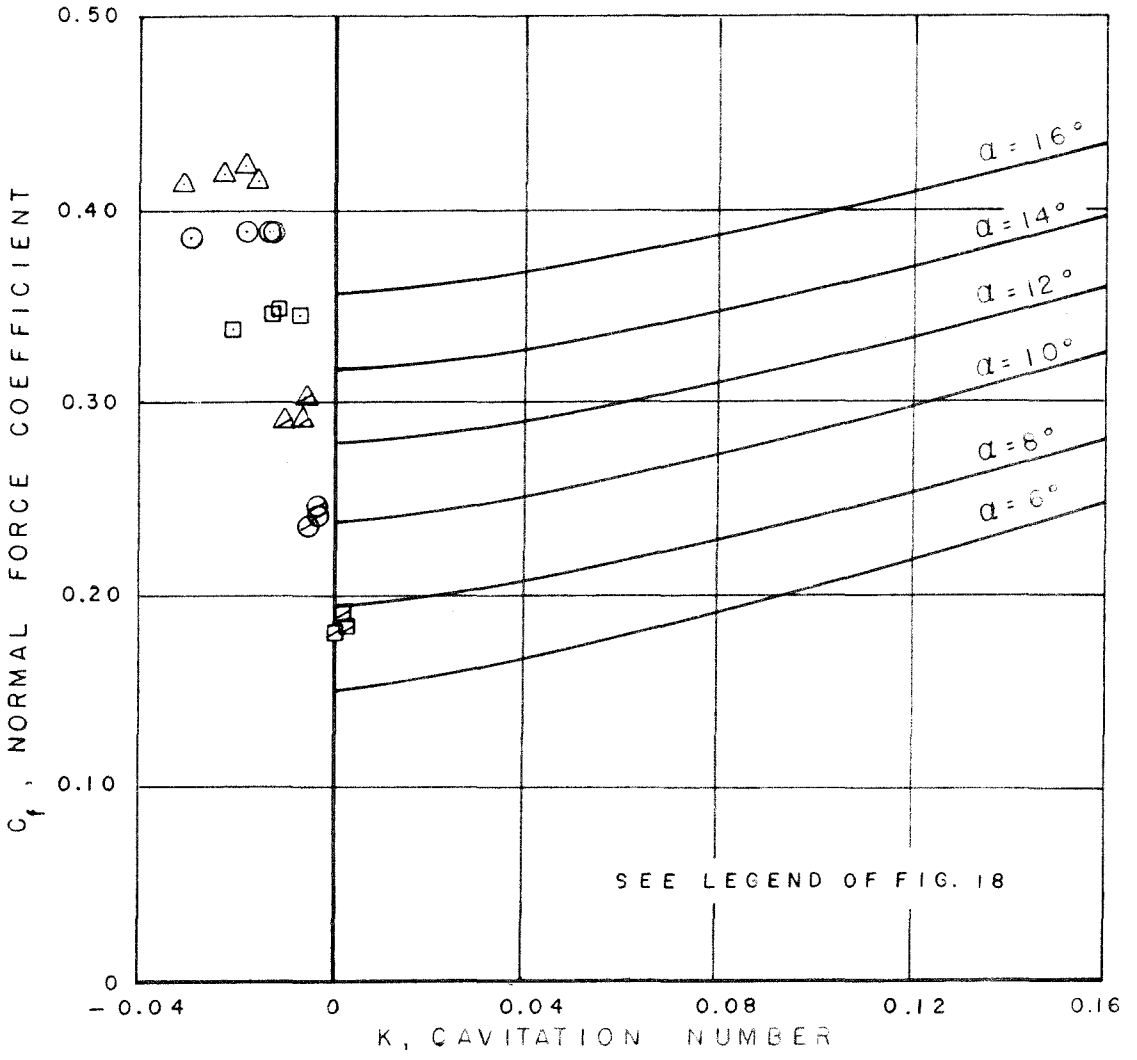

Fig. 22. The experimental normal force coefficient versus cavitation number, at six angles of attack and S/c = 0.05, as compared to Wu's exact infinite fluid theory.

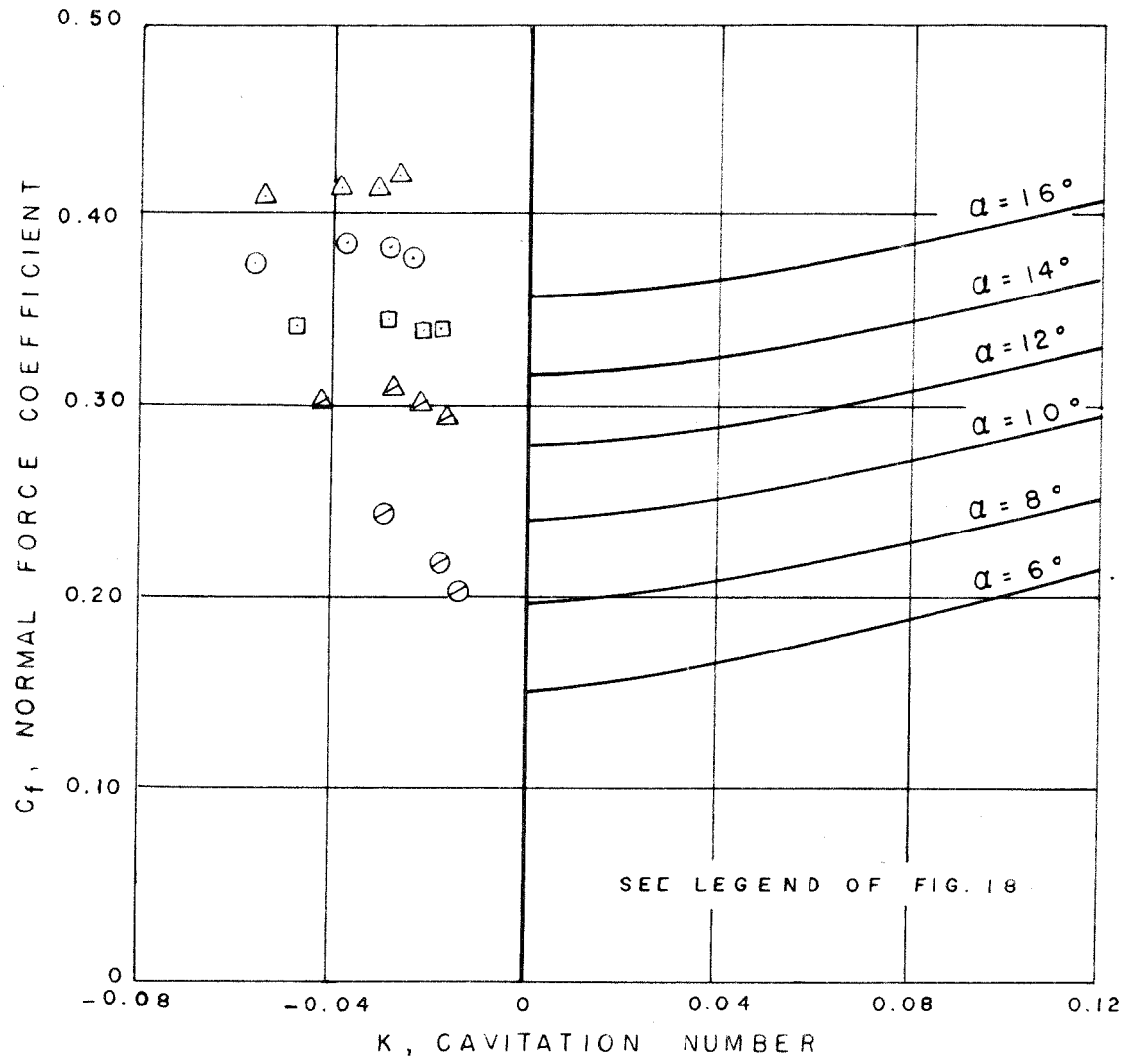

Fig. 23. The experimental normal force coefficient versus cavitation number, at six angles of attack and S/c = -0.06, as compared to Wu's exact infinite fluid theory.

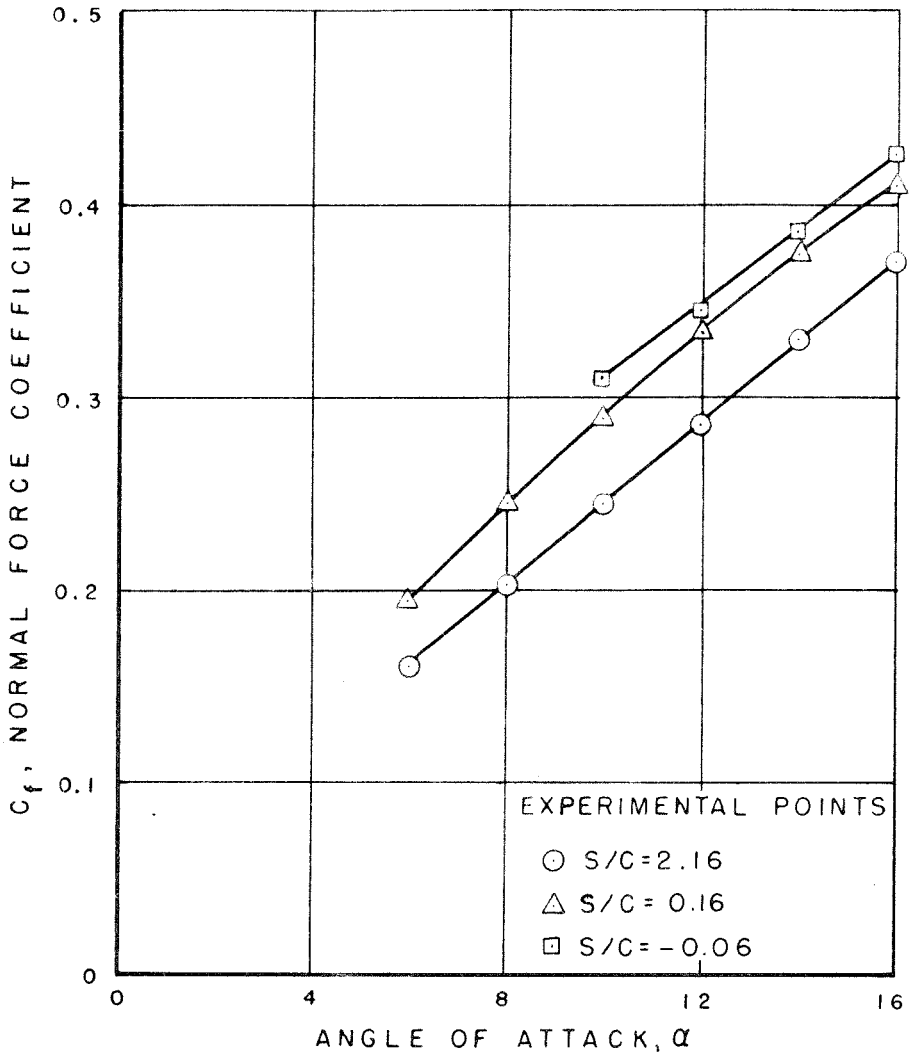

Fig. 24a. The effect of angle of attack on the normal force coefficient at K = 0 and three submergence ratios.

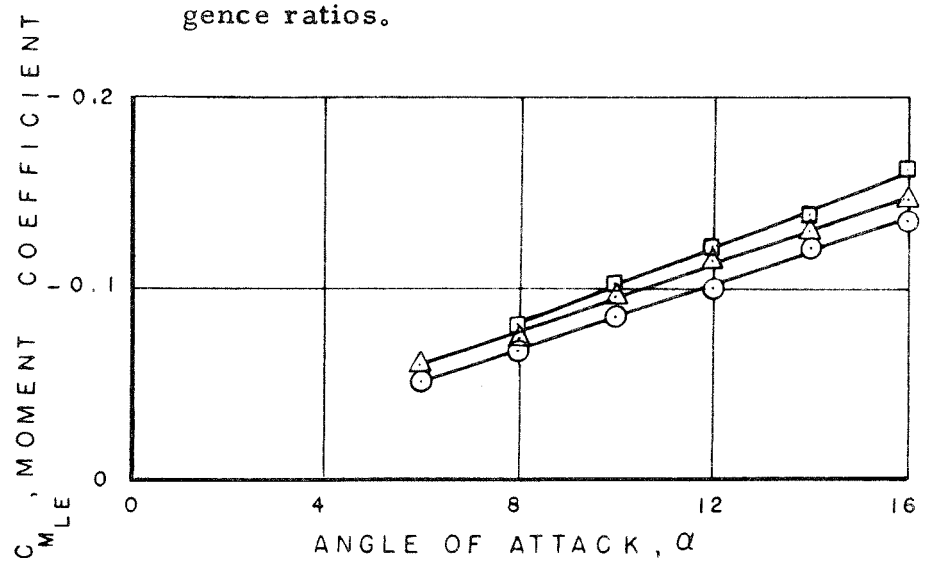

Fig. 24b. The effect of angle of attack on the moment coefficient at K = 0 and three submergence ratios.

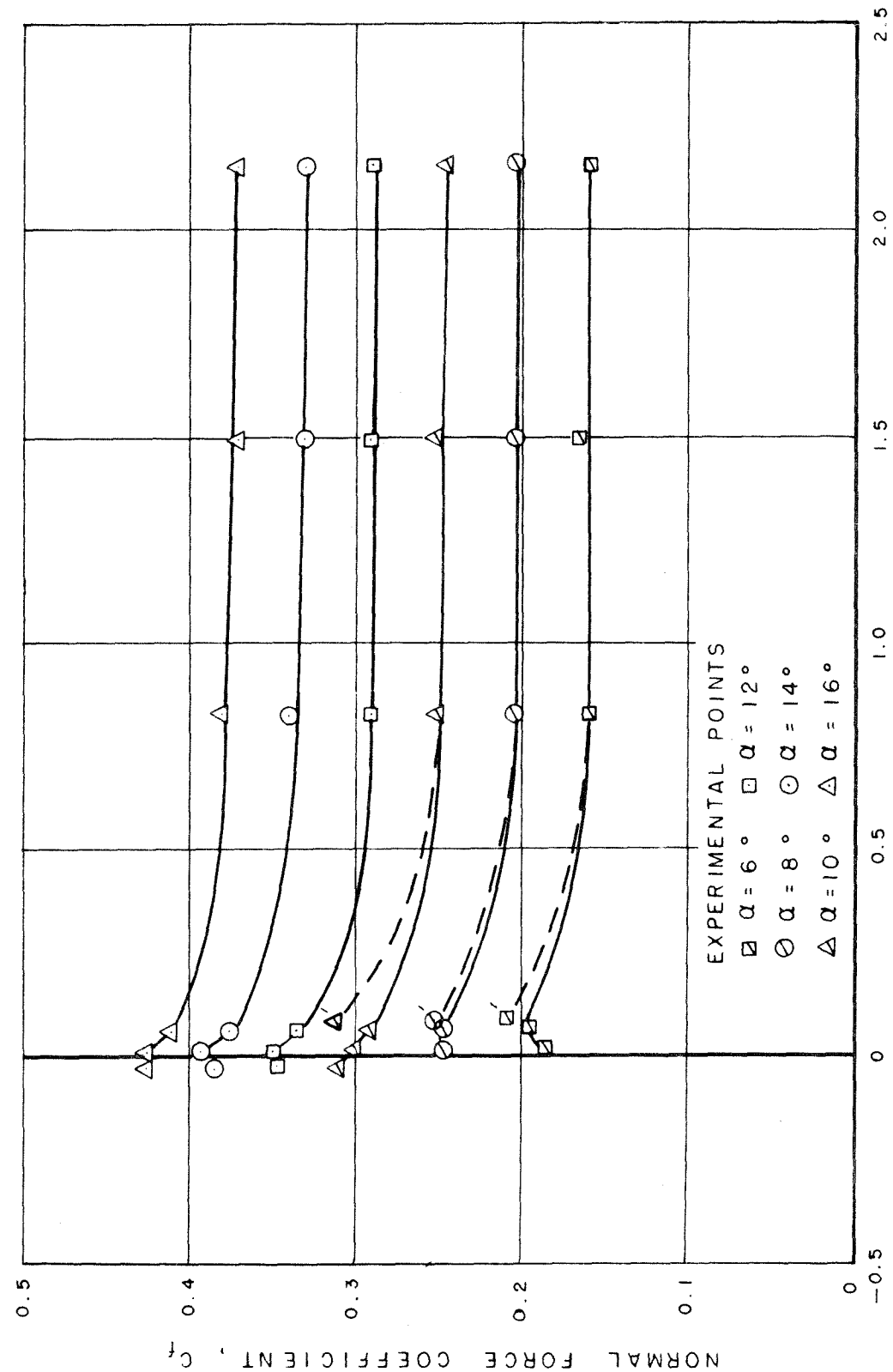

Fig. 25. The effect of submergence on the normal force coefficient at six angles of attack and K = 0. (The primed points are those obtained with the skimmer operating.)

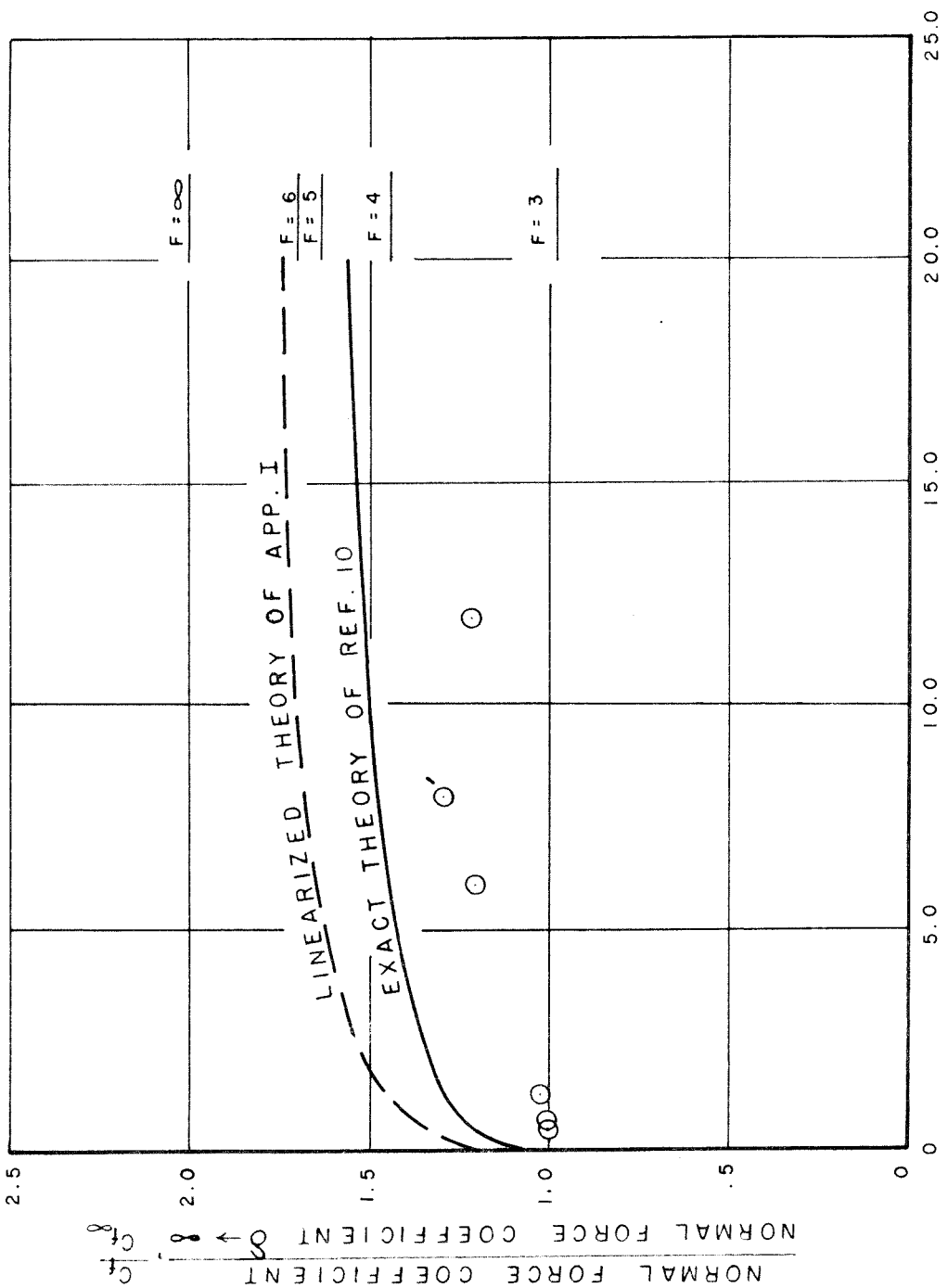

Fig. 26. A comparison of the experimental normal force coefficient ratios to the theories of Green and App. I at $\alpha = 8^0$ and $K = 0$. The Froude number asymptotes of Cumberbatch for $\delta = 0$ are also shown.

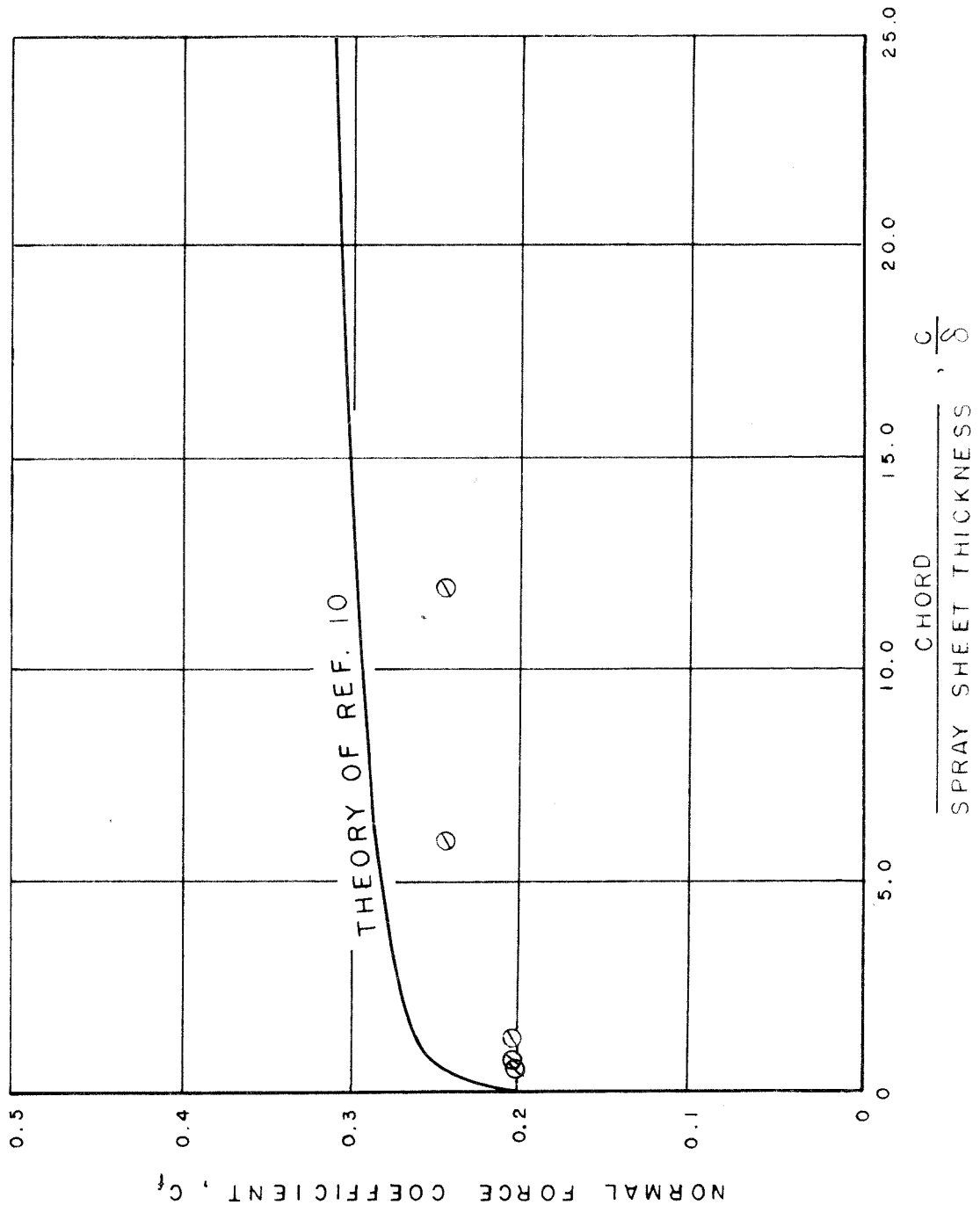

Fig. 27. The normal force coefficient versus the chord to spray sheet thickness ratio showing the experimental points and the theory of Green at $\alpha = 8^{\circ}$ and $K = 0$.

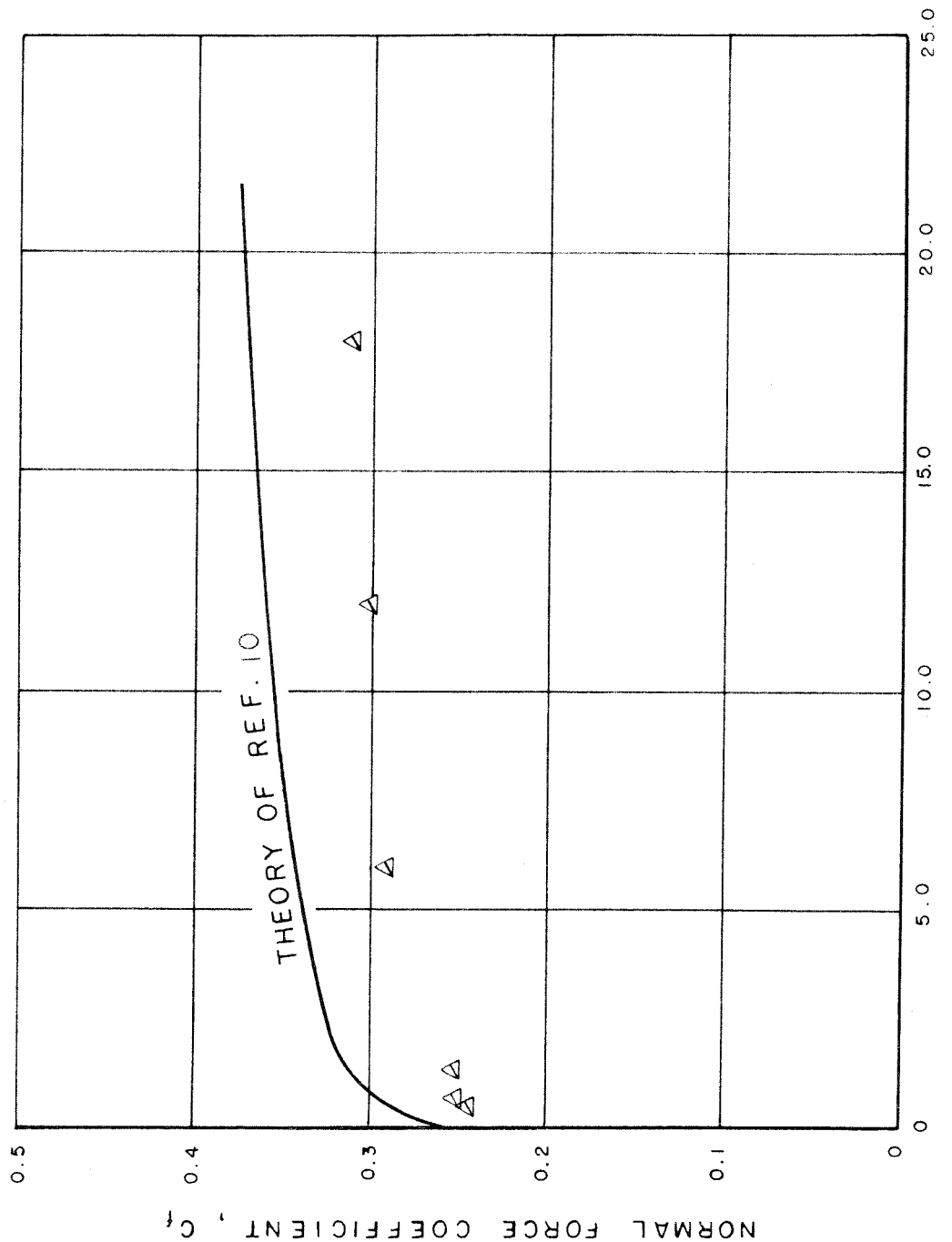

Fig. 28. The normal force coefficient versus the chord to spray sheet thickness ratio showing the experimental points and the theory of Green at $\alpha = 10^0$ and $K = 0$.

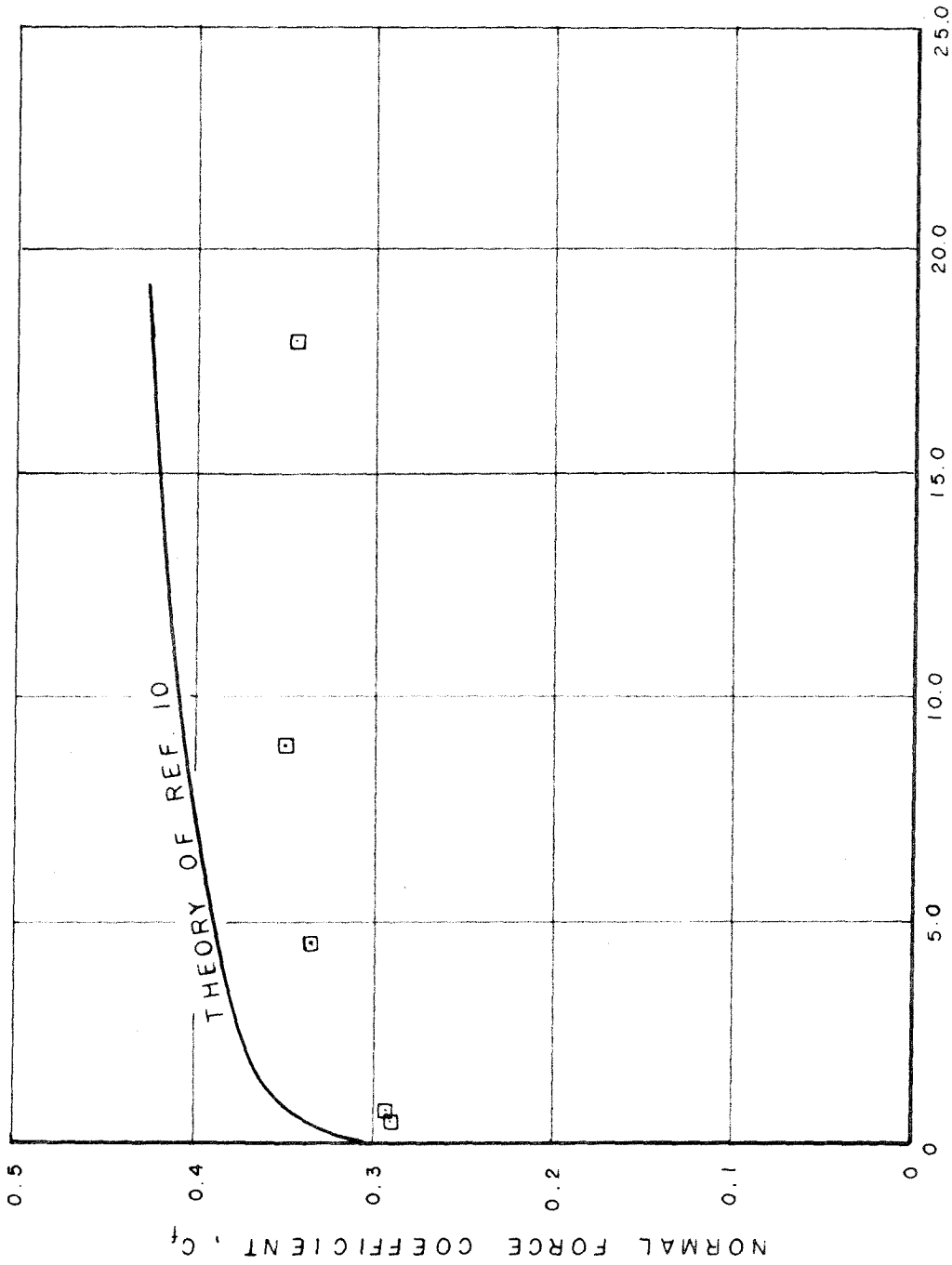

Fig. 29. The normal force coefficient versus the chord to spray sheet thickness ratio showing the experimental points and the theory of Green at $\alpha = 12^{\circ}$ and $K = 0$.

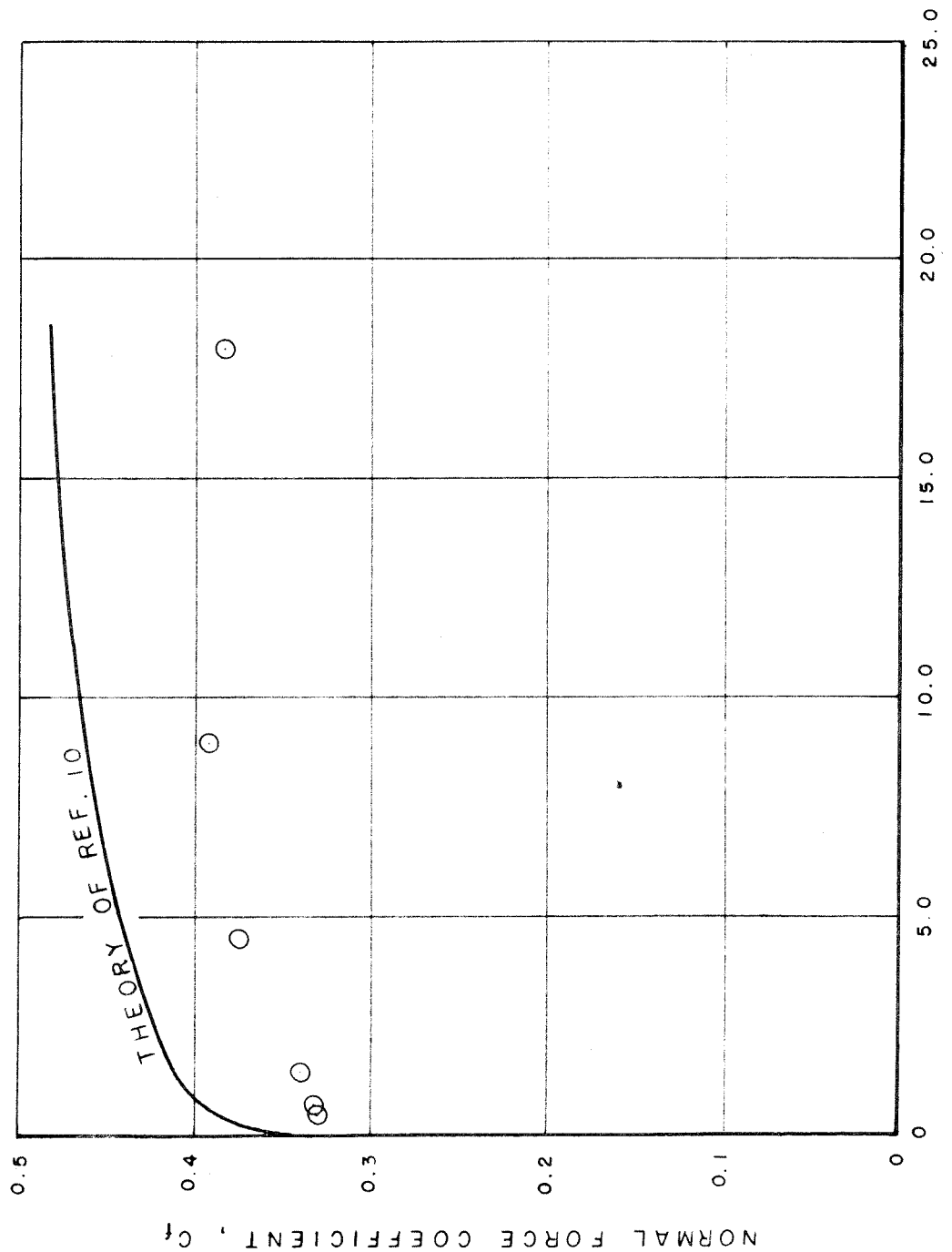

Fig. 30. The normal force coefficient versus the chord to spray sheet thickness ratio showing the experimental points and the theory of Green at $\alpha = 14^0$ and $K = 0$.

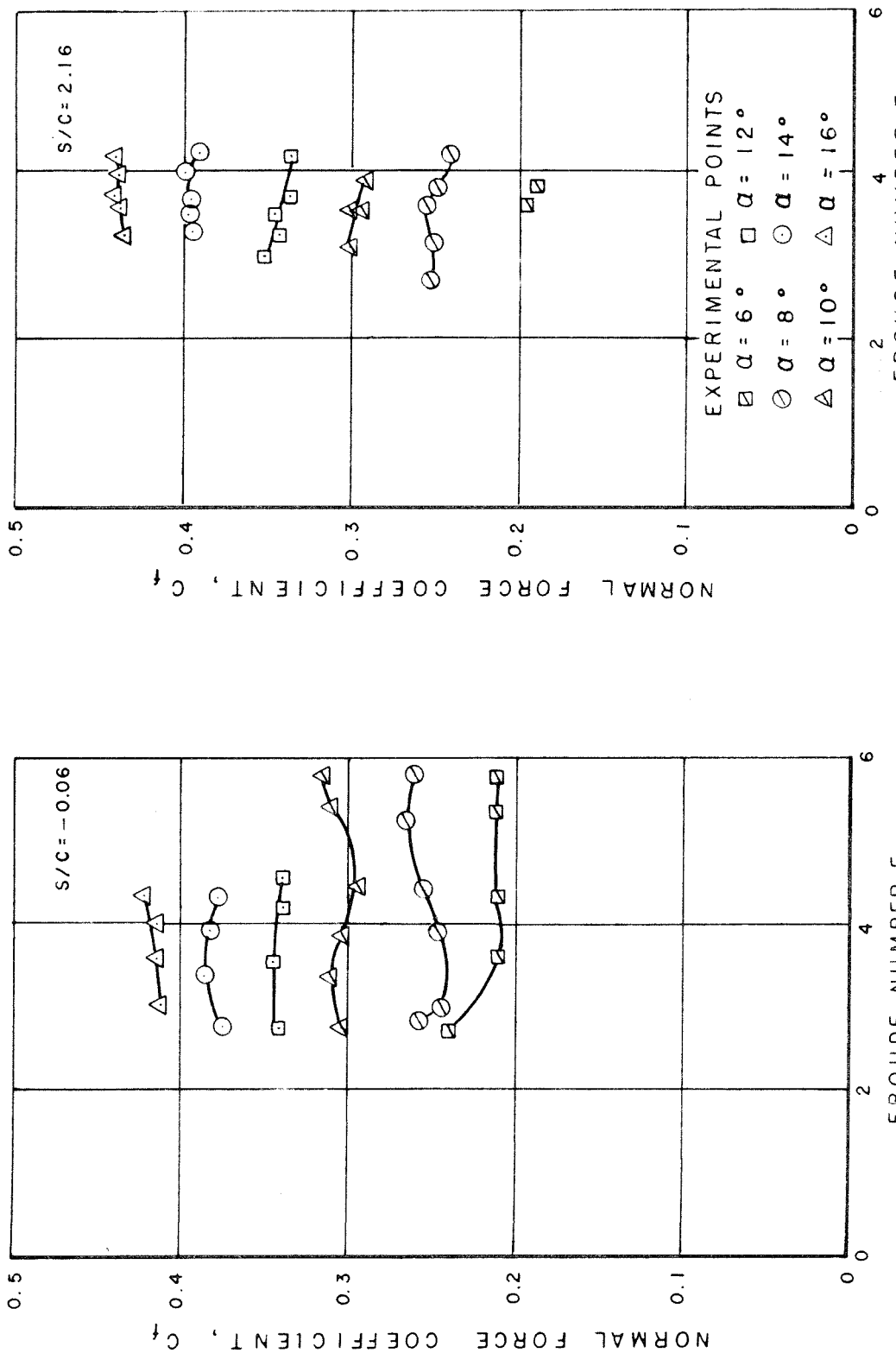

Fig. 31. The effect of Froude number on the normal force coefficient at six angles of attack and two submergence ratios.

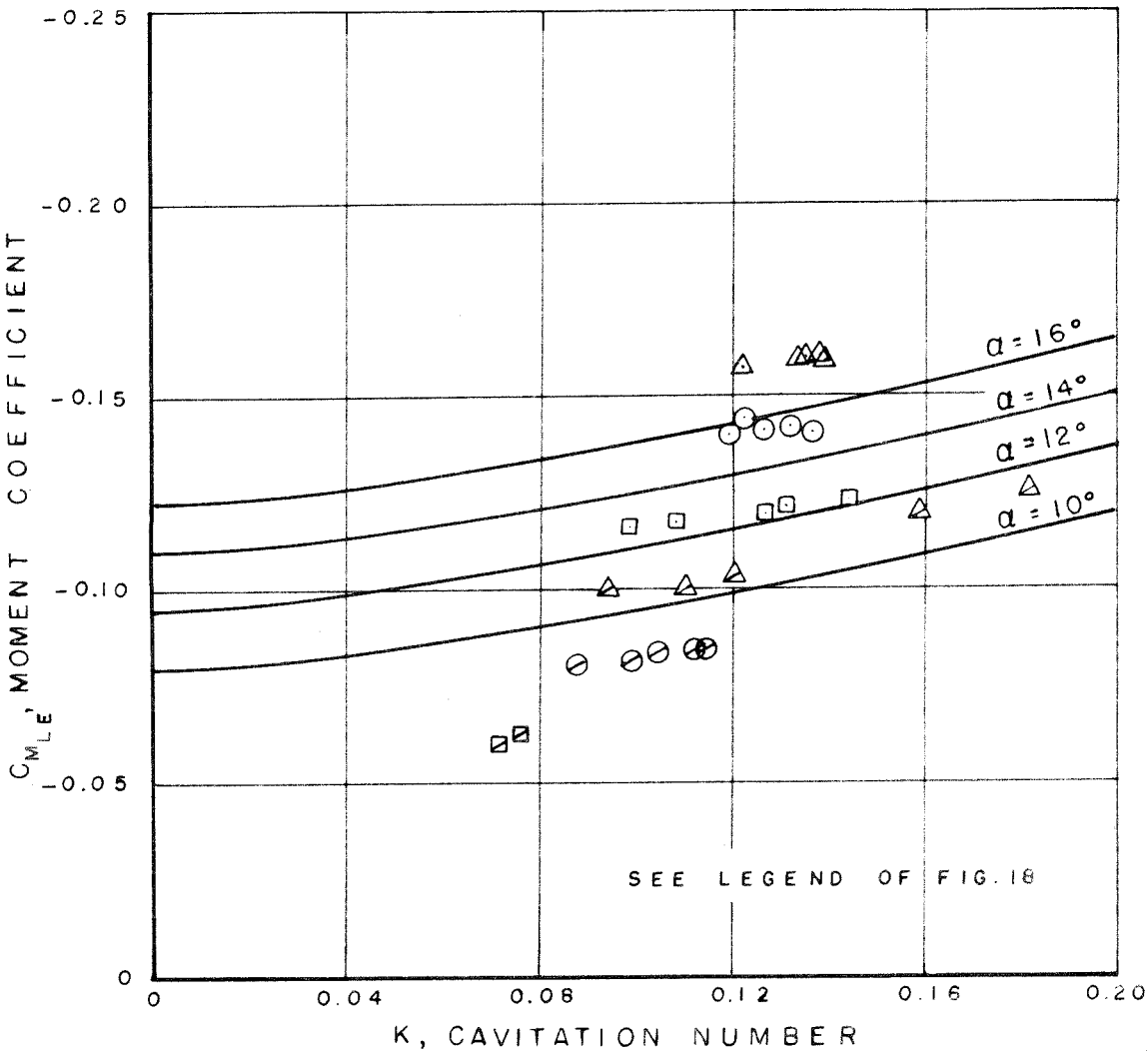

Fig. 32. The experimental moment coefficient about the leading edge versus cavitation number, at six angles of attack and S/c = 2.16, as compared to Wu's exact infinite fluid theory.

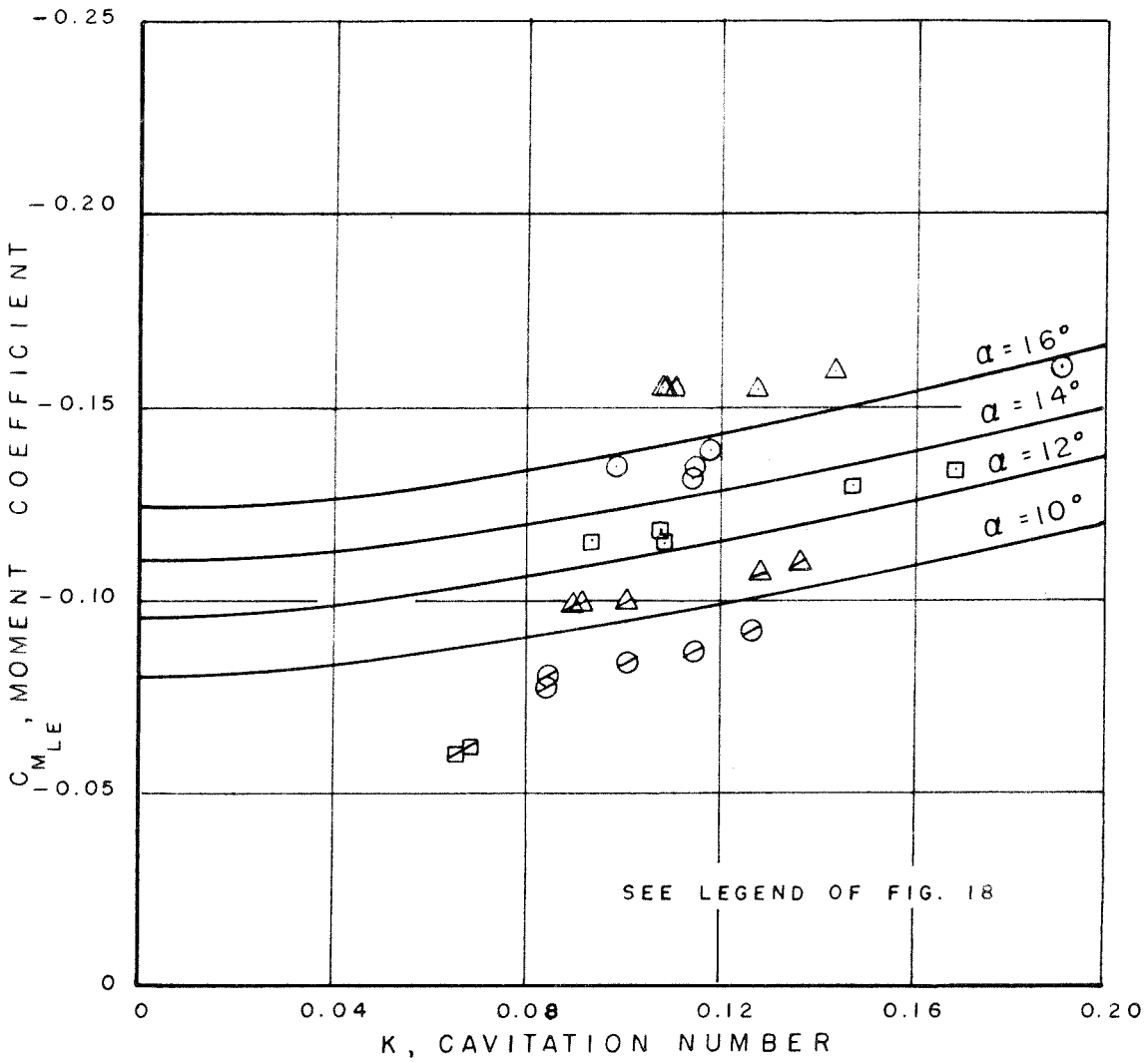

Fig. 33. The experimental moment coefficient about the leading edge versus cavitation number, at six angles of attack and S/c = 1.50, as compared to Wu's exact infinite fluid theory.

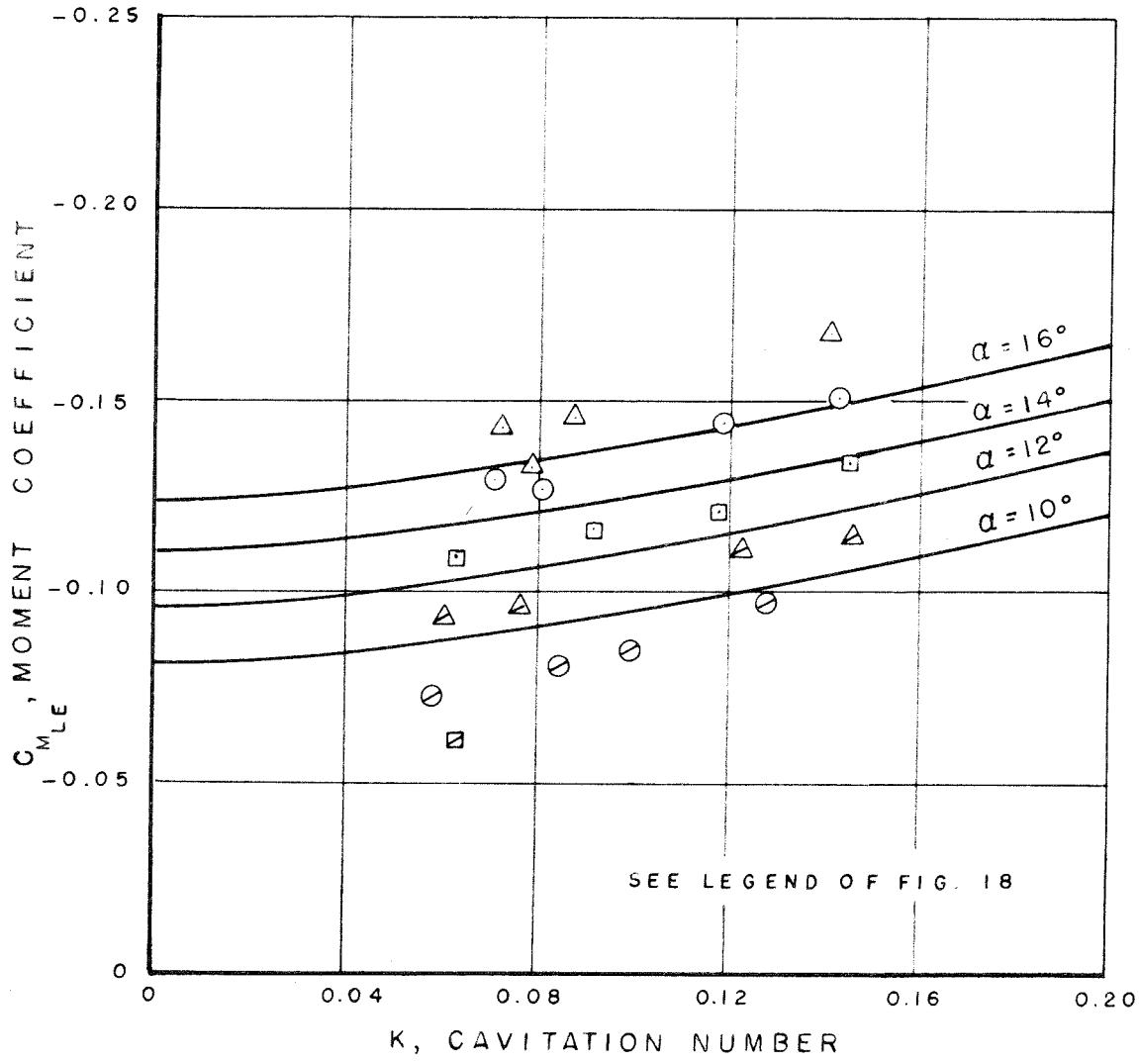

Fig. 34. The experimental moment coefficient about the leading edge versus cavitation number, at six angles of attack and S/c = 0.83, as compared to Wu's exact infinite fluid theory.

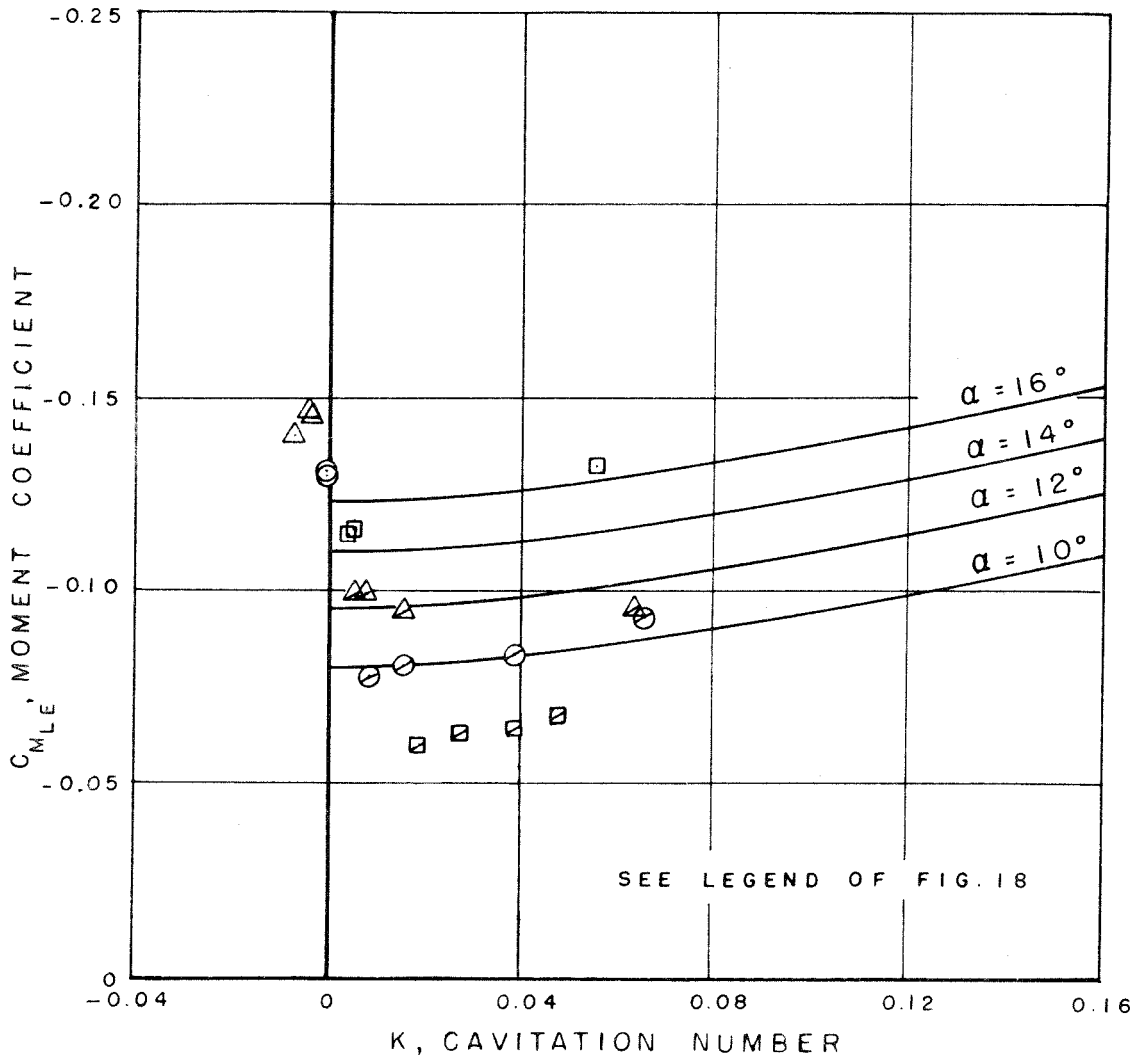

Fig. 35. The experimental moment coefficient about the leading edge versus cavitation number, at six angles of attack and S/c = 0.16, as compared to Wu's exact infinite fluid theory.

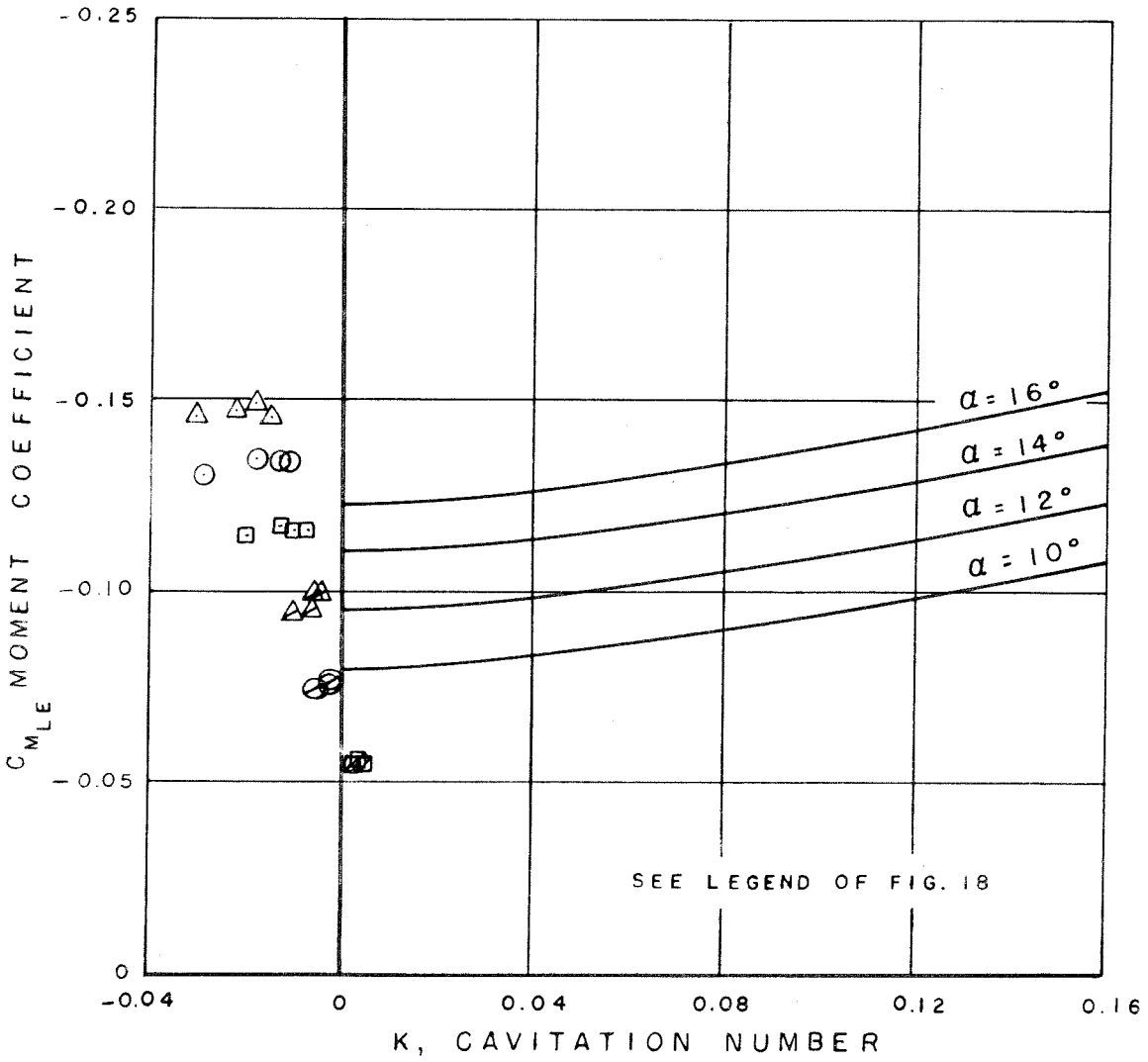

Fig. 36. The experimental moment coefficient about the leading edge versus cavitation number, at six angles of attack and S/c = 0.05, as compared to Wu's exact infinite fluid theory.

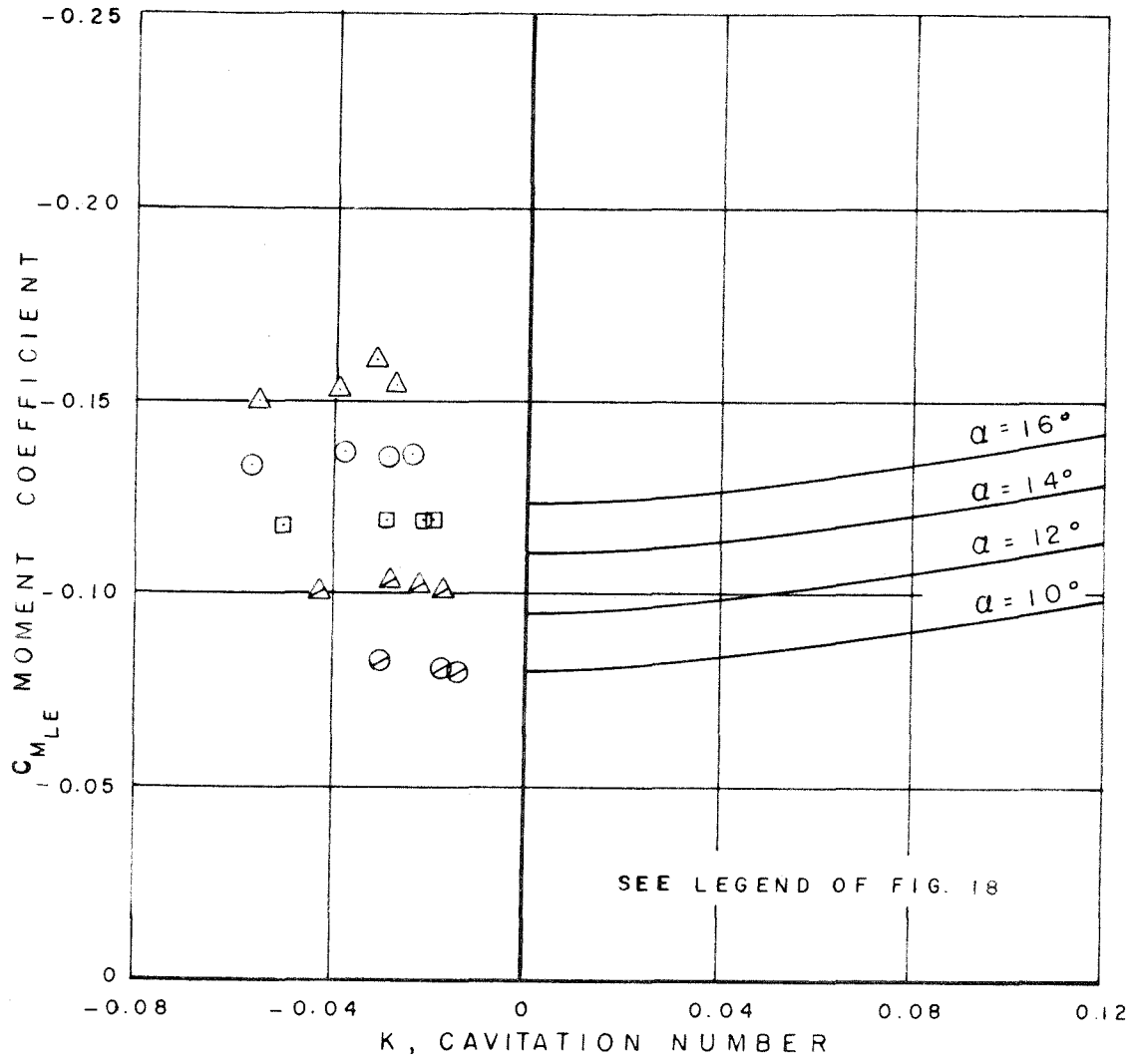

Fig. 37. The experimental moment coefficient about the leading edge versus cavitation number, at six angles of attack and S/c = -0.06, as compared to Wu's exact infinite fluid theory.

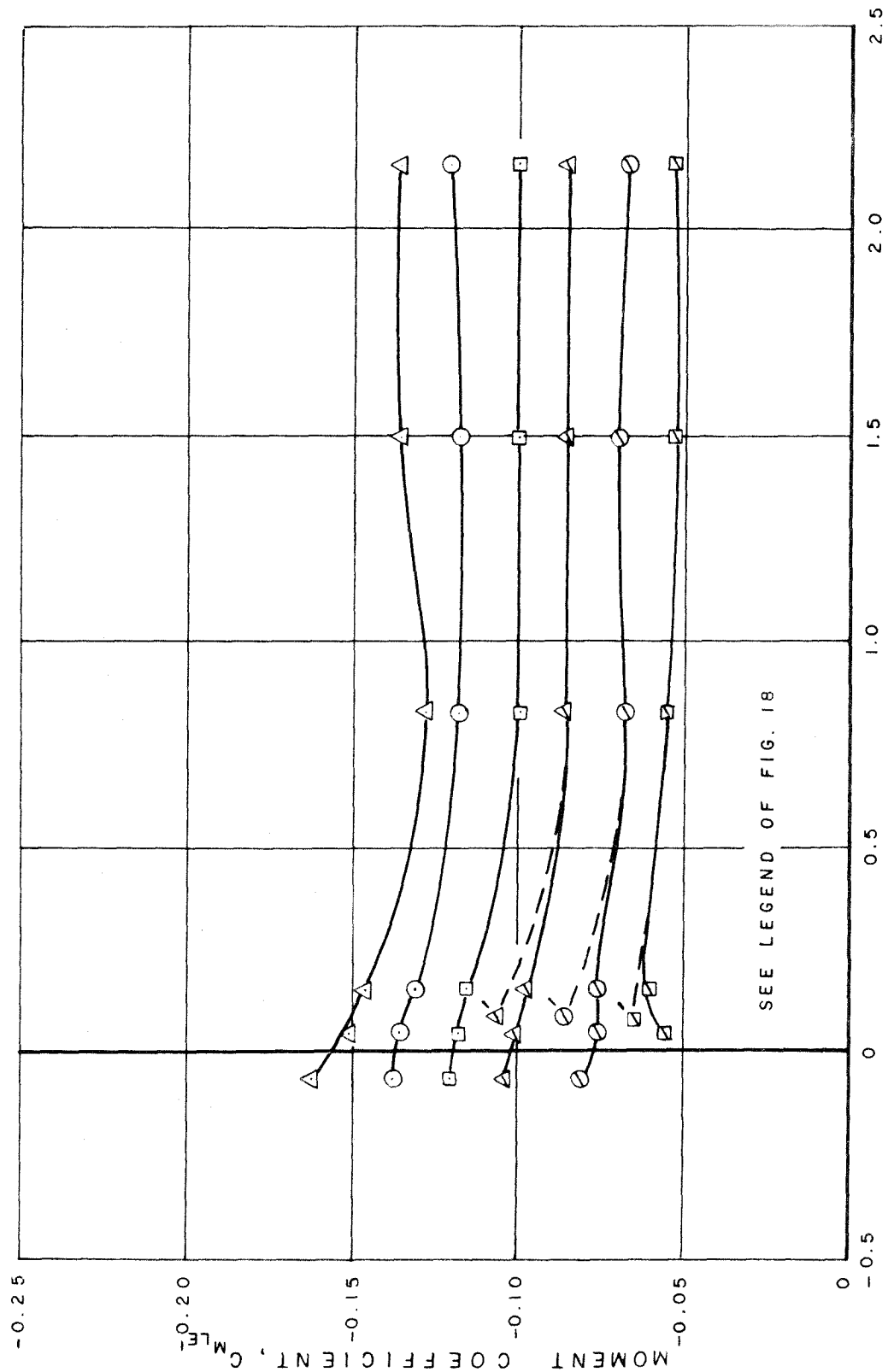

Fig. 38. The effect of submergence on the moment coefficient at six angles of attack and K = 0. (The primed points are those obtained with the skimmer operating.)

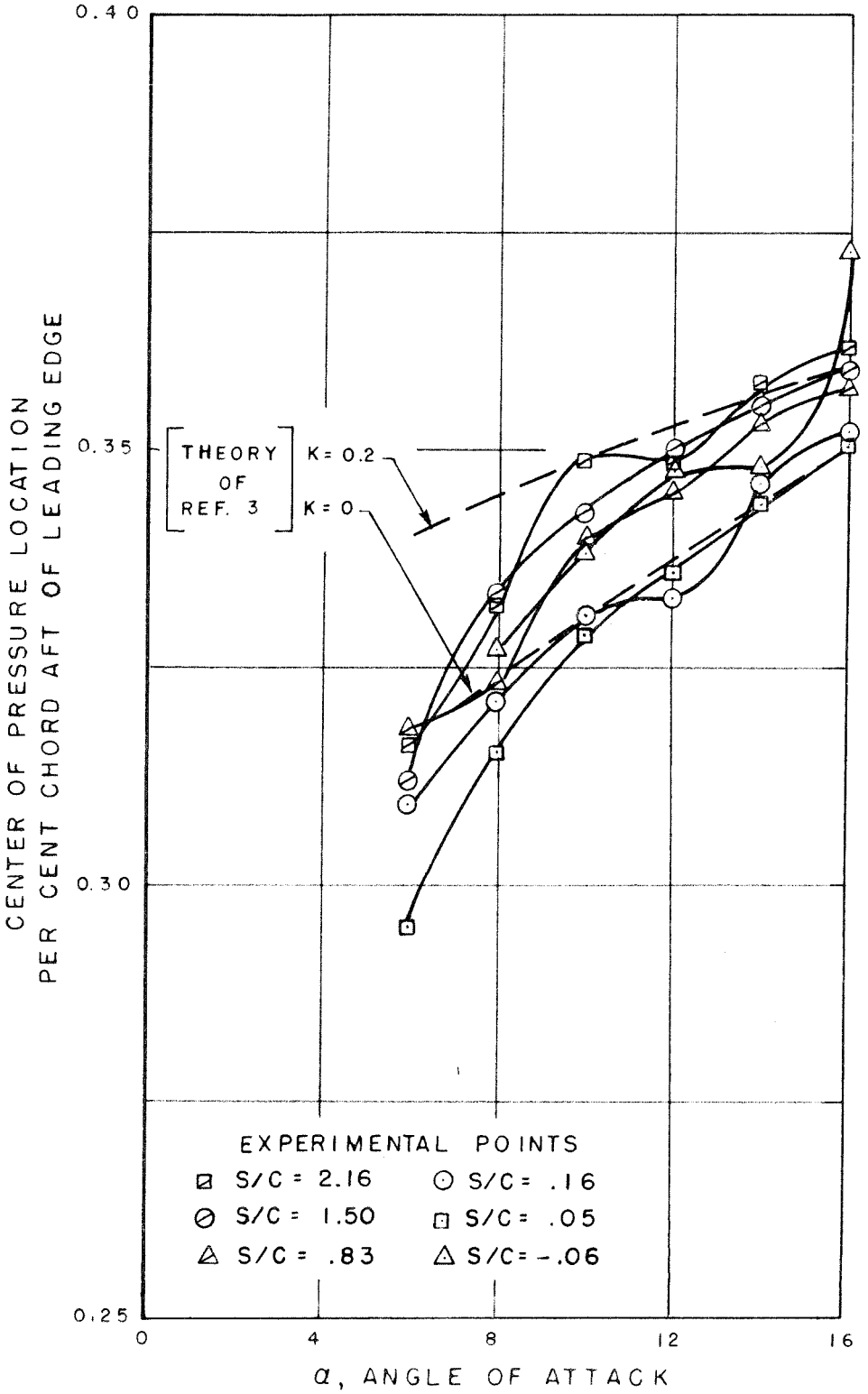

Fig. 39. The experimental center of pressure location versus angle of attack at six submergence ratios as compared to Wu's exact infinite fluid theory.

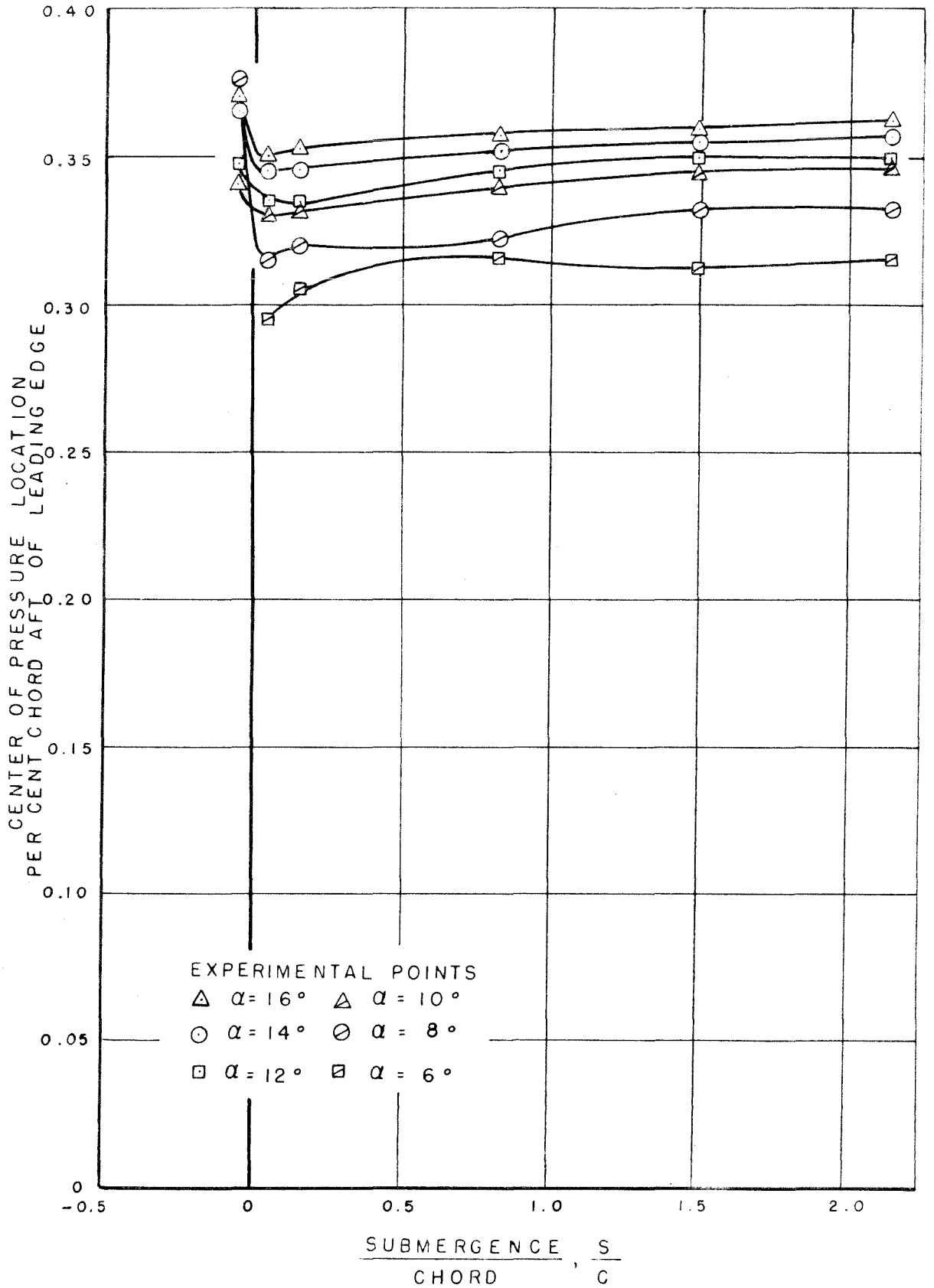

Fig. 40. Center of pressure location versus submergence at six angles of attack.

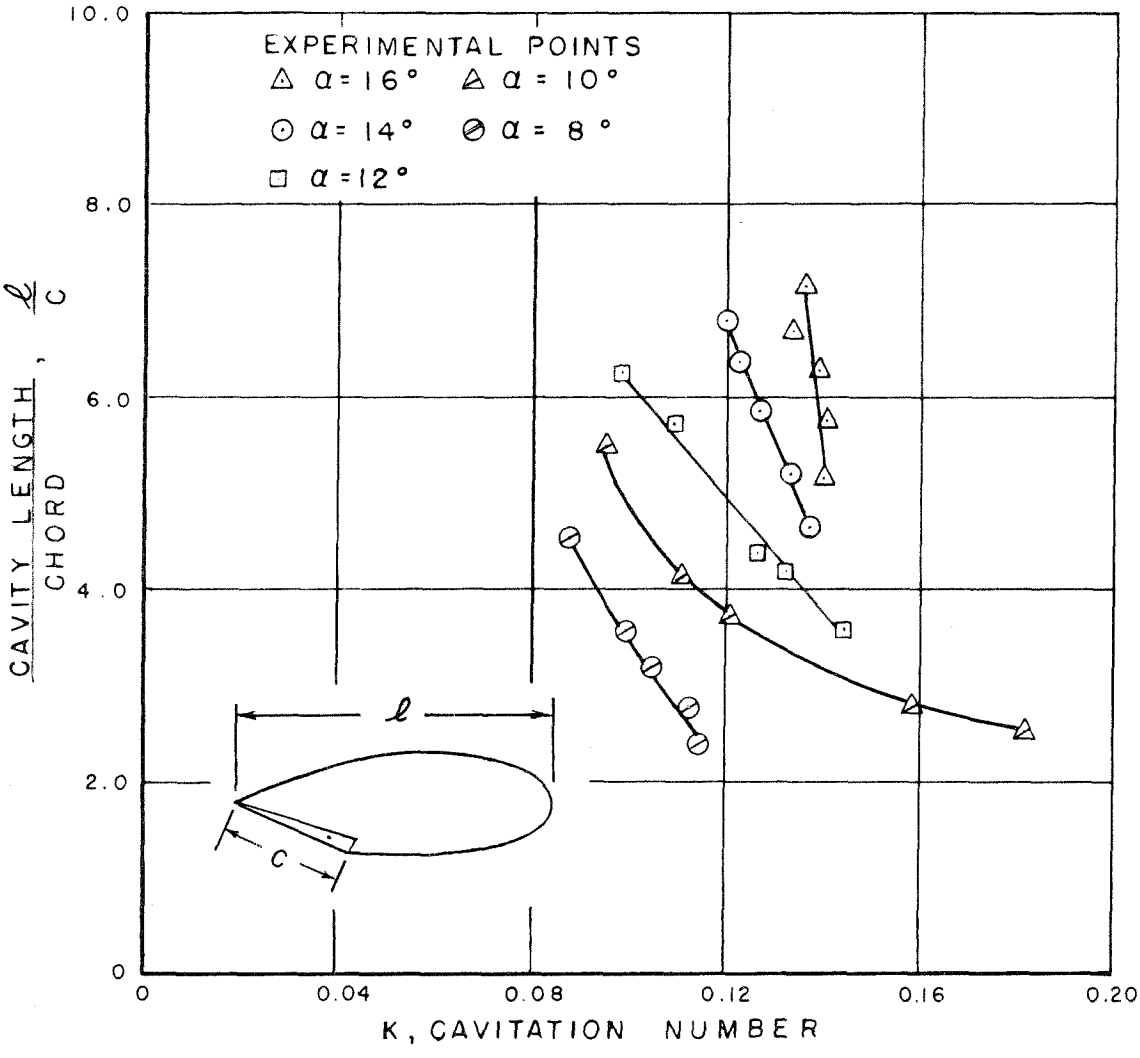

Fig. 41. Cavity length ratios versus cavitation number at five angles of attack and S/c = 2.16.

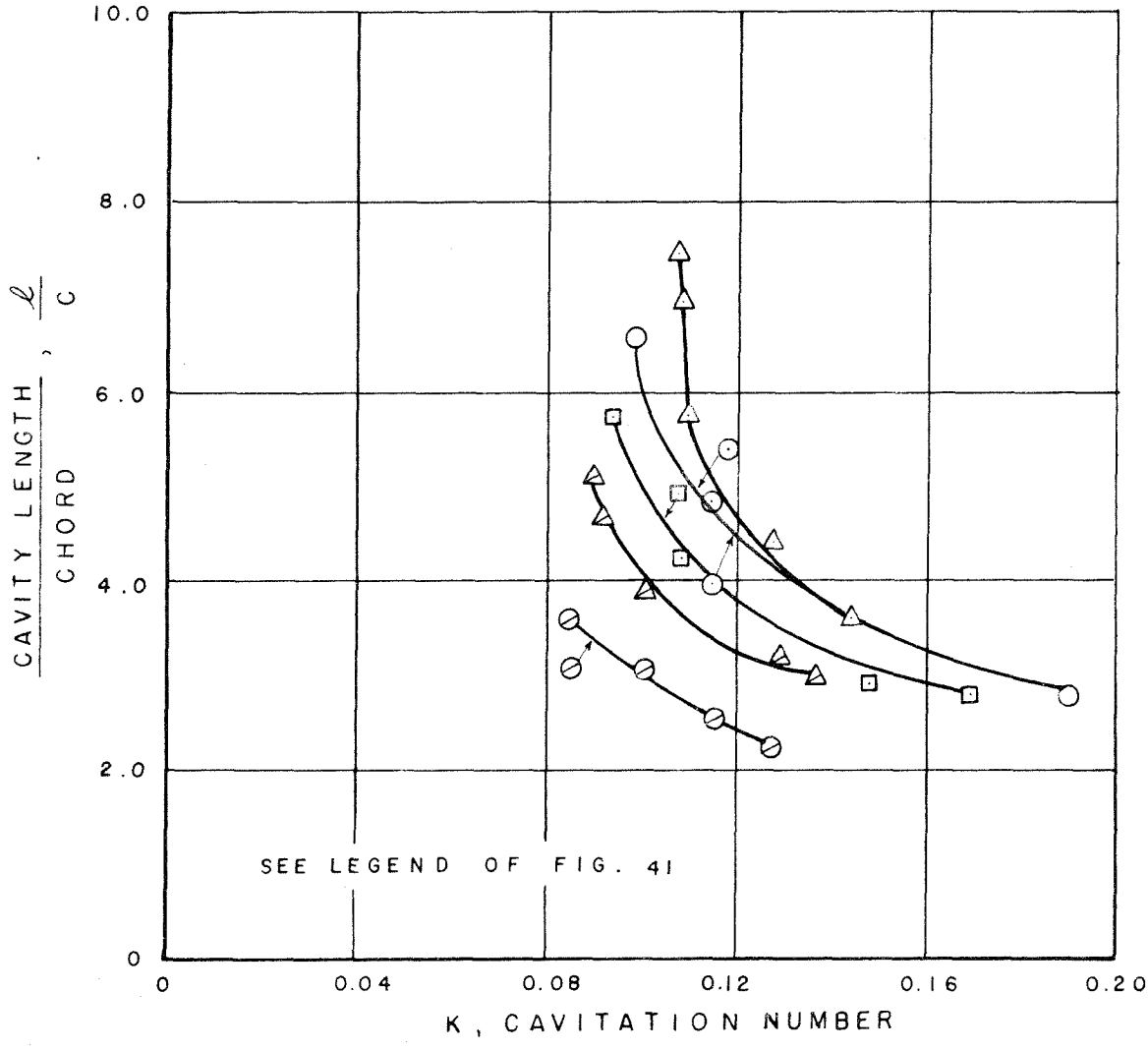

Fig. 42. Cavity length ratios versus cavitation number at five angles of attack and S/c = 1.50.

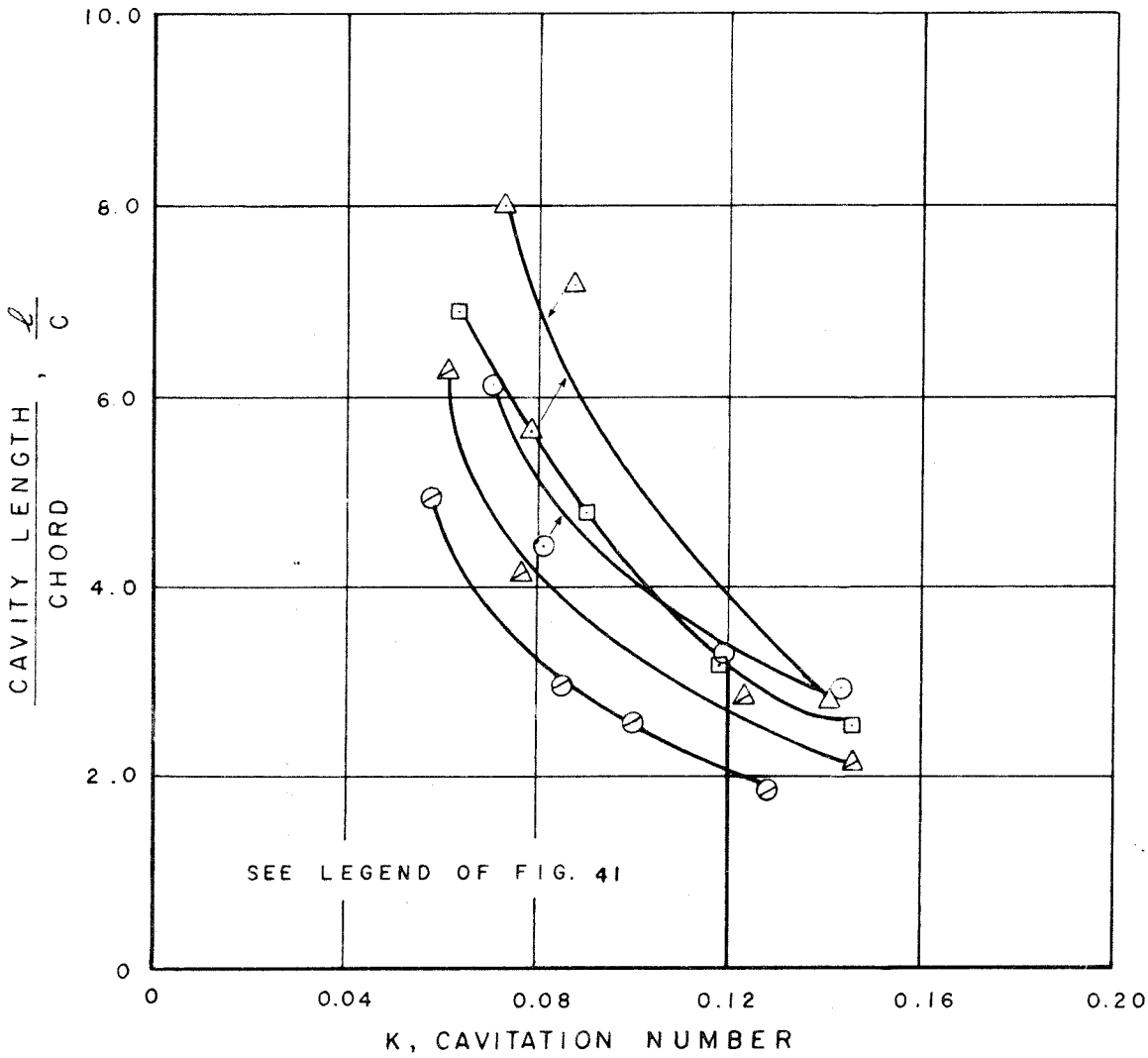

Fig. 43. Cavity length ratios versus cavitation number at five angles of attack and S/c = 0.83.

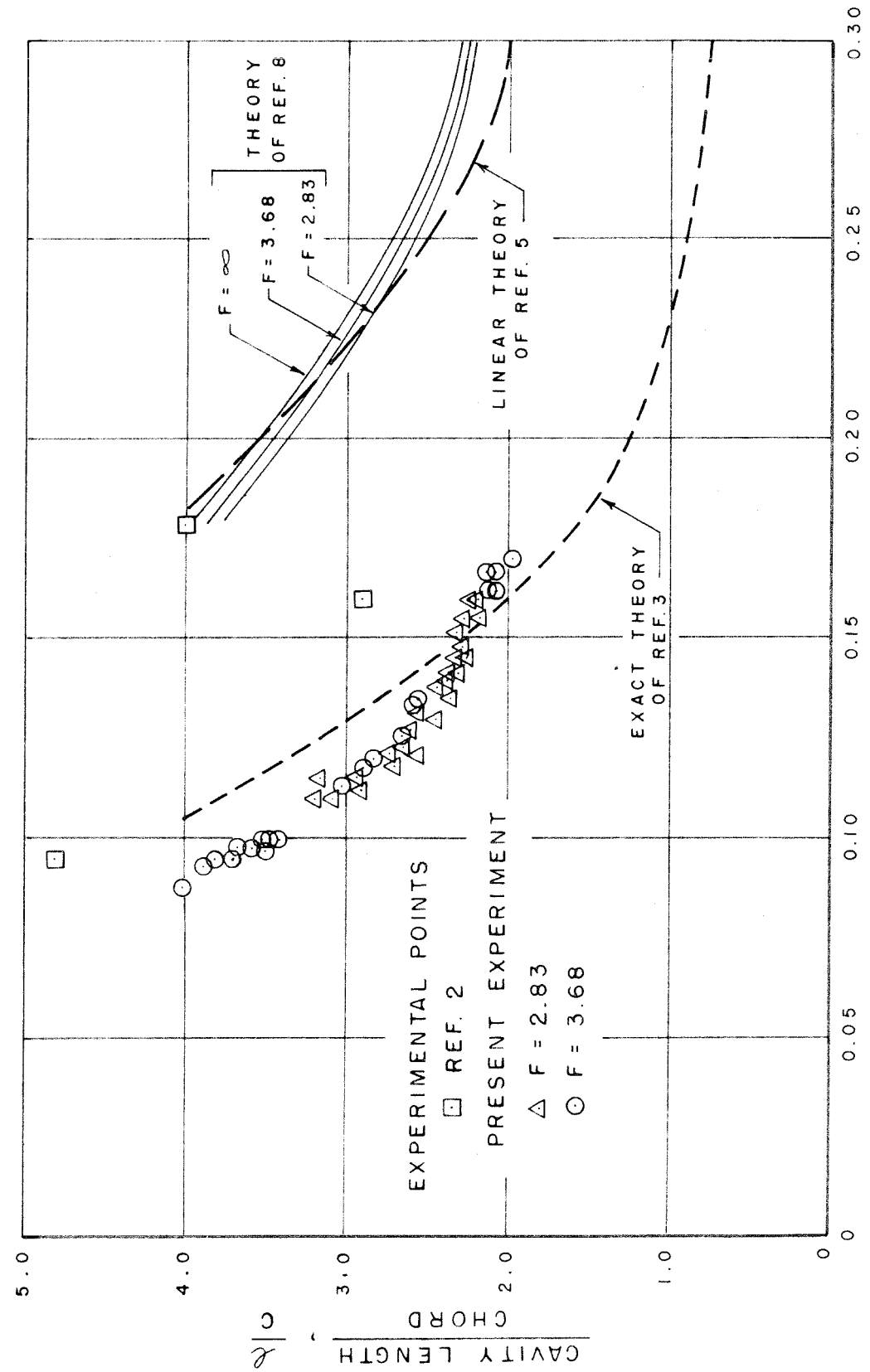

Fig. 44. The experimental cavity length ratios, at S/c = 1.60, $\alpha = 8^{\circ}$, F = 2.83 and F = 3.68, versus cavitation number as compared to the experiment of Silberman and the theories of Wu and Parkin.

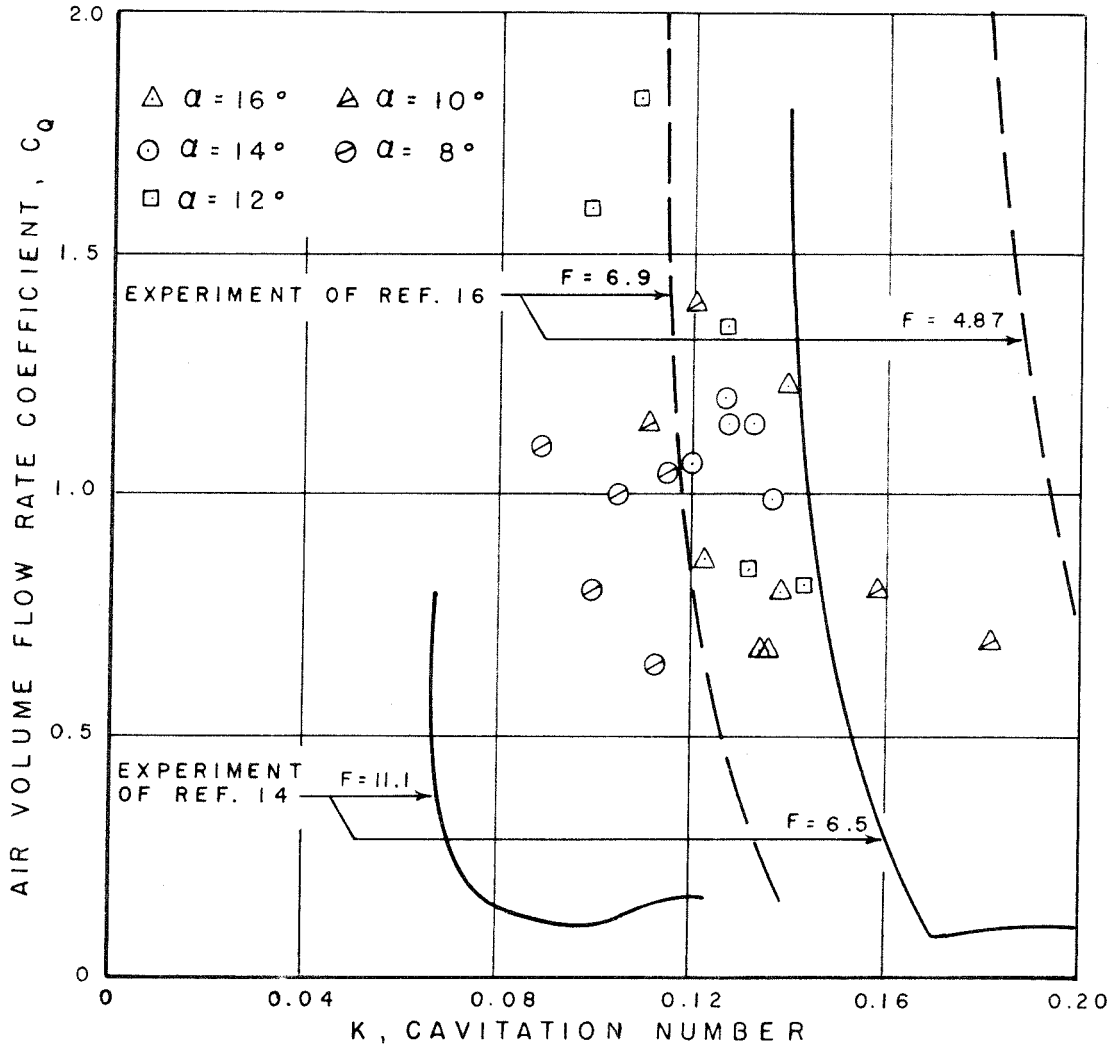

Fig. 45. The experimental air volume flow rate coefficient versus cavitation number at five angles of attack and S/c = 2.16 as compared to the experiments of Swanson and O'Neill and Cox and Clayden.

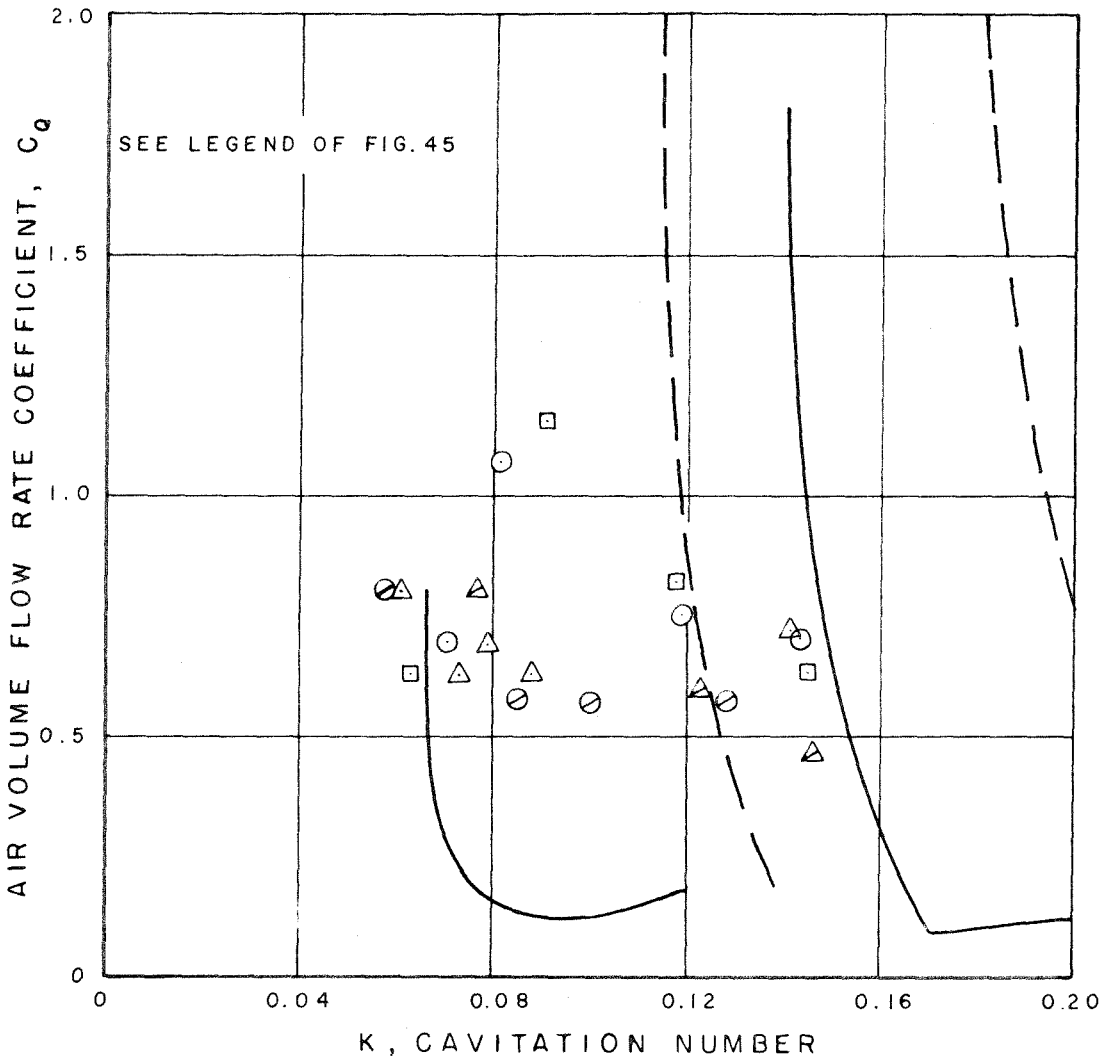

Fig. 46. The experimental air volume flow rate coefficient versus cavitation number at five angles of attack and S/c = 0.83 as compared to the experiments of Swanson and O'Neill and Cox and Clayden.